Studies on neutralizing anti-heparin-binding epidermal growth factor-like growth factor (HB-EGF) antibodies for drug development of cancer treatment

（抗ヘパリン結合性上皮成長因子（HB-EGF）中和抗体による抗癌治療薬に関する研究）

Shuji Sato

佐藤 秀司

2013

Index

1. Abbreviations:

ADAM, a disintegrin and metalloprotease

ARG, amphiregulin

BSA, bovine serum albumin

BSA-conjugate, BSA-conjugated sHB-EGF

BTC, betacellulin

CTF, C-terminal fragment of HB-EGF

DT, diphtheria toxin

EGF, epidermal growth factor

EGFR, EGF receptor

ELISA, enzyme-linked immunosorbent assay

FMAT, fluorometric microvolume assay technology

HB-EGF, heparin-binding EGF-like growth factor

HRGβ, heregulinβ

HRP, horseradish peroxidase

HUVEC, human umbilical vein endothelial cells

KinExA, kinetics exclusion assay

KLH, keyhole limpet hemocyanin

KLH-conjugate, KLH-conjugated sHB-EGF

mAb, monoclonal antibody

MFI, median fluorescence intensity

NHDF, normal human dermal fibroblasts

PLZF, promyelocytic leukaemia zinc finger protein

PMA, phorbol 12-myristate 13-acetate

proHB-EGF, membrane-bound form of HB-EGF

sHB-EGF, soluble form of HB-EGF

TGF-α, transforming growth factor-α

uc-proHB-EGF, uncleavable mutant of proHB-EGF

VEGF, vascular endothelial cell growth factor

2. General introduction

2.1. Background

According to the report released by the United Nations, the current world population of over 7 billion is forecast to grow to 9.2 billion by 2050 (Fig. 0-1A). In association with the population growth, people aged 65 and over of 5.2 billion in 2010 will reach 15 billion in 2050. In particular, advanced countries face the aging society. In Japan, the ratio of 65 and over was 7.1% in 1970, whereas it increased to 23% in 2010 (Fig. 0-1B). It is estimated that this trend will make the population 39% in 2050. As people grow older, the number of those developing cancer increases (Fig. 0-1C). Cancer occurs not only in association with genetic factors but with environmental factors. Approximately 5–10% of cancers are entirely hereditary. The remaining causes of cancers are said to be environmental factors including tobacco, alcohol, infection, radiation, diet, obesity, environmental pollutants, and so forth. The older people are, the more likely that those are exposed to the risk factors. Cells, as tissue components, grow under the restricted control and do not proliferate more than necessity. However, cancer cells do not stop to proliferate as a result of a loss of the control, and invade nearby parts of the body. The cancer cells further spread to more distant parts of the body through the lymphatic system or bloodstream. In cancer cells, genomic amplification or mutations of cell growth-regulating genes are frequently seen. Resulting over-expression or constitutive activation of oncogenes and down-regulated or disabled tumor suppressor genes induce the endless cancer cell proliferation. It also has been revealed that multiple genetic changes in the oncogenes and tumor suppressor genes are likely to induce cancer progression (Knudson, 2001).

A primary choice for the exclusion of cancer tissues, especially for cancer tissues at an early stage, is a surgical excision. However, in case of unresectable advanced or metastatic cancers, anti-cancer drug can be an important choice for patients. These days, with the aim of enhancing a

therapeutic efficacy and of reducing adverse effects, molecularly-targeted anti-cancer drugs are under the active development. Epidermal growth factor receptor (EGFR) is one of the molecules governing not only the proliferation of normal epidermal cells but that of cancer cells, and is over-expressed in many types of cancer (Salomon et al, 1995); therefore, EGFR inhibitor has been pursued for therapeutic applications and several EGFR-targeting drugs including small molecule compounds and antibodies have been marketed for the treatment of cancers. Activation of EGFR is triggered by multiple ligands such as EGF, amphiregulin (ARG), transforming growth factor-α (TGF-α), betacellulin (BTC), and heparin-binding epidermal growth factor-like growth factor (HB-EGF). The activation of EGFR by the multiple ligands may be blocked by the EGFR inhibitors. However, at the same time, they may cause unnecessary adverse events by excessively disturbing the activation of EGFR by all the ligands. From that perspective, the inhibition of an EGFR ligand, which is substantially involved in tumor progression, might become a potential therapy. This approach may reduce adverse events such as a severe skin rash, which is seen by the treatment of anti-EGFR inhibitors.

Among the EGFR ligands, I selected HB-EGF, which has been reported to be over-expressed in multiple cancer types, and generated anti-HB-EGF monoclonal antibodies (mAbs) and characterized them in the Chapter I. Furthermore, in the Chapter II, I explored the therapeutic value of one of the most potent neutralizing antibodies, Y-142, in comparison with mAbs clinically used.

2.2. Ovarian cancer

Ovarian cancer occurs as a result of aberrant genomic amplification or accumulation of genetic mutations, which cause unregulated cell growth. In recent years, as many as 160,000 patients have been annually diagnosed with ovarian cancer in Japan, US, UK, France, Germany, Spain and Italy, and BRICs (Fig. 0-2A). New cases diagnosed as ovarian cancer are predicted to reach 200,000 in

2025. At present, ovarian cancer occupies 5% of cancer death rate of women, and fifth-most-frequent cause of cancer death overall in women. Epidemiological studies showed that genetic, reproductive, and environmental factors can affect the risk of ovarian cancer (Sueblinvong et al, 2009). Approximately 5–10% of ovarian cancers are hereditary. Among them, 90% of the cases are related with BRCA gene mutations (Prat et al, 2005). The remaining 10% is associated with hereditary nonpolyposis colorectal cancer. Older women, infertile women and those with a condition called endometriosis have an increased risk. On the other hand, a reduced risk of ovarian cancer is associated with a reduced number of menstrual cycles, such as increased parity and the use of oral contraceptives, as well as with early age at first pregnancy and older age of final pregnancy. Patients with an unresectable advanced ovarian cancer have a 5-year survival rate of less than 30%, whereas more than 90% of those with an early-stage ovarian cancer survive more than 5 years (SEER, 2007). This indicates that early detection is inevitable for the improved survival. Signs and symptoms of ovarian cancer are frequently absent early on. The asymptomatic phenotype of ovarian cancer makes its early-stage detection difficult. In 2007, the Gynecologic Cancer Foundation announced the national consensus of common symptoms of ovarian cancer: abdominal or pelvic pain, difficulty eating or feeling full quickly, bloating, and urinary urgency or frequency. Medical attention should be paid when the symptoms continue.

For patients eligible for chemotherapy, the combination of paclitaxel and carboplatin are prescribed for more than 90% of ovarian cancer patients. Based on a previous clinical study, the combined therapy is known to give the patients a median survival period of 29 months. The combination therapy of paclitaxel and carboplatin, however, develops severe neurotoxicity and neutropenia. Therefore, the emergence of anti-cancer drug with an efficacy and with a reduced adverse effect is being awaited.

2.3. Gastric cancer

Approximately 300,000 people are annually diagnosed with gastric cancer in Japan, US, the 5 European countries and BRICs (Fig. 0-2B). The cause of gastric cancer includes food habit, smoking, alcohol intake, and infection with the Helicobacter pylori (Plummer et al, 2004; Tramacere et al, 2012; Eslick, 2006). Overweight and obesity are also associated with increased risk of gastric cancer (Yang et al, 2009). Meanwhile, vegetables and fruit are protective against gastric cancer (Lunet et al, 2005). In Japan and Korea, a gastric cancer screening system using photofluorography is established because of the high incidence of the gastric cancer (Jung et al, 2011). The screening system allows the 5-year survival rate of Japanese gastric cancer patients to be 62%, while those of US and the European countries are less than 30%. Gastric cancer is one of the deadliest cancers, and ranks second worldwide in terms of cancer death rates.

Although a combined therapy with docetaxel/carboplatin/5-FU is widely used for patients with an unresectable gastric cancer, it can come with adverse events including neutropenia and gastrointestinal toxicity. In case of the unresectable gastric cancer, the median survival period of the patients is as short as 10 months. Therefore, elucidation of biological mechanism in gastric cancer is an urgent task and will help identify an effective therapy.

2.4. Antibody drug

Antibody is present in the body, and works as an immunoresponse factor with the binding ability to a target molecule. Antibody drug is an artificially generated antibody, which maintains innate antibody characters. To date, more than 30 kinds of antibody drug have been launched onto the market, including 14 for the treatment of cancers (Table 0-1). In addition, more than 160 antibodies are currently in clinical development. Compared to small molecules, the history of antibody drugs is short, as indicated by the fact that most of the antibody drugs were approved in the last two decades.

However, 3 out of top 10 medical drugs in global sales in 2011 were occupied by antibody drugs (Cegedim Strategic Data). There are some rationales behind this phenomenon. Unlike orally-available small molecules, antibody drugs need to be intravenously administered. However, because of its long half-life in blood (~ 2 weeks; Keizer et al, 2010), antibody drugs can be administered on a once-per-week to once-per-month basis. Another advantage of antibody drugs over small molecules is absence of structure-based adverse events because antibodies originally present in the blood. This means that the dose of antibody drug can be raised to maximize its efficacy without increasing the risk of adverse events. Antibody does not become passively incorporated because of its large molecular weight (approximately 150 kDa), meaning that antibody-targeted molecules are limited to cell surface proteins or secreted proteins. At the same time, however, the large molecular weight is suitable for the inhibition of protein-protein interaction such as a ligand-receptor binding. In addition, antibody unites cytotoxic functions mediated through immunological players including NK cells and complements. Moreover, the higher success rate helps to expand the antibody drug market: antibody drugs come on the market with the possibility of 20% once its clinical trial starts, whereas small molecules do with that of 5% (Chapman et al, 2007).

The functionality of antibody drug depends on target molecule functions as well as on its isotype. When the target molecule is a ligand or receptor involved in cell proliferation, antibody can inhibit the proliferation by blocking the ligand-receptor interaction. EGFR family member strongly induces cancer cell proliferation and antibody drugs against EGFR are known to be able to inhibit the proliferation by blocking the ligand-receptor interaction, the mechanism of which is called neutralizing. Bevacizumab, an antibody drug against vascular endothelial cell growth factor (VEGF), is also a neutralizer against VEGF functions. VEGF is a potent angiogenic protein and promotes new blood vessel formation to carry nutrition through. The anti-VEGF antibody starves cancer cells to death by inhibiting the VEGF-derived angiogenesis.

Antibody combines immunological functions including antibody-dependent cell-mediated cytotoxicity (ADCC) and complement-dependent cytotoxicity (CDC). ADCC is exhibited by NK cells expressing IgG Fc receptor, FcγRIIIa. Through the binding to FcγRIIIa, some IgG class antibodies (IgG_1 and IgG_3 in case of human IgG) activate NK cells. Perfolin protein secreted by the activated NK cells enhances the permeability of target cell, and granzyme sequentially secreted from the NK cells induces apoptosis in the target cells. CDC occurs as a result of the activation of a classical complement pathway by the binding of complement factor to IgG Fc region. As a result, target cell reach to death by having its cell membrane disrupted or preyed by phagocytes. CDC is one of the functions of anti-CD20 antibody, rituximab. Normal heamatopoietic cells express CD55 and CD59 on cell surface. These molecules help the cells escape from CDC by suppressing the activation of complement.

Antibody also can be used as a drug delivery tool. Drug, which is conjugated to antibody, can be delivered to target cells expressing the antigen molecule of the antibody. High specificity of antibody to the antigen molecule enables the drug to specifically attack the target cells without damaging irrelevant cells.

2.5. HB-EGF

HB-EGF is a cell growth factor with a heparin-binding ability, which was first isolated from the conditioned medium of U-937, a macrophage-like cell line (Higashiyama et al, 1991). HB-EGF is expressed as a membrane protein called proHB-EGF, which is composed of a signal peptide, propeptide, heparin-binding domain, EGF-like domain, juxtamembrane domain, transmembrane domain, and cytoplasmic domain (Fig. 0-3; Higashiyama et al, 1992). The propeptide domain is cleaved soon after proHB-EGF is presented at the cell surface (Ono et al, 1994). Under stress conditions such as osmotic stress or chemotherapy, proteases including matrix metalloprotease-3, -7,

a disintegrin and metalloprotease (ADAM) 9, 10, 12, and 17 (Suzuki et al, 1997; Yu et al, 2002; Izumi et al, 1998; Asakura et al, 2002; Lemjabbar et al, 2002; Yan et al, 2002; Sunnarborg et al, 2002), cleave proHB-EGF, which results in the release of its extracellular domain, a soluble form of HB-EGF (sHB-EGF) containing the heparin-binding and EGF-like domains (Fig. 0-4). The heparin-binding domain is a 21-amino acid stretch rich in basic amino acids, and located at the position of 93rd to 113th of proHB-EGF (Thompson et al, 1994). The binding of sHB-EGF to heparin sulfate proteoglycan through this domain enhances the biological activity of sHB-EGF such as the phosphorylation of EGFR and cell migration (Aviezer et al, 1994; Higashiyama et al, 1993). The EGF-like domain is shared by EGFR ligands, and consists of 36–40 amino acids containing a 6-cysteine motif (Carpenter et al, 1991). This domain is required for the HB-EGF binding to its receptors EGFR and ERBB4 (Shin et al, 1994). Through the activation of the receptors, sHB-EGF exhibits different biological activities. Namely, sHB-EGF induces cell proliferation as well as chemotaxis through the activation of EGFR, while the ERBB4 activation leads to chemotaxis, not to cell proliferation (Elenius et al, 1997). More detailed analysis showed that the homo- and heterodimers of EGFR family members can function as a sHB-EGF receptor when either of EGFR or ERBB4 is included in the dimmers (Fig. 0-5; Riese et al, 1996). sHB-EGF, released by the ectodomain shedding of proHB-EGF, is involved in a variety of physiological processes including tissue development (Iwamoto et al, 2003; Jackson et al, 2003; Mine et al, 2005), skin wound healing (Shirakata et al, 2005), and pregnancy (Das et al, 1994; Raab et al, 1996), as well as pathological processes such as cardiac hypertrophy (Asakura et al, 2002), pulmonary hypertension (Powell et al, 1993), atherosclerosis (Miyagawa et al, 1995; Peoples et al, 1995), and oncogenic transformation (Fu et al, 1999). The over-expression of HB-EGF mRNA as well as HB-EGF protein in ovarian cancer tissues have been reported (Tanaka et al, 2005). sHB-EGF protein is also detected in the peritoneal fluid from ovarian cancer patients (Yagi et al, 2005; Miyamoto et al, 2004). Furthermore,

it has been shown that the over-expression of ADMA17, one of proteases for HB-EGF, is associated with the over-expression of HB-EGF, meaning that HB-EGF signaling cascade itself may be enhanced in ovarian cancer (Tanaka et al, 2005). In the Chapter I and II, the biological activities of anti-HB-EGF mAbs on sHB-EGF were characterized with cell lines derived from ovarian cancer tissues.

Membrane-bound form of HB-EGF, proHB-EGF, exhibits unique functions distinguished from sHB-EGF, such as a diphtheria toxin (DT) receptor (Naglich et al, 1992), a cell adhesion molecule (Raab et al, 1996), and a juxtacrine growth factor (Higashiyama et at, 1995), other than acting as a precursor of sHB-EGF. DT binding to proHB-EGF is potentiated by CD9 or heparin-like molecules (Mitamura et al, 1992; Shishido et al, 1995), and the sequential internalization of the DT-proHB-EGF complex causes the inhibition of protein synthesis, which is resulted from the ADP ribosylation activity of DT on peptide elongation factor EF-2. As a cell adhesion molecule, proHB-EGF contributes to blastocyst adhesion to the uterus in the process of implantation in mice (Raab et al, 1996). In vitro analyses revealed that proHB-EGF forms a complex with CD9 and integrin $\alpha 3\beta 1$ at cell-cell contact sites (Nakamura et al, 1995). The complex is predicted to be associated with the cell adhesion function of proHB-EGF. Some other molecules, which have not been identified yet, might interact with the complex (Singh et al, 2007). The juxtacrine activity of proHB-EGF was first noted in a co-culture system, where proHB-EGF-over-expressing cells were seeded on EGFR-over-expressing cells (Higashiyama et al, 1995). To isolate and assess the signaling initiated by proHB-EGF separately from that initiated by sHB-EGF, the proHB-EGF-over-expressing cells were fixed with formalin, thereby preventing the release of sHB-EGF. In this co-culture system, the proHB-EGF-over-expressing cells promoted DNA synthesis and prevented apoptosis in the EGFR-over-expressing cells in some of the studies (Higashiyama et al, 1995; Nakagawa et al, 1996; Takemura et al, 1997). In contrast, they inhibited DNA synthesis and promoted apoptosis in the EGFR-over-

expressing cells in a modified co-culture condition without using the formalin-fixation (Iwamoto et al, 1999). The functions of proHB-EGF were also evaluated by analyzing the effects of proHB-EGF over-expression on autonomous cellular events. The proHB-EGF over-expression suppressed or promoted cell proliferation in different cell lines (Miyoshi et al, 1997; Takemura et al, 1999). Thus, the roles of proHB-EGF have not been consistently or clearly elucidated. In the Chapter III, I identified the cell proliferation and survival functions of proHB-EGF by examining anti-HB-EGF mAb effect. In gastric cancer tissues, from which a cell line used in the Chapter III is derived, the over-expression of HB-EGF was reported (Hirata et al, 2009; Yasumoto et al, 2011). The author believes that the identification of the proHB-EGF function will lead to the deeper understanding of gastric cancer.

Recent studies showed that the C-terminal fragment of proHB-EGF (CTF) acts as a signaling molecule. After sHB-EGF is released by the ectodomain shedding of proHB-EGF, CTF, the remnant of proHB-EGF, translocates into nucleus, and guides promyelocytic leukaemia zinc finger protein (PLZF), which suppresses the expression of CyclinA (Li et al, 1997; Yeyati et al, 1999), out of nucleus. The nuclear export of PLZF by CTF leads to the gene expression of CyclinA, resulting in the acceleration of S-phase (Nanba et al, 2003). More recently, the interaction of CTF with BCL6, which is a transcriptional repressor of CyclinD2, was reported (Kinugasa et al, 2007). Translocation of CTF into nucleus promotes degradation of BCL6 in ubiquitin/proteasome pathway, inducing the gene expression of CyclinD2 (Hirata et al, 2009). The resulting induction of CyclinD2 gene is predicted to drive cell cycle. In HB-EGF expression-positive gastric cancer tissues, an inverse correlation of the expressions of BCL6 and CyclinD2 was reported, suggesting the CTF contribution to cancer cell proliferation in clinical cancer tissues (Hirata et al, 2009). However, there has been no evidence showing the direct involvement of proHB-EGF in cancer cell proliferation and survival, which is discussed in the Chapter III.

2.6. HB-EGF inhibitors

Generation of anti-HB-EGF antibodies by a hybridoma approach has been thought difficult because of the high homology of HB-EGF over species (Fig. 0-6; Hamaoka et al, 2010). When it comes to neutralizing antibodies, only few mAbs have been reported. DE10 is the first publicized neutralizing mAb against human HB-EGF. The antibody is cross-reactive to rat HB-EGF and partially inhibits sHB-EGF-induced cell proliferation (Khong et al, 2000). Another neutralizing antibody KM3566 was generated with an HB-EGF-null mouse by a hybridoma approach. It is announced that a clinical phase I study of its humanized version has initiated with the indication of ovarian cancer patients in US (Miyamoto et al, 2011). However, judging from the biological data of DE10 and KM3566, it seemed to me that more potent neutralizing antibody could be generated.

CRM197 was previously identified as a mutein of diphtheria toxin (DT) with an amino acid replacement of a glycine with a glutamic acid at the 52^{nd} amino acid position (Uchida et al, 1971; Giannini et al, 1984). Among two domains A and B consisting of DT, A domain is responsible for its ADP ribosylation activity, while B domain is able to bind to HB-EGF (Mekada et al, 1988). The A domain ADP-ribosylates a peptide elongation factor EF-2, which causes cytotoxicity through the inhibition of protein synthesis. Because of the amino acid replacement in the A domain of CRM197, the cytotoxicity of CRM197 through the ADP ribosylation activity is 10^6 times less than that of wild-type DT (Kageyama et al, 2007). However, CRM197 retains the binding and inhibitory activity to HB-EGF at a level comparable to wild-type DT, and shows HB-EGF-specific binding (Mitamura et al, 1995; Prenzel et al 1999). The molecular mechanism of CRM197 cytotoxicity is likely due to the inhibition of HB-EGF activity as wells as to the remaining ADP ribosylation activity (Kageyama et al, 2007). In 2004, the result of phase I clinical trial was disclosed, where CRM197 was administered to 25 patients with an advanced cancer (Buzzi et al, 2004). One case of

a breast cancer showed a complete regression, and two cases of a breast cancer and a neuroblastoma resulted in a partial regression. No severe adverse event was observed with the administration of 1.7 to 3.5 mg/kg. However, the study revealed the instability of CRM197 in human blood. The half-life of CRM197 is about 18 hours, which is much shorter than that of a typical human antibody (~ 2 weeks). In the Chapter II, the biological property of Y-142 was compared with CRM197 as well as cetuximab and bevacizumab.

2.7. Figures

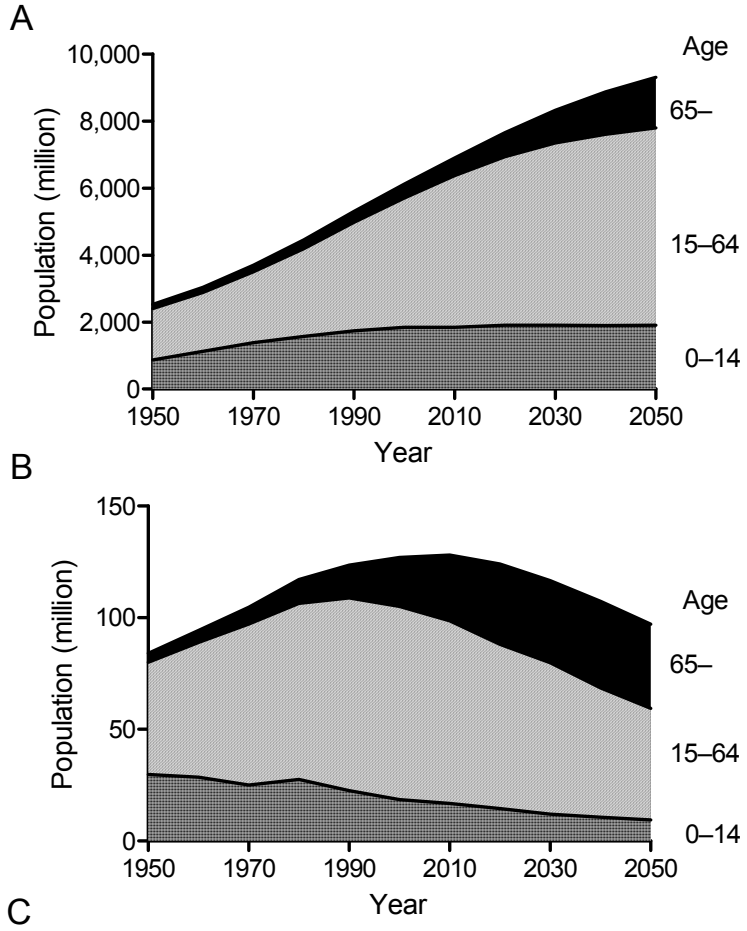

Fig. 0-1. Demographic change and cancer prevalence

A. Changes in world population. B. Changes in Japan's population. Modified from the United Nations, World Population Prospects: The 2010 Revision. C. Cancer prevalence in Japan. Modified from Matsuda et al, 1995.

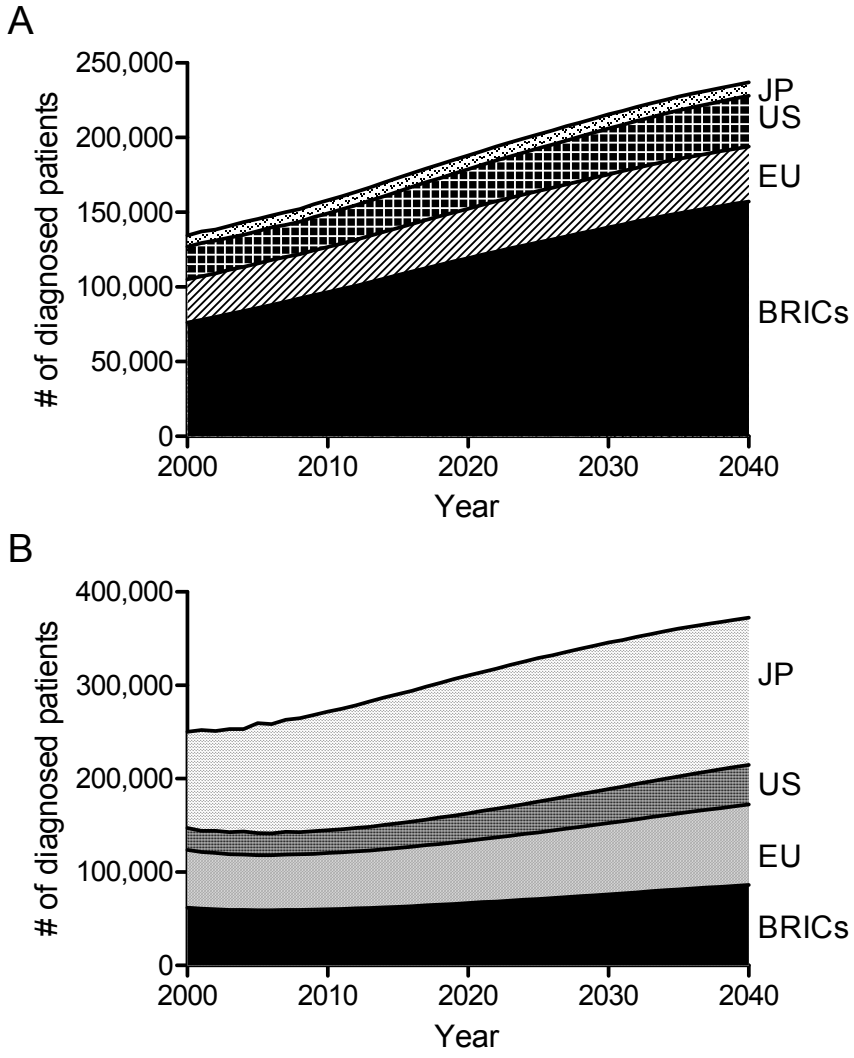

Fig. 0-2. Increase in new cases of ovarian and gastric cancers

Newly diagnosed cases of ovarian (A) and gastric cancers (B). Patient number was graphed with a reference of EpiDatabase. JP, Japan; EU includes UK, France, Germany, Spain, and Italy; BRICs includes Brazil, Russia, India, and China.

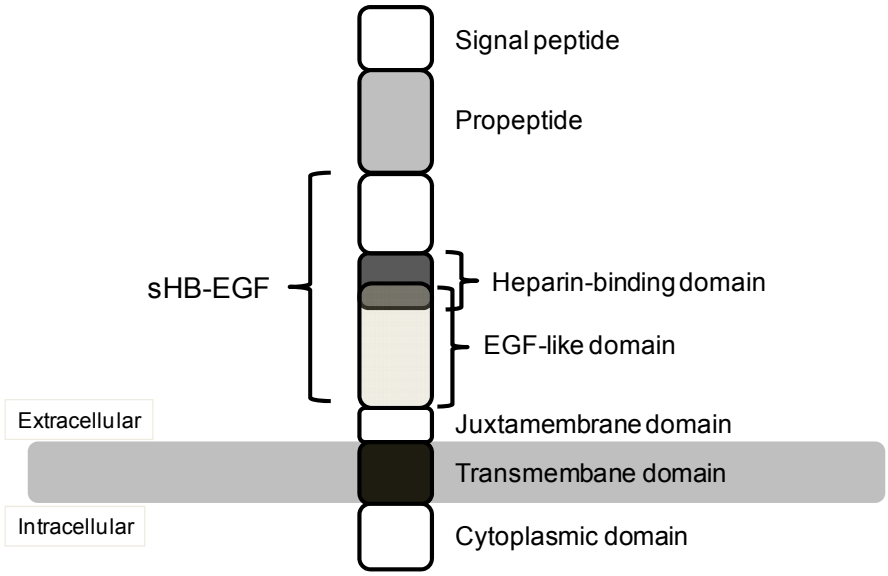

Fig. 0-3. HB-EGF domain structure

proHB-EGF domain structure is depicted. Propeptide is cut off soon after proHB-EGF is presented at cell surface. Ectodomain shedding occurs at the site of juxtamembrane domain.

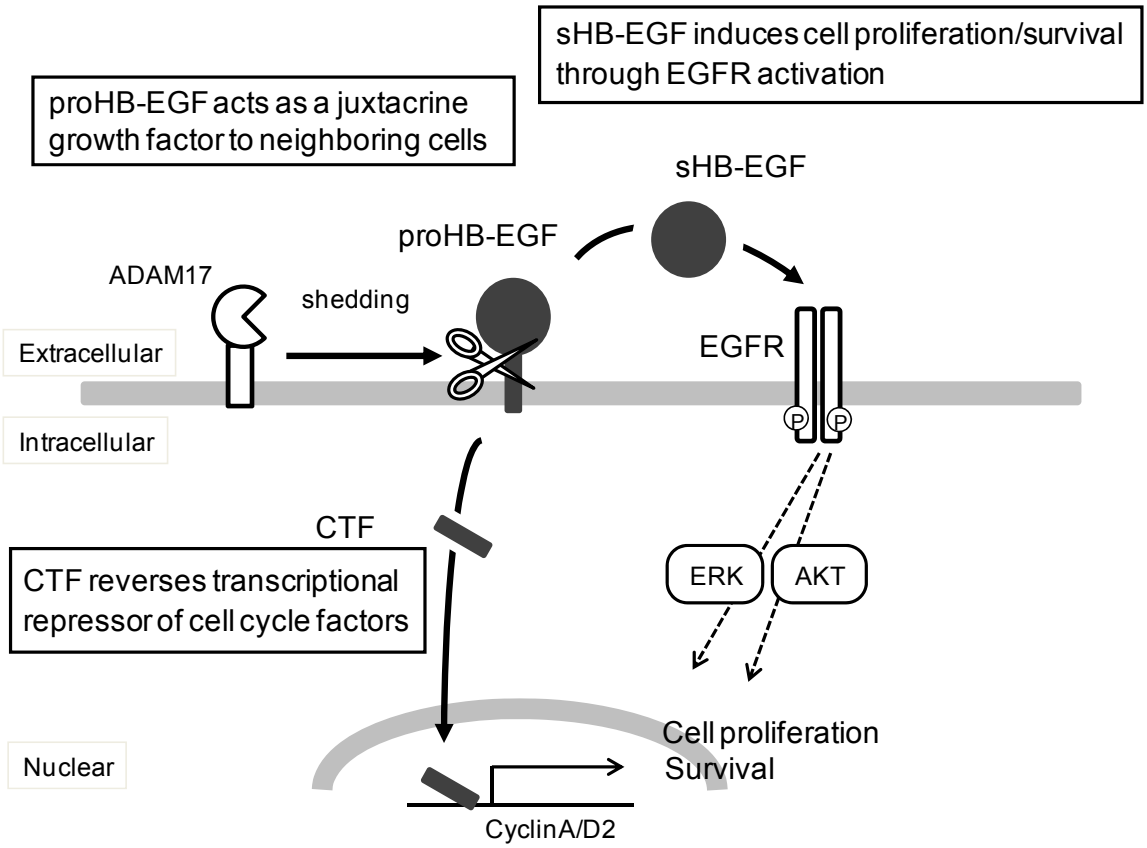

Fig. 0-4. HB-EGF cellular signaling

proHB-EGF is cleaved by a protease such as ADAM17. Soluble form of HB-EGF (sHB-EGF) activates EGFR-ERK and EGFR-AKT pathways, leading to cell proliferation and survival, respectively. C-terminal fragment (CTF) translocates into a nucleus and induces CyclinA/CyclinD2 expression by inhibiting their transcriptional repressors.

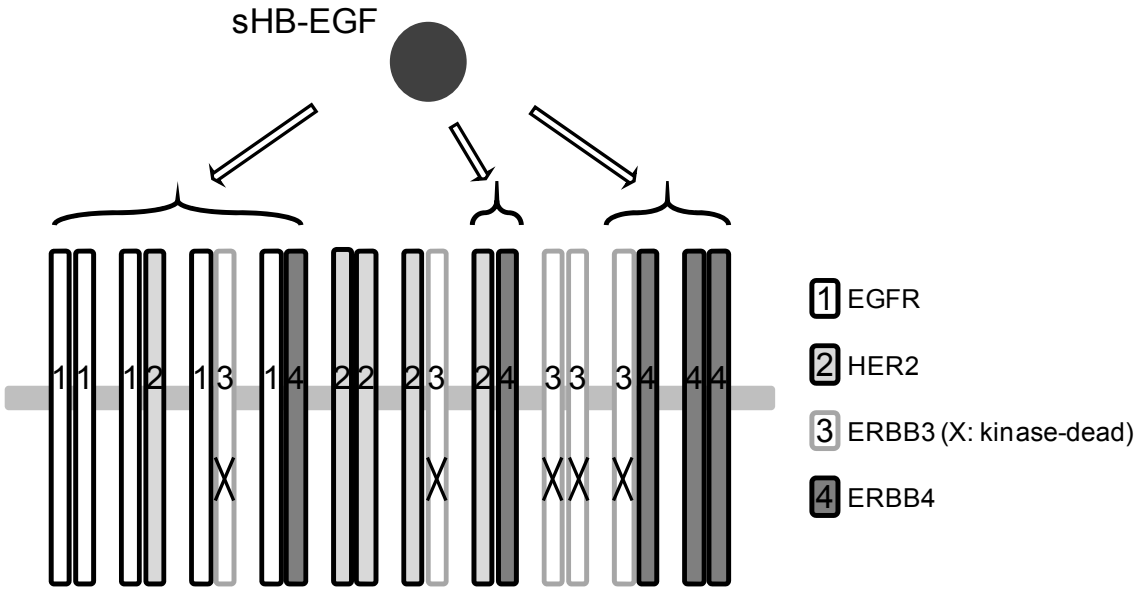

Fig. 0-5. Binding preference of sHB-EGF

sHB-EGF binds to a homo- or hetero-dimers, composed of EGFR or ERBB4. Modified from Miyamoto et al, 2007.

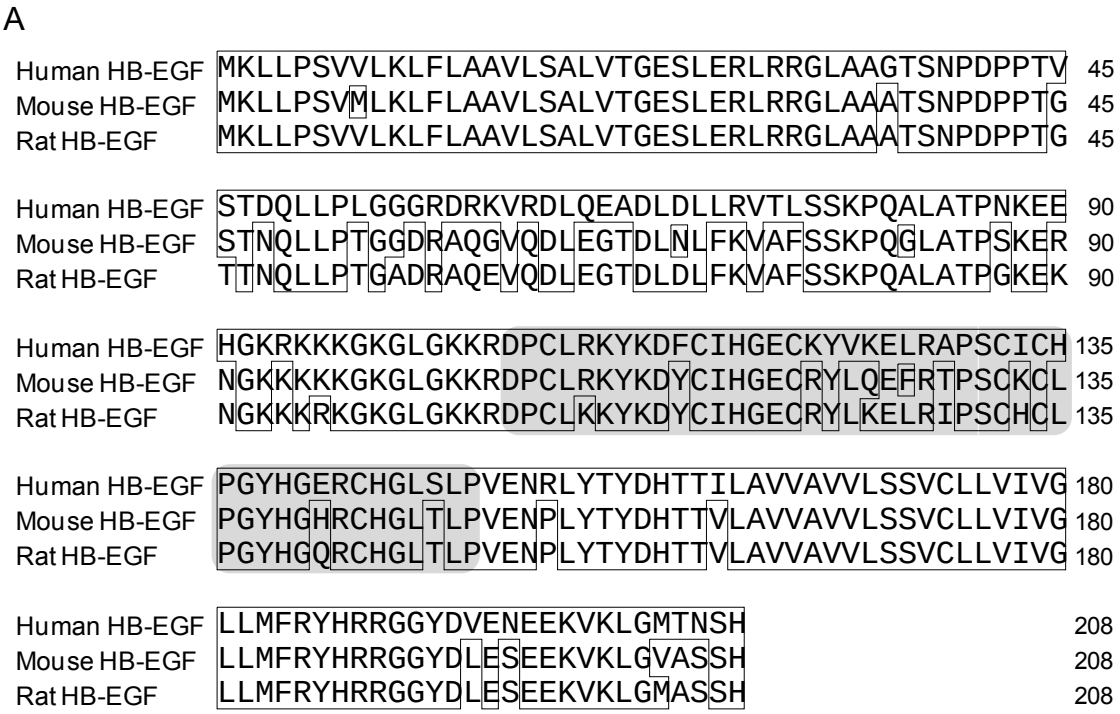

B

	Mo	Ra
Hu	80.8	81.7
Mo	—	92.3

C

	Mo	Ra
Hu	73.6	75.9
Mo	—	87.4

D

	Mo	Ra
Hu	77.3	79.5
Mo	—	86.4

Fig. 0-6. Amino acid alignment of human, mouse, and rat HB-EGF

A. Amino acid alignment of proHB-EGF. Amino acids identical to human proHB-EGF are boxed. EGF-like domain is highlighted in gray. Amino acid identity of human, mouse, and rat proHB-EGF (B), human, mouse, and rat sHB-EGF (C), and the EGF-like domain in human, mouse, and rat HB-EGF (D). Hu, human; Mo, mouse; Ra, rat.

2.8. Table

Table 0-1. Anti-cancer antibody drug in the market

Generic name	Brand name	Target	Type	Indication	Approval	
					US	JP
Mogamulizumab	Poteligeo	CCR4	Humanized	T cell lymphoma	Non-approved	2012
Pertumumab	Perjeta	HER2	Humanized	Metastatic breast cancer	2012	Non-approved
Brentuximab vedotin	Adcetris	CD30	Chimeric (monomethyl auristatin-conjugate)	Hodgkin lymphoma	2011	Non-approved
Ipilimumab	Yervoy	CTLA-4	Human	Metastatic melanoma	2011	Non-approved
Ofatumumab	Arzerra	CD20	Human	Chronic lymphocytic leukemia	2009	Non-approved
Panitumumab	Vectibix	EGFR	Human	Colon cancer	2006	2010
Bevacizumab	Avastin	VEGF	Humanized	Colon cancer	2004	2007
Cetuximab	Erbitux	EGFR	Chimeric	Head and neck cancer Colon cancer	2004	2008
Iodine 131 Toshitumomab	Bexxar	CD20	Mouse (^{131}I-labeled)	Non-hodgkin lymphoma	2003	Non-approved
Ibritumomab tiuxetan	Zevalin	CD20	Mouse (^{90}Y-labeled)	Non-hodgkin lymphoma	2002	2008
Alemutuzumab	Campath/MabCampath	CD52	Humanized	Chronic lymphocytic leukemia	2001	Non-approved
Gemtuzumab azogamicin	Myotarg	CD33	Humanized (calicheamicin-conjugate)	Acute myeloid leukemia	2000	2005
Trastuzumab	Herceptin	HER2	Humanized	Metastatic breast cancer	1998	2001
Rituximab	Rituxan/MabThera	CD20	Chimeric	Non-hodgkin lymphoma	1997	2001

3. Chapter I: Characterization of a variety of neutralizing anti-HB-EGF monoclonal antibodies by different immunization methods

3.1. Introduction

The development of neutralizing anti-HB-EGF mAbs with various biochemical or biological profiles is helpful for the advancement of HB-EGF research. In addition, more potent neutralizing anti-HB-EGF mAbs might expedite progress in the clinical research of HB-EGF. In addition, if the neutralizing anti-HB-EGF mAbs are cross-reactive to mouse HB-EGF, they could be useful for the evaluation of its anti-tumor activity as well as adverse events in mouse models of cancer.

Previous studies have shown that the same immunogen can elicit different antibody responses in different mouse strains (Stollar et al, 1973; Hoffenbach et al, 1985; Kasai et al, 1987) and different forms of the antigen can also alter antibody responses (Baraldo et al, 2004; Defendini et al, 1990; Karle et al, 2003). However, the antibody responses were tested with antisera in these studies, and little information is known about the effects of different mouse strains and immunogen types on the characteristics of individual mAbs.

In this study, I succeeded in generating a variety of neutralizing anti-HB-EGF mAbs by using different mouse strains as well as different preparations of the immunogen HB-EGF. Here, I discuss the characteristics of the mAbs and their correlation to the epitope bin and the immunization method.

3.2. Materials and Methods

3.2.1. Preparation of recombinant proteins

To prepare recombinant human, mouse, or rat sHB-EGF, the expression plasmids were constructed by cloning human, mouse, or rat sHB-EGF cDNA encoding amino acids 1–148 of

proHB-EGF into the pcDNA3.1 vector (Invitrogen). Because pro-peptide sequence of mouse and rat HB-EGF were not cleaved in human-derived 293F cells (Invitrogen), mouse and rat sHB-EGF cDNA encoding amino acids 1–62 was replaced with a corresponding sequence of human sHB-EGF cDNA. sHB-EGF expression plasmid was transfected into 293F cells by using 293fectin (Invitrogen) according to the supplier's recommendation. sHB-EGF was purified from the culture supernatant of the 293F cells with HiTrap Heparin HP (GE Healthcare), followed by a purification with a TSKgel CM-5PW column (Tosoh).

I also produced recombinant EGFR ectodomain fused to the human IgG_1 Fc region (EGFR-hFc). EGFR ectodomain cDNA (amino acids 1–645 of human EGFR) was inserted into pcDNA3.1 already containing the hFc gene. The expression plasmid was transfected into 293F cells as described above, and the recombinant EGFR-hFc protein was purified from the culture supernatant with rProteinA Sepharose FF (GE Healthcare), and subsequently with a Superdex 200 10/300 column (GE Healthcare).

3.2.2. Generation of anti-HB-EGF mAbs

BALB/c mice (8 weeks old, Japan Clea) were immunized subcutaneously with 10 μg of keyhole limpet hemocyanin-conjugated human sHB-EGF (KLH-conjugate) 3 times, and then 5 μg of KLH-conjugate or 5 μg of recombinant human sHB-EGF protein was intravenously injected as a final boost. I also performed co-immunization with the KLH-conjugate and human proHB-EGF-expressing cells. In brief, 1×10^7 proHB-EGF-expressing 293F cells were injected intraperitoneally 4 times on a weekly basis and at a final boost. KLH-conjugate was subcutaneously immunized at the first and fourth injections. CD1 mice (8 weeks old, Charles River) were immunized subcutaneously with 10 μg of KLH-conjugate or with 10 μg of BSA-conjugated sHB-EGF (BSA-conjugate) 3 times, followed by an intravenous final boost with 5 μg of the same antigen. C57BL

and C3H mice (8 weeks old, Japan Clea) were immunized with the KLH-conjugate alone in the same way. Five mice were used for each immunization. In all cases, other than the injection of the proHB-EGF-expressing cells, immunizations were carried out every 2 weeks. Three days after the final boost, the spleen was isolated from each mouse, and the splenocytes were fused with P3X63Ag8U.1 mouse myeloma cells (American Type Culture Collection) at a ratio of 1:1 by using the Hybrimune Electrofusion System (Cyto Pulse Sciences). The fused cells were seeded in a semi-solid selective culture media including hypoxanthine-aminopterin-thymidine, and the grown hybridoma clones were manually transferred to 96-well plates. Hybridomas secreting anti-HB-EGF mAbs were screened using FMAT. First, biotinylated sHB-EGF was prepared with Biotin Labeling Kit-NH_2 (Dojindo). Next, the biotinylated sHB-EGF was captured with streptavidin beads (Polysciences), and then incubated with hybridoma culture supernatant and Cy5-labeled anti-mouse IgG Fc antibody (Jackson ImmunoResearch Laboratories) in Can Get Signal solution I (Toyobo) in FMAT 384-well plates (Applied Biosystems) for 7 h at room temperature. The mAb bound to the beads was detected by measuring fluorescence intensity of Cy5 by 8200 Cellular Detection System (Applied Biosystems).

The animal studies were carried out in strict accordance with the recommendations in the Guide for the Care and Use of Laboratory Animals of the National Institutes of Health. The protocol was approved by the Committee on the Ethics of Animal Experiments of Takeda Pharmaceutical Company Limited (Permit Number: 2802).

3.2.3. mAb preparation

Hybridoma clones secreting anti-HB-EGF mAbs were expanded in a culture media containing 10% Ultra-low IgG fetal bovine serum (Invitrogen). Hybridoma culture supernatant was mixed with rProteinA Sepharose in MAPSII Binding Buffer (Bio-Rad) and incubated with end-over-end

rotation overnight at 4°C. After a washing step with PBS, the bound mAb was eluted with 0.1 M glycine-HCl (pH 3.0) containing 0.15 M NaCl and was immediately neutralized with 1 M Tris-HCl (pH 8.0). The buffer was then exchanged to PBS by ultrafiltration with Amicon Ultra-4 Centrifugal Filter (Millipore).

3.2.4. sHB-EGF/EGFR-hFc binding assay

The inhibitory activity of the hybridoma culture supernatant against the binding of sHB-EGF to EGFR-Fc was detected as described previously (Jin et al, 2009) .In brief, recombinant EGFR-hFc protein was captured by anti-human IgG Fc antibody (Jackson ImmunoResearch Laboratories) immobilized on 96-well plates. Hybridoma culture supernatant was incubated with 6 ng/mL biotinylated sHB-EGF and with 50 ng/mL sodium heparin on the plates for 1 hour at 37°C, followed by incubation with horseradish peroxidase-labeled (HRP-labeled) streptavidin (Jackson ImmunoResearch Laboratories) for 1 hour at 37°C. The plates were washed with PBS containing 0.05% Tween-20 after each incubation step. SureBlue TMB Microwell Substrate (KPL) was added to each well and incubated for 2 min. The reaction was stopped by 1 M H_2SO_4 and the absorbance at 450 nm was measured by a SPECTRA MAX plate reader (Molecular Devices). The inhibitory activity of hybridoma culture supernatant was determined by measuring the binding of sHB-EGF to EGFR-hFc. I selected 210 hybridoma clones, whose culture supernatant inhibited sHB-EGF binding to EGFR by more than 70% and confirmed their inhibitory activity by an EGFR phosphorylation assay.

3.2.5. EGFR phosphorylation assay

EGFR phosphorylation was detected as described previously (Giorgio et al, 2011). Briefly, SK-OV-3 ovarian cancer cells (American Type Tissue Collection) were seeded at 1×10^4 cells/well in

McCoy's 5A containing 10% serum in a 96-well plate for 1 day and were then serum-starved for 1 day. Hybridoma culture supernatant or various concentrations of purified mAb were pre-incubated with 10 ng/mL human sHB-EGF for 30 minutes at room temperature, and the reaction mixture was added to SK-OV-3 cells. After a 30-minute incubation period at 37°C, phosphorylated EGFR was detected by Human Phospho-EGFR DuoSet IC ELISA Kit (R&D Systems). Inhibitory activity of hybridoma culture supernatant was determined by measuring the phosphorylation of EGFR. All the culture supernatants tested inhibited the sHB-EGF-induced EGFR phosphorylation by more than 50%. To accurately measure the neutralizing activity of the mAb clones, I confirmed their neutralizing activity with protein A-purified antibodies. In the case of purified mAbs, the phosphorylation of EGFR in the presence of each purified mAb was calculated as the percentage of the maximum phosphorylation induced by sHB-EGF in the absence of mAb. The maximum phosphorylation was considered as 100% and basal phosphorylation in the absence of sHB-EGF and mAb as 0%. IC_{50} values of purified mAbs were calculated using Prism (GraphPad).

3.2.6. Colony formation assay

Colony formation assay was performed as described previously (Beerli et al, 1996). In brief, RMG-I ovarian cancer cells (Japanese Collection of Research Bioresources) were seeded at 750 cells/well in RPMI1640 containing 0.35% agarose, 10% serum, and 1 ng/mL human sHB-EGF in the presence of 10 μg/mL anti-HB-EGF mAb, into Hydrocell 96-well plates (CellSeed). After 1-week culture period, formed colonies were stained with 0.5 μM Calcein-AM (Invitrogen) and detected with an Acumen eX^3 instrument (TTP Labtech). The number of colonies per well in the presence of anti-HB-EGF mAb was calculated as the percentage of the number of colonies induced by sHB-EGF in the absence of anti-HB-EGF antibody. The number of colonies in the absence of

sHB-EGF and mAb was considered 0%. IC_{50} values of purified mAbs were calculated using a SAS preclinical package (SAS).

3.2.7. Species specificity test

ELISA was performed as described previously (Engvall et al, 1971). Human, mouse, or rat sHB-EGF was immobilized at a concentration of 1 μg/mL onto 96-well plates overnight at 4°C. Various concentrations of anti-HB-EGF mAb were then added to each well and incubated for 1 hour at 37°C, followed by incubation with HRP-labeled anti-mouse IgG antibody (Jackson ImmunoResearch Laboratories). The plates were washed with PBS containing 0.05% Tween-20 after each incubation step. SureBlue TMB Microwell Substrate was then added to the 96-well plates, and the reaction was stopped after 2 minutes by adding 1 M H_2SO_4. The mAb binding to sHB-EGF was detected by measuring the absorbance at 450 nm by a Spectra Max plate reader. EC_{50} values were calculated with Prism.

3.2.8. Flow cytometry

Human proHB-EGF expression plasmid was prepared by cloning the full-length human proHB-EGF cDNA into pEF1 vector (Invitrogen). 293F cells were transfected with the proHB-EGF expression plasmid as described above. Three days after transfection, cells were reacted with 2 μg/mL anti-HB-EGF mAb for 1 hour on ice, followed by incubation with 2 μg/mL Alexa488-labeled anti-mouse IgG (Invitrogen) for 1 hour on ice. Cells were washed with PBS after each antibody incubation step. The binding of anti-HB-EGF mAb was measured by detecting fluorescence intensity with a Cytomics FC 500 instrument (Beckman Coulter). The median fluorescence intensity (MFI) ratio was calculated by dividing the MFI of mAb-treated sample by that of a control mAb-treated sample. MFI ratio was then used as a measure of the binding activity

to proHB-EGF. The control sample was prepared by incubating cells with mouse IgG control (BD Pharmingen) instead of anti-HB-EGF mAb.

3.2.9. Epitope binning study

The epitope binning study was performed using the FMAT assay. Anti-HB-EGF mAbs were biotinylated with Biotin Labeling Kit-NH_2. In brief, polystyrene beads (Spherotech) were coated with human sHB-EGF and incubated with 0.1 μg/mL biotinylated anti-HB-EGF mAb, 5 μg/mL unlabeled anti-HB-EGF mAb, and 0.33 μg/mL streptavidin-Alexa Fluor 647 (Invitrogen) in Can Get Signal solution I in FMAT 384-well plates for 7 hours at room temperature. Biotinylated mAbs on the beads were detected by measuring Alexa Fluor 647 with 8200 Cellular Detection System. Inhibited binding of the biotinylated mAb to sHB-EGF by unlabeled mAb was calculated using the formula:

Binding inhibition (%) = $(1 - A/B) \times 100$

where A represents total fluorescence in the presence of unlabeled mAb and B represents total fluorescence in the absence of unlabeled mAb. Clustering analysis was performed with the percent inhibition of all combinations of mAb pairs by using Ward's methods with Euclidean distance. I first classified the mAbs into 3 epitope bins, namely, A, B, and C, which were distinguished by the hierarchical dendrogram and the color-coded map (Fig. 1-3). I then subdivided epitope bin A into A1, A2, A3, and A4, and epitope bin C into C1 and C2, based on visual inspection of the hierarchical dendrogram (Fig. 1-3).

3.3. Results

3.3.1. Generation of anti-HB-EGF mAbs

To maximize the chances of obtaining neutralizing anti-HB-EGF mAbs, I tested various immunization methods and screened hybridomas in a high-throughput manner. I used mice with 4 different genetic backgrounds (BALB/c, C57BL, C3H, and CD1) as hosts. Carrier protein-conjugated forms of HB-EGF were used as immunogens through all the immunizations to enhance the antibody response. The four mouse strains were immunized subcutaneously with KLH-conjugated sHB-EGF (KLH-conjugate). In addition, BSA-conjugated sHB-EGF (BSA-conjugate) was tested in CD1 mice (BSA/CD1), and 2 other immunizations were tested in BALB/c mice: KLH-conjugate immunization plus a final boost of sHB-EGF (KLH/sHB-EGF/BALB/c), and co-immunization with KLH-conjugate plus proHB-EGF-expressing 293F cells (KLH/cell/BALB/c). I used an electrofusion system for high-efficiency hybridoma production, and subsequent fluorometric microvolume assay technology (FMAT) assay to screen anti-HB-EGF mAb-secreting hybridoma clones with hybridoma culture supernatant as the antibody source. Using this approach, I identified 3,337 HB-EGF-specific mAb-secreting hybridoma clones. The rates of obtaining HB-EGF-specific mAb-secreting hybridoma clones for each immunization are summarized in Table 1-1.

3.3.2. Neutralizing activity of anti-HB-EGF mAbs

Hybridoma clones secreting neutralizing anti-HB-EGF mAbs were then screened by 2 assays. I selected 210 hybridoma clones, whose culture supernatant inhibited sHB-EGF binding to EGFR by more than 70%. The culture supernatant was then applied to EGFR phosphorylation assay using SK-OV-3 ovarian cancer cells, and they all inhibited the sHB-EGF-induced EGFR phosphorylation by more than 50% (Table 1-1). Because antibody concentrations in culture supernatants differed for each hybridoma clone, I then tested their neutralizing activity in the EGFR phosphorylation assay by using protein A-purified mAbs and confirmed that they possessed a neutralizing activity against sHB-EGF-induced EGFR phosphorylation. I found that they neutralized the sHB-EGF-induced

EGFR phosphorylation with a broad range of IC_{50} values, ranging from 5.5×10^{-11} M to 7.6×10^{-7} M ('All' column in Fig. 1-1A). I further tested the effect of the neutralizing mAbs against sHB-EGF-dependent cancer cell growth by measuring colony formation of RMG-I ovarian cancer cells. Eighty-nine anti-HB-EGF mAbs, which possessed IC_{50} values of less than 5×10^{-9} M in the EGFR phosphorylation assay, were applied to the colony formation assay ('All' column in Fig. 1-1B). The IC_{50} values of neutralizing anti-HB-EGF mAbs in the EGFR phosphorylation and colony formation assays were positively correlated (Fig. 1-1C), suggesting that the inhibition of sHB-EGF-induced EGFR phosphorylation leads to suppression of the sHB-EGF-dependent cancer cell growth.

3.3.3. Binding activities of neutralizing anti-HB-EGF mAbs to sHB-EGF and proHB-EGF

As a method to characterize the neutralizing mAbs, I evaluated the binding activities of the mAbs to human, mouse, and rat sHB-EGF by ELISA and to human proHB-EGF by flow cytometry. The EC_{50} values to human sHB-EGF ranged from 1.3×10^{-11} M to 7.8×10^{-10} M ('All' column in Fig. 1-2A). I found that the range of EC_{50} values to mouse and rat sHB-EGF was much broader (1.6×10^{-11} M to 3.0×10^{-6} M and 1.4×10^{-11} M to 1.0×10^{-7} M, respectively) than that to human sHB-EGF ('All' column in Figs. 1-2B, 1-2C). Likewise, the neutralizing anti-HB-EGF mAbs showed a diverse binding activity to proHB-EGF. Some mAbs showed a strong binding activity to proHB-EGF ('All' column in Fig. 1-2D).

3.3.4. Epitope binning study of neutralizing anti-HB-EGF mAbs

On the basis of the findings described above, I hypothesized that neutralizing anti-HB-EGF mAbs might recognize different epitopes. I carried out an epitope binning study by measuring their competitive binding to human sHB-EGF in the FMAT assay. Of the 210 neutralizing mAbs, I used 156 that provided a sufficient amount for this assay from a small-scale hybridoma culture. At first,

129 mAbs were tested, and of those, 119 mAbs were classified into 3 epitope bins, designated A, B, and C, which were distinguished by the hierarchical dendrogram and the color-coded map (Fig. 1-3). The remaining 10 mAbs were not categorized into any of these epitope bins. Because mAbs in epitope bins A and C showed heterogenous properties regarding neutralizing and/or binding activities (data not shown), I decided to subdivide these bins. Therefore, based on the visual inspection of the hierarchical dendrogram in Fig. 1-3, I further subdivided epitope bin A into A1, A2, A3, and A4, and epitope bin C into C1 and C2. Another 27 mAbs were additionally purified and sorted into the epitope bins by performing the competitive binding assay with several representative mAbs from each epitope bin. Finally, 146 neutralizing anti-HB-EGF mAbs were classified into epitope bins A1 (n = 19), A2 (n = 12), A3 (n = 8), A4 (n = 16), B (n = 28), C1 (n = 29), and C2 (n = 34).

The epitope binning study allowed me to identify characteristics of the antibodies that were unique to each epitope bin. The mAbs in epitope bins A3, C1, and C2 exhibited potent neutralizing activities, whereas those in epitope bins A1 and B had weaker activity (Figs. 1-1A, 1-1B). The mAbs in epitope bins C1 and C2 were highly cross-reactive to mouse and rat sHB-EGF, while the mAbs in epitope bin B were less cross-reactive to mouse and rat sHB-EGF (Figs. 1-2B, 1-2C). The mAbs in epitope bin A3 cross-reacted selectively to mouse HB-EGF, while those in epitope bins A1 and A4 cross-reacted specifically to rat HB-EGF. The mAbs in epitope bin A2 showed a profile similar to those in epitope bin A4 in terms of neutralizing and binding activities to sHB-EGF (Figs. 1-1A, 1-1B, 1-2A–1-2C). However, epitope bin A2 consisted of mAbs with a weaker binding activity to proHB-EGF than those in epitope bin A4 (Fig. 1-2D). The mAbs in epitope bin B demonstrated the strongest binding activity to proHB-EGF, as well as to sHB-EGF (Figs. 1-2A, 1-2D). Meanwhile, the mAbs in epitope bin C1 and C2 showed a weak binding activity to proHB-EGF instead of their binding activities to human sHB-EGF comparable to the mAbs of other

epitope bins. These epitope bin-specific characteristics indicated that the epitope bins of the mAbs were properly determined.

3.3.5. Unique epitope bin population by mouse strain and immunogen type

I analyzed each epitope bin population by immunization method to determine whether mouse strain or immunogen type affected the antibody characteristics. Of the 146 antibodies classified in the epitope binning study, I excluded the mAbs from C57BL and C3H mice because both strains produced very few neutralizing mAbs (Table 1-1). As shown in Fig. 1-4, I found that epitope bin populations were strikingly different among the immunization methods. These results clearly indicated that mouse strain and immunogen type can both affect antibody functionality.

3.4. Discussion

Previously reported neutralizing anti-HB-EGF mAbs, DE10 and KM3566, were generated using the carrier-free recombinant sHB-EGF protein as the immunogen (Khong et al, 2000; Miyamoto et al, 2011). In these studies, hybridoma clones were generated by a conventional polyethylene glycol fusion method, and HB-EGF mAb-secreting clones were screened by ELISA. Antigen-null mice are useful tools while obtaining antibodies against an autoantigen because they do not develop immune tolerance to the antigen (Amagai et al, 2007). Because of the high homology between the amino acid sequences of human and mouse HB-EGF, HB-EGF-null mice were used for the generation of anti-HB-EGF mAbs (Khong et al, 2000; Miyamoto et al, 2011). However, the reported number of anti-HB-EGF mAbs from the antigen-null mouse was limited. Herein, I succeeded in identifying 3,337 hybridoma clones secreting HB-EGF-specific antibody, including 210 neutralizing mAb clones from wild-type mice. I leveraged multiple approaches to efficiently obtain neutralizing anti-HB-EGF mAbs. I immunized different mouse strains with different forms of HB-EGF as the

immunogen. I used KLH- or BSA-conjugated forms of sHB-EGF for an enhanced immune response. An electrofusion system and a homogeneous high-throughput screening assay enabled me to obtain and evaluate a large number of hybridoma clones. I speculate that the combination of these approaches contributed to the identification of the unprecedented number of the neutralizing mAbs.

A subset of the mAbs obtained here showed a previously unreported cross-reactivity to mouse HB-EGF. The mAbs in epitope bins C1 and C2 showed a strong binding activity to mouse and rat sHB-EGF (Fig. 1-2B, 2C). Their neutralizing activity was evaluated only against human sHB-EGF (Fig. 1-1A); however, these antibodies are likely to be effective neutralizers against mouse and rat sHB-EGF, making them useful tools for validating in vivo sHB-EGF functions caused by blocking HB-EGF/EGFR signaling in these animals. I also found that the mAbs in epitope bin C2 showed a potent neutralizing activity, with IC_{50} values of less than 1×10^{-10} M in a colony formation assay (Fig. 1-1B). Some mAbs completely inhibited 1 ng/mL of sHB-EGF-induced colony formation at a dose as low as 0.1 nM (data not shown). Although it is difficult to directly compare the neutralizing activities in different cell-based assays, the neutralizing activities of the mAbs obtained here seemed to be more potent than those of previously reported mAbs (Khong et al, 2000; Miyamoto et al, 2011). In addition, the neutralizing activity of anti-HB-EGF mAbs in the EGFR phosphorylation assay was well correlated with that in the colony formation assay (Fig. 1-1C). This finding strongly suggests that blockage of sHB-EGF/EGFR signaling is a promising therapy for treating sHB-EGF-dependent cancers.

As shown in Table 1-1, KLH-conjugate immunizations of different mouse strains produced anti-HB-EGF mAb-positive and neutralizing mAb-positive hybridoma clones at different rates. CD1 mice produced neutralizing anti-HB-EGF mAbs at a higher positive rate than did the other mouse strains (0.72% vs. 0.11%, 0.06%, and 0.08%), which probably reflects the highest positive rate of anti-HB-EGF mAbs in CD1 mice. In contrast, the positive rate of neutralizing mAbs in C3H mice

was only 0.08%, although its positive rate was as high as 8.0% for HB-EGF-specific mAbs. Thus, the production rates for HB-EGF-specific and neutralizing mAbs were mouse strain-dependent. In the BALB/c immunizations, sHB-EGF injection at the final boost (KLH/sHB-EGF/BALB/c) resulted in a higher positive rate for neutralizing mAbs than KLH-conjugate (KLH/BALB/c) (0.91% vs. 0.11%), although the positive rates for anti-HB-EGF mAbs were similar (7.8% vs. 5.7%). In the CD1 immunizations, BSA-conjugate gave a higher positive rate for neutralizing mAbs than did KLH-conjugate (1.97% vs. 0.72%), although the positive rates for anti-HB-EGF mAbs were similar (11.6% vs. 13.2%). These results suggested that the type of immunogen also affected the production rates for anti-HB-EGF mAbs and neutralizing mAbs.

The population of epitope bins was markedly different between mouse strains and immunogen types. The mAbs in epitope bin A2 were obtained only from BSA/CD1 and those in epitope bin A3 were obtained only from KLH/BALB/c and KLH/sHB-EGF/BALB/c. In addition, the mAbs in epitope bins A4 and B were obtained primarily from CD1 and BALB/c mice, respectively. Although further analysis is required to clarify the mechanism behind this phenomenon, these results demonstrate that immunization methods using different mouse strains and immunogen types produce neutralizing anti-HB-EGF mAbs with various features.

Considering the variation of mAb characteristics, I classified the neutralizing antibodies by using an epitope binning study. To date, multiple methods have been established for epitope binning (Ladner, 2007). Although competitive assays using ELISA or Biacore are convenient, these methods are not practical for epitope binning of large number of mAbs. Therefore, I chose to use the FMAT assay (Swartzman et al, 1999), which enabled me to classify antibodies in a high-throughput manner and gave me several insights for HB-EGF studies. Because I used only neutralizing mAbs in the FMAT assay, I expected that all the mAbs could competitively bind to sHB-EGF by recognizing an epitope in sHB-EGF that is critical for EGFR binding. However, the

mAbs in epitope bin B did not competitively bind to sHB-EGF with those in epitope bins A and C (Fig. 1-3), suggesting that the mAbs in epitope bin B and those in epitope bins A and C recognize different epitopes and inhibit sHB-EGF binding to EGFR by different approaches. In fact, previous studies have demonstrated that multiple sites are involved in the interaction between EGF and EGFR. Two domains (I and III) in the extracellular portion of EGFR have been shown to play important roles in ligand binding (Defize et al, 1989; Lax et al, 1989; Lax et al, 1991). Crystal structure analysis has proposed that the interface between EGF and EGFR consists of 3 sites (Ogiso et al, 2002). One of them is located in domain I and the other 2 in domain III. Binding studies using sHB-EGF and proHB-EGF also provided interesting information. The mAbs in epitope bins C1 and C2 showed a weaker binding activity to proHB-EGF but a stronger binding activity to sHB-EGF compared to the mAbs in epitope bins A2, A3, and A4 (Figs. 1-2A, 1-2D). This result is likely due to the different conformations of sHB-EGF and the ectodomain of proHB-EGF.

In this study, I obtained a number of neutralizing anti-HB-EGF mAbs by using different immunization methods and several high-throughput approaches. I found that the neutralizing activities of these mAbs, as well as their binding features, were defined by the epitope bin. Some of the tested neutralizing mAbs showed a potent anti-cell proliferation activity against cancer cells, suggesting that they may be effective anti-cancer agents. My findings further provide evidence that the immunization method has an effect on the production rates of mAbs and their characteristics.

3.5. Figures

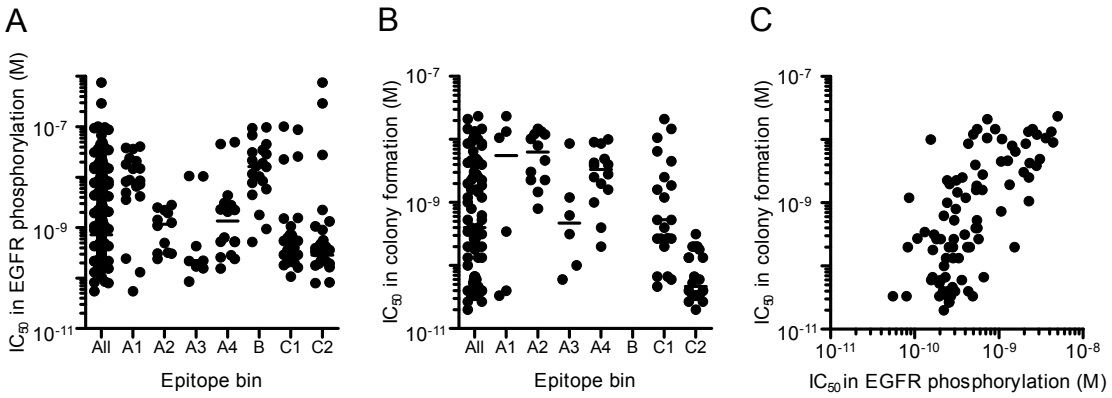

Fig. 1-1. Neutralizing activity of anti-HB-EGF mAbs against sHB-EGF functions

(A) Neutralizing activity of anti-HB-EGF mAbs against sHB-EGF-induced EGFR phosphorylation in SK-OV-3 cells. The plots represent the IC_{50} values of mAbs used in the epitope binning study (Fig. 1-3). The horizontal line indicates the median IC_{50} value. (B) Neutralizing activity of anti-HB-EGF mAbs against sHB-EGF-induced colony formation in RMG-I cells. I used the 89 mAbs with IC_{50} values of less than 5×10^{-9} M in the EGFR phosphorylation assay, and this plot represents the IC_{50} values of the 83 mAbs with IC_{50} values of less than 1×10^{-7} M. The horizontal line indicates the median IC_{50} value. (C) Correlation of neutralizing activities of anti-HB-EGF mAbs against sHB-EGF-induced EGFR phosphorylation and colony formation. Each dot represents the IC_{50} values of 83 mAbs with an IC_{50} value of less than 1×10^{-7} M in the colony formation assay (Fig. 1B). The data were analyzed by the Spearman's test (two-tailed). The Spearman correlation was $r = 0.6730$ ($P < 0.0001$).

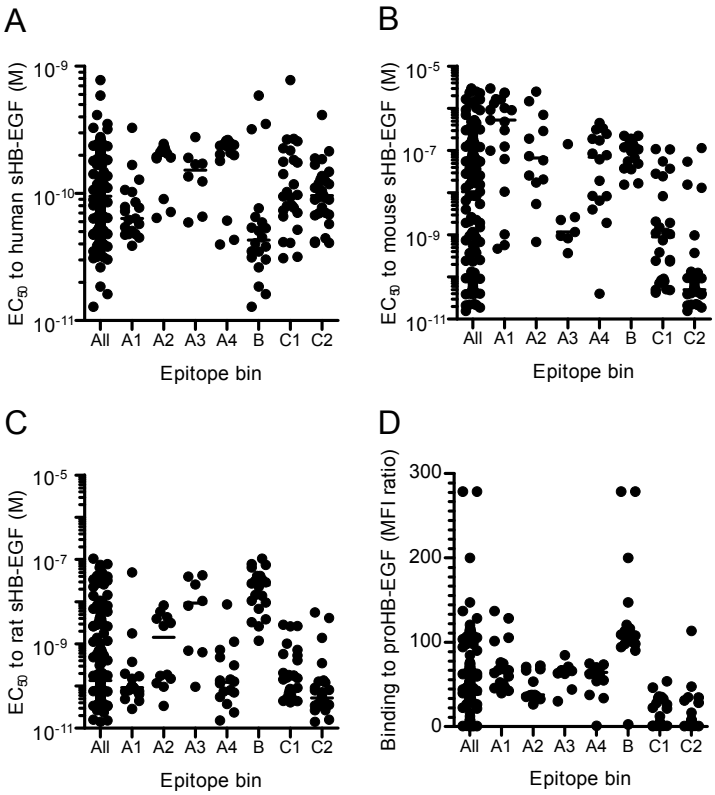

Fig. 1-2. Binding activities of neutralizing anti-HB-EGF mAbs to HB-EGF

Binding activity of anti-HB-EGF mAbs to (A) human sHB-EGF, (B) mouse HB-EGF, and (C) rat sHB-EGF. The binding activities were determined by ELISA. The plots represent EC_{50} values of mAbs used in the epitope binning study (Fig. 1-3). The horizontal line indicates the median EC_{50} value. (D) Binding activity of anti-HB-EGF mAbs to proHB-EGF was measured by flow cytometry. The plots represent median fluorescence intensity (MFI) ratio of the mAbs used in the epitope binning study (Fig. 1-3). The MFI ratio of anti-HB-EGF mAb to a control sample was used as the measure of binding activity to proHB-EGF. The horizontal line indicates the median MFI ratio.

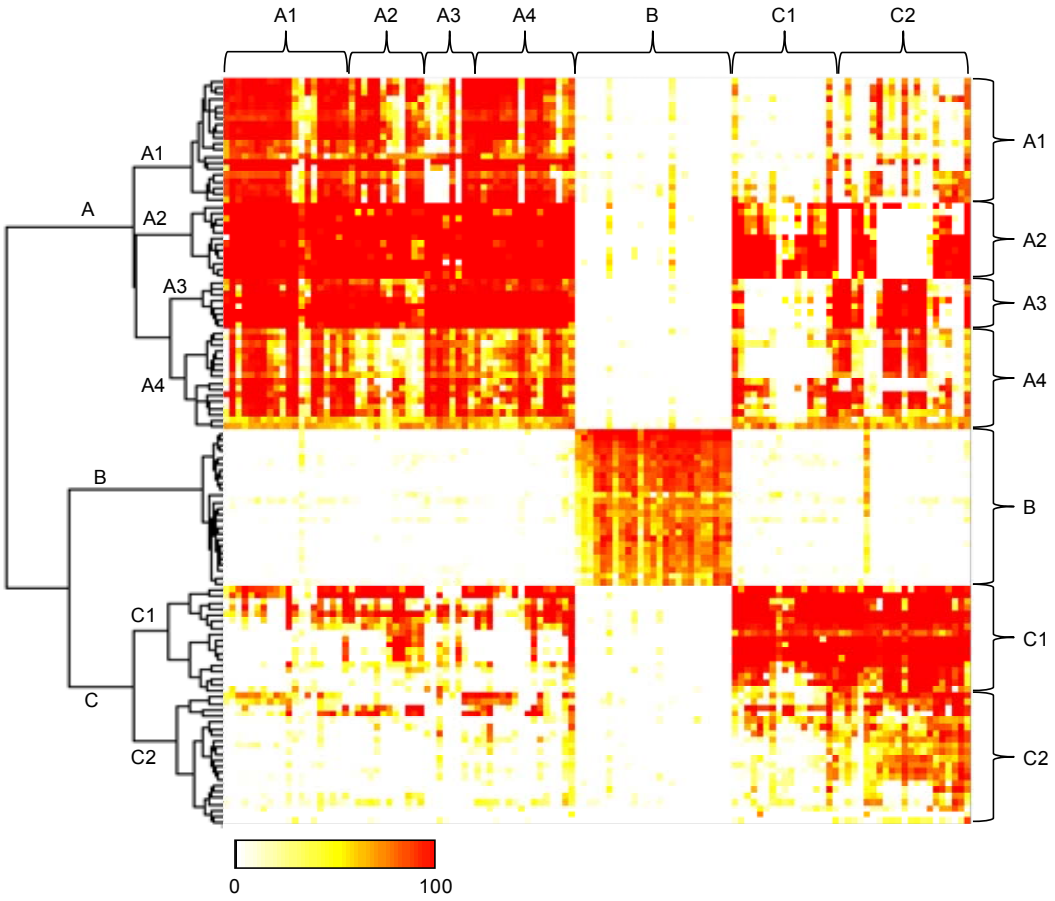

Fig. 1-3. Epitope binning study of anti-HB-EGF mAbs

The competitive binding of all mAb pairs to sHB-EGF was measured in the FMAT assay. Binding of biotinylated anti-HB-EGF antibody to sHB-EGF was detected in the presence of a label-free anti-HB-EGF antibody. Horizontal and vertical axes indicate unlabeled and biotinylated mAbs, respectively. Data were analyzed by Ward's method with Euclidean distance. Dendrogram on the left axis represents the similarity of each mAb in the competitive binding pattern to sHB-EGF. The color scale from 0 to 100 shows the competitive binding of the 2 mAbs.

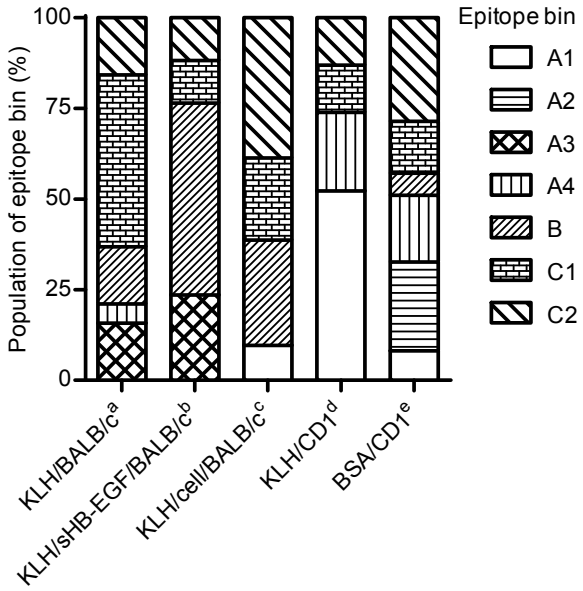

Fig. 1-4. Difference of epitope bin population by mouse strain and immunogen type

Epitope bin populations were analyzed based on the immunization method used to generate the mAbs. [a-c]BALB/c immunization with [a]KLH-conjugated sHB-EGF; [b]the KLH-conjugate and a final boost of sHB-EGF; [c]co-immunization of the KLH-conjugate and proHB-EGF-expressing cells; [d,e]CD1 immunization with [d]the KLH-conjugate; [e]BSA-conjugated sHB-EGF.

3.6. Table

Table 1-1. Summary of anti-HB-EGF mAb generation by mouse strain and immunogen.

Immunization	Total	HB-EGF binder	Neutralizing mAb
KLH/BALB/c[a]	17,952	1,018 (5.7%)	19 (0.11%)
KLH/sHB-EGF/BALB/c[b]	2,640	207 (7.8%)	24 (0.91%)
KLH/cell/BALB/c[c]	5,280	589 (11.2%)	33 (0.63%)
KLH/C57BL[d]	1,670	30 (1.8%)	1 (0.06%)
KLH/C3H[e]	2,640	210 (8.0%)	2 (0.08%)
KLH/CD1[f]	5,720	754 (13.2%)	41 (0.72%)
BSA/CD1[g]	4,576	529 (11.6%)	90 (1.97%)
Total	40,478	3,337 (8.2%)	210 (0.52%)

The number of hybridoma clones of mAb for each immunization is shown. The production rates are noted in parentheses. [a-c]BALB/c immunization with [a]KLH-conjugated sHB-EGF; [b]the KLH-conjugate and a final boost of sHB-EGF; [c]co-immunization of the KLH-conjugate and proHB-EGF-expressing cells; [d]C57BL immunization with the KLH-conjugate; [e]C3H immunization with the KLH-conjugate; [f,g]CD1 immunization with [f]the KLH-conjugate; [g]BSA-conjugated sHB-EGF

4. Chapter II: An anti-HB-EGF monoclonal antibody inhibits cancer cell proliferation and multiple angiogenic activities of HB-EGF: a potential anti-cancer therapeutic agent

4.1. Introduction

Recent studies have revealed a variety of physiological and pathological functions of HB-EGF (Iwamoto et al, 2003; Jackson et al, 2003; Mine et al, 2005; Shirakata et al, 2005; Das et al, 1994; Raab et al, 1996; Asakura et al, 2002; Powell et al, 1993; Miyagawa et al, 1995; Peoples et al, 1995; Fu et al, 1999). More recently, increasing evidence has demonstrated that HB-EGF is over-expressed in multiple types of cancer (Kobrin et al, 1994; Naef et al, 1996; Mishima et al, 1998; Thøgersen et al, 2001; Miyamoto et al, 2004) and the over-expression has been shown to correlate with poor prognosis (Thøgersen et al, 2001; Tanaka et al, 2005; Hoffmann et al, 2009). Due to these findings, anti-HB-EGF agents have been actively pursued for therapeutic applications. An HB-EGF inhibitor of the diphtheria toxin mutant, CRM197, is in phase I clinical development for the treatment of advanced ovarian cancers (Tsujioka et al, 2011). Anti-HB-EGF antibody KHK2866, a humanized version of KM3566, is currently in phase I clinical trials for solid cancers (Miyamoto et al, 2011). In this study, I report the characterization of anti-HB-EGF mAb, Y-142, by analyzing its functional activities and binding epitope. The potent biological activity of Y-142 was compared with those of the HB-EGF inhibitor CRM197, the anti-VEGF antibody bevacizumab, and the anti-EGFR antibody cetuximab.

4.2. Materials and Methods

4.2.1. Materials

Human, mouse, and rat sHB-EGF, and EGFR-hFc were prepared as described in the Chapter I. EGFR ligands, anti-EGFR, anti-ERBB4, and anti-HB-EGF polyclonal antibodies, FITC-labeled

anti-CD31, anti-vascular endothelial growth factor (VEGF), biotinylated anti-VEGF, horseradish peroxidase (HRP)-labeled anti-phosphotyrosine antibodies were purchased from R&D Systems. Anti-phosphorylated ERK1/2 and anti-phosphorylated AKT antibodies were purchased from Cell Signaling Technology. Alexa488-labeled anti-rabbit IgG antibody was obtained from Invitrogen. Mouse control IgG, HRP-labeled streptavidin, HRP-labeled anti-mouse, anti-goat IgG antibodies, Cy5-labeled goat anti-mouse IgG Fcγ specific antibody, and anti-human IgG Fc antibody were purchased from Jackson ImmunoResearch Laboratories. Cetuximab and CRM197 were from ImClone and Sigma Aldrich, respectively. Sulfo-tagged anti-mouse antibody and streptavidin were purchased from Meso Scale Discovery. Sulfo-tagged anti-phosphotyrosine antibody was prepared by labeling anti-phosphotyrosine antibody (Millipore) with MSD Sulfo Tag reagent (Meso Scale Discovery).

4.2.2. Antibody preparation

Anti-HB-EGF mAb Y-142 was generated through the KLH/cell/BALB/c immunization campaign in the Chapter I. Y-142 was purified from its hybridoma culture supernatant with rProteinA Sepharose (GE Healthcare).

4.2.3. Cell culture

Ovarian cancer cell line SK-OV-3, breast cancer cell line T47D, and colorectal cancer cell line SW480 cells were purchased from American Type Culture Collection and maintained with McCoy's 5A, RPMI1640, and Leibovit'z L-15 media supplemented with 10% serum, respectively. Normal human dermal fibroblasts (NHDF) and human umbilical vein endothelial cells (HUVEC) were purchased from Lonza and maintained with FGM-2 and EGM-2 kits (Lonza), respectively.

4.2.4. Binding specificity test

Human, mouse, or rat sHB-EGF prepared in the Chapter I was immobilized on an MSD 384-well plate (Meso Scale Discovery). Non-specific binding was blocked with PBS containing 1% BSA. Y-142 was then added to each well and incubated for 1 hour at room temperature. Sulfo-tagged anti-mouse IgG antibody was added and incubated for 1 hour at room temperature. MSD Read Buffer T (Meso Scale Discovery) was added and chemiluminescence was measured with a Sector Imager 6000 (Meso Scale Discovery). EGFR ligand specificity of Y-142 was determined by incubating various concentrations of Y-142 for 1 hour in an EGFR ligand-immobilized 384-well plate followed by incubating HRP-labeled anti-mouse IgG antibody for 1 hour at room temperature. TMB Peroxidase EIA Substrate (BIORAD) was then added to the 384-well plate and the reaction was stopped after 15 minutes by adding 1N H_2SO_4. Antibody binding to EGFR ligand was then detected by measuring the absorbance at 450 nm using a SPECTRA MAX instrument (Molecular Devices).

4.2.5. Biophysical measurement of K_D

KinExA experiments were performed using a KinExA 3200 instrument (Sapidyne) at 22°C. sHB-EGF was reconstituted into PBS. sHB-EGF and Y-142 samples were prepared in vacuum-degassed HBS-P buffer (10 mM HEPES, 150 mM NaCl, and 0.005% Tween-20) from GE Healthcare with filtered 0.01% BSA and 0.02% sodium azide. For the detection antibody, Cy5-labeled goat anti-mouse IgG, Fcγ specific was used. For each KinExA experiment, 20 μg of sHB-EGF was diluted into 1 mL of 50 mM sodium carbonate (pH 9.2) which was added directly to 50 mg of azlactone beads (UltraLink Biosupport, Thermo Scientific), and rocked overnight at 4°C. After rocking, the beads were rinsed once with 1 M Tris-HCl (pH 8.5) containing 1% BSA and rocked for 1 hour at room temperature in the same buffer. Coupled beads were added to the bead

reservoir in the KinExA instrument and diluted to 30 mL with HBS-N (10 mM HEPES and 150 mM NaCl, GE Healthcare) containing 0.02% sodium azide which was also the running buffer for the KinExA instrument. All antigen-coupled beads were used immediately after preparation.

For K_D-controlled experiments, 12 concentrations of sHB-EGF at a range of 4.04 fM–207 pM were equilibrated at room temperature for 72 hours with 1.03 pM Y-142 binding sites. The volume flowed through the bead pack for each sample in the K_D-controlled titration was 23 mL at a flow rate of 0.25 mL/min. For antibody-controlled experiments, 12 concentrations of sHB-EGF at a range of 4.67 fM–239 pM were equilibrated at room temperature for 24 hours with 35.6 pM Y-142 binding sites. The volume flowed through the bead pack for each sample in the antibody-controlled titration was 3 mL at a flow rate of 0.25 mL/min. K_D-controlled data and antibody-controlled data were simultaneously fit with a dual-curve positive cooperativity model using KinExA software (Version 3.13, Sapidyne).

4.2.6. sHB-EGF binding inhibition to EGFR

Anti-human IgG Fc antibody was immobilized onto a 96-well plate overnight at 4°C. After the plates were blocked with PBS containing 20% Immunoblock (Dainippon Sumitomo Pharma), EGFR-hFc was added and reacted for 1 hour at room temperature. Y-142 was then added and incubated at a concentration of 6.7 nM in the presence of 0.63 nM biotinylated sHB-EGF and 25 ng/mL of sodium heparin for 1 hour at 37°C, followed by adding HRP-labeled streptavidin and incubating for 1 hour at 37°C. SureBlue TMB Microwell Substrate was then added and the reaction was stopped after 15 minutes by adding 1N H_2SO_4. Absorbance at 450 nm was measured using SPECTRA MAX. The binding of sHB-EGF to EGFR-hFc in the presence of Y-142 was calculated as the percentage of the maximum binding that was measured of sHB-EGF binding to EGFR-hFc in

the absence of Y-142. The minimum binding control signal was detected in the absence of sHB-EGF and Y-142.

4.2.7. EGFR phosphorylation assay

In the EGFR phosphorylation assay, SK-OV-3 cells were plated at 1×10^4 cells/well in McCoy's 5A containing 1% serum into a 96-well plate. After a 1-day culture, cells were incubated with 10 nM sHB-EGF or ARG together with Y-142 for 30 minutes at 37°C. Cells were lysed in Cell lysis buffer (Cell Signaling Technology) with a protease inhibitor cocktail (Roche Applied Science) and a phosphatase inhibitor cocktail (Sigma Aldrich). Cell lysates were then incubated in an anti-EGFR polyclonal antibody-coated plate for 1 hour at room temperature, followed by an incubation with HRP-labeled anti-phosphotyrosine antibody for 1 hour at room temperature. After an incubation with TMB Peroxidase EIA Substrate for 15 minutes, the reaction was stopped by adding 1N H_2SO_4. EGFR phosphorylation was detected by measuring the absorbance at 450 nm using an Envision plate reader (Perkin Elmer). EGFR phosphorylation in the presence of Y-142 was calculated as the percentage of the maximum EGFR phosphorylation measured in the absence of Y-142. The minimum phosphorylation control was signal detected in the absence of sHB-EGF and Y-142.

4.2.8. ERBB4 phosphorylation assay

T47D cells were seeded at 2.5×10^4 cells/well into a 96-well plate with RPMI1640 containing 10% serum and cultured for 1 day. After being plated, the cells were serum-starved for 1 day and then treated with 10 nM sHB-EGF together with various concentrations of Y-142 for 30 minutes at 37°C. Cell lysates were prepared as in the EGFR phosphorylation assay described above and then incubated in an anti-ERBB4 polyclonal antibody-coated MSD 384-well plate for 1 hour at room temperature. To detect receptor phosphorylation, sulfo-tagged anti-phosphotyrosine antibody was

incubated for 1 hour at room temperature. MSD Read Buffer T was then added as a substrate and chemiluminescence was measured with a Sector Imager 6000. ERBB4 phosphorylation in the presence of Y-142 was calculated as the percentage of the maximum ERBB4 phosphorylation measured in the absence of Y-142. The minimum phosphorylation control was signal detected in the absence of sHB-EGF and Y-142.

4.2.9. ERK1/2 and AKT phosphorylation assays

For the detection of the phosphorylation of ERK1/2 or AKT, SK-OV-3 cells were plated as described above. The plated cells were then fixed with 3.8% paraformaldehyde for 1 hour at room temperature, washed with PBS containing 0.05% Tween-20 (wash buffer) three times, and blocked with wash buffer containing 1% BSA, 2% goat serum, 0.3 % cold fish skin gelatin, 0.1% TritonX-100, and 0.05% sodium azide. Cells were then incubated with anti-phosphorylated ERK1/2 antibody or anti-phosphorylated AKT antibody overnight at 4°C, washed three-times with wash buffer, and incubated with Alexa488-labeled anti-rabbit IgG antibody for 2 hours at room temperature. In order to measure total protein in each well, cells were incubated with Alexa647 succinimidyl ester (Invitrogen) in wash buffer. Phosphorylated ERK1/2 and AKT as well as total protein were detected with an ImageXpress Micro instrument (Molecular Devices). The levels of phosphorylation for ERK1/2 and AKT were normalized with the total amount of protein in each well. Phosphorylation levels were calculated as the percentage of the maximum phosphorylation levels detected in the absence of Y-142. The minimum control signal was detected in the absence of sHB-EGF and Y-142.

4.2.10. Cell proliferation assay

SK-OV-3 cells were added at 3×10^3 cells/well in McCoy's 5A containing 1% serum and HUVEC were added at the same density in EBM-2 (Lonza) containing 5% charcoal-stripped serum (Hyclone) to 96-well plates and cultured for 1 day. Cells were further cultured in the presence of 10 nM sHB-EGF with various concentrations of Y-142, cetuximab, or CRM197 for 3 days. Cell proliferation was detected with CellTiter-Glo (Promega) using Envision. Cell proliferation of SK-OV-3 cells and HUVEC calculated as the percentage of the proliferation level measured in the absence of sHB-EGF, Y-142, cetuximab, and CRM197.

4.2.11. Tube formation assay

NHDF were seeded at 1×10^4 cells/well with an FGM-2 kit into a clear-bottom black 96-well plate and cultured for 3 days. One thousand HUVEC were seeded onto the monolayer of NHDF with EBM-2 media containing 2% charcoal-stripped serum in the presence of 50 nM sHB-EGF with various concentrations of Y-142, cetuximab, or CRM197. After a 4-day incubation period, HUVEC were stained with FITC-labeled anti-CD31 antibody. CD31-positive cells were detected using an Acumen ex3 instrument (TTP Labtech). Tube formation in the presence of Y-142, cetuximab, or CRM197 was calculated as the percentage of the tube formation detected without the presence of sHB-EGF, Y-142, cetuximab, and CRM197.

4.2.12. VEGF measurement

Anti-VEGF mAb was immobilized in an MSD high binding plate overnight at 4°C. Each well was then blocked with PBS containing 1% BSA for 1 hour at room temperature. Culture supernatant from the tube formation assay described above was then added into each well and the plate was incubated for 1 hour at room temperature. Biotinylated anti-VEGF antibody was then reacted for 1 hour at room temperature followed by an incubation with sulfo-tagged streptavidin for

1 hour at room temperature. Read T Buffer was then added as a substrate and chemiluminescence was measured with a Sector Imager 6000 instrument. The VEGF amount in the culture supernatant was calculated as a percentage of the VEGF amount in the absence of sHB-EGF, Y-142, cetuximab, and CRM197.

4.2.13. Western blot

sHB-EGF was boiled in laemmli sample buffer (BIORAD) with or without 10 mM dithiothreitol for 5 minutes at 95°C. Various amounts of the non-reduced or reduced sHB-EGF were then subjected to sodium dodecyl sulfate-polyacrylamide gel electrophoresis. sHB-EGF was detected with either 3 μg/mL of Y-142 or 3 μg/mL of anti-HB-EGF polyclonal antibody as the primary antibody, followed by incubation with HRP-labeled anti-mouse IgG antibody or HRP-labeled anti-goat IgG antibody, respectively, as the secondary antibody.

4.2.14. Epitope mapping

Expression plasmids of proHB-EGF alanine mutants were prepared with a KOD Plus Mutagenesis Kit (TOYOBO). Each expression plasmid was transfected into SW480 with Lipofectamine LTX with Plus reagent (Invitrogen) in 96-well plates. Two days after the transfection, cells were washed once with PBS(+) (PBS with 0.5 mM $CaCl_2$ and 0.5 mM $MgCl_2$) and then incubated in 1% BSA-containing PBS for 30 minutes at 4°C. Cells were then washed three times with PBS(+) and incubated with 200 nM Y-142 or anti-HB-EGF polyclonal antibody for 30 minutes at 4°C. After the washing steps, HRP-labeled anti-mouse IgG or HRP-labeled anti-goat IgG-antibody was added to detect Y-142 or anti-HB-EGF polyclonal antibody, respectively. After washing twice with PBS(+), TMB Peroxidase EIA Substrate was added to each well and incubated for 15 minutes. The reaction was stopped by adding 1N H_2SO_4. Antibody binding was detected by

measuring the absorbance at 450 nm using an Envision instrument. In order to take into consideration the differences among proHB-EGF expression levels, the binding of Y-142 to each proHB-EGF mutant was normalized with that of the anti-HB-EGF polyclonal antibody by each mutant. The percent binding of Y-142 was then calculated using the following formula: Y-142 binding (%) = (A/B)/(C/D) × 100, where A represents the absorbance at 450 nm of the indicated concentrations of Y-142 in mutant proHB-EGF, B represents the absorbance (450 nm) of 200 nM anti-HB-EGF polyclonal antibody in mutant proHB-EGF, C represents the absorbance (450 nm) of 200 nM Y-142 in wild-type proHB-EGF, and D represents the absorbance (450 nm) of anti-HB-EGF polyclonal antibody in wild-type proHB-EGF.

4.3. Results

4.3.1. Binding specificity of Y-142

Neutralizing anti-HB-EGF antibodies were generated by a hybridoma approach in the Chapter I. In the study, I characterized one of the anti-HB-EGF mAbs, Y-142. I first tested the binding profile of Y-142 to EGF ligands using ELISA (Fig. 2-1A). Y-142 showed comparable binding to sHB-EGF and amphiregulin (ARG), but not to the other four EGFR ligands. I then examined species specificity of Y-142 by testing its binding to human, mouse and rat sHB-EGF. As shown in Fig. 2-1B, Y-142 bound to human sHB-EGF but not to mouse and rat sHB-EGF.

4.3.2. Biophysical measurement of K_D for Y-142 to sHB-EGF

The K_D value of Y-142 to human sHB-EGF was measured using the kinetic exclusion assay (KinExA) method. K_D-controlled titration data were obtained by using a range of sHB-EGF concentrations equilibrated with a constant Y-142 binding site concentration (2x the molecular concentration) of 1.03 pM. For antibody-controlled experiments, several concentrations of sHB-

EGF were equilibrated with a constant Y-142 binding site concentration of 35.6 pM. In a dual-curve analysis, the K_D-controlled curve contains most of the K_D information while the antibody-controlled curve returns a value for the binding site concentration of the mAb. The latter parameter can be compared to the nominal binding site concentration of the mAb which can determine if the estimated K_D should be adjusted for the activity of the antigen in certain cases (Darling et al, 2004). The K_D-controlled titration data and antibody-controlled titration data were initially fit in a dual-curve analysis with a standard 1:1 equilibrium binding model. It was observed, however, that the titration curves collected under both K_D- and antibody-controlled conditions decreased with a slope steeper than that described by the standard 1:1 model. This steeper slope can only be explained by use of a positive cooperativity model. In the positive cooperativity model, the binding of sHB-EGF to one mAb binding site causes the affinity of the second binding site of the antibody to increase (Blake et al, 2003). Hence, a positive cooperativity equilibrium model was used to fit the dual-curve titration data which provided an improved fit to the dual curve data set, yielding an effective K_D = 1.50 pM (Fig. 2-2). In addition, the resulting Hill coefficient (n = 1.68) was greater than 1 which also indicated positive cooperativity (n = 1 signifies independent binding) (Blake et al, 2004).

4.3.3. Neutralizing activity of Y-142 against sHB-EGF and ARG signaling

As the over-expression of HB-EGF in cancer tissues has been reported (Kobrin et al, 1994; Naef et al, 1996; Mishima et at, 1998; Thøgersen et al, 2001; Miyamoto et al, 2003), the neutralization of sHB-EGF functionality is expected as a promising therapeutic potential. Neutralizing activity of Y-142 against sHB-EGF was therefore evaluated in both biochemical and cell-based assays. EGFR is one of the HB-EGF receptors, and the binding of sHB-EGF to EGFR leads to phosphorylation of EGFR and its downstream signaling. I found that the binding of sHB-EGF to EGFR-hFc was completely blocked with Y-142, whereas a control mouse IgG had no effect (Fig. 2-3A). The sHB-

EGF blocking activity of Y-142 was translated with the complete inhibition of sHB-EGF-induced EGFR phosphorylation (Fig. 2-3B). In addition to EGFR, sHB-EGF binds to and activates signaling pathway (Higashiyama et al, 1991; Beerli et al, 1996); indeed I showed that Y-142 could neutralize the sHB-EGF-induced phosphorylation endogenously expressed ERBB4 on T47D cells (Fig. 2-3C). Importantly, the neutralizing activity of Y-142 affected EGFR downstream signaling events. As shown in Figs. 2-3D and 2-3E, Y-142 neutralized sHB-EGF-induced phosphorylation of ERK1/2 and AKT, respectively. Taken together, these results showed that sHB-EGF binds to and activates EGFR and ERBB4, and that Y-142 can neutralize sHB-EGF-induced EGFR and ERBB4 signaling.

In a binding specificity test, Y-142 recognized ARG as well as sHB-EGF, which were both EGFR ligands (Fig. 2-1A). I then tested if Y-142 could neutralize the biological activity of ARG, which is a known ligand of EGFR. I hypothesized that Y-142 would be able to neutralize the functionality of ARG because of its neutralizing activity against sHB-EGF and cross-reactivity to ARG. However, I was able to show that phosphorylation of EGFR induced by ARG was only partially neutralized by Y-142 (Fig. 2-3F), whereas Y-142 completely blocked the sHB-EGF-induced EGFR phosphorylation (Fig. 2-3B). These results suggested that Y-142 could neutralize both sHB-EGF and ARG functional activities, albeit ARG activity on EGFR is only partially blocked by Y-142.

4.3.4. Comparison of sHB-EGF neutralizing activity of Y-142 with cetuximab and CRM197

The neutralizing activity of Y-142 against sHB-EGF was compared with two known inhibitors of the EGFR pathway: cetuximab and CRM197. Cetuximab, an anti-EGFR mAb used as a cancer therapeutic agent, suppresses EGFR-dependent cancer cell growth by inhibiting EGFR activation. CRM197, a mutant diphtheria toxin, binds to proHB-EGF and the subsequent internalization of CRM197 causes the inhibition of protein synthesis. I observed that sHB-EGF-induced SK-OV-3

cell proliferation was completely inhibited by Y-142 and cetuximab, and partially inhibited by CRM197 (Fig. 2-4A). Y-142 showed a more potent effect in suppressing cell proliferation than cetuximab. IC_{50} values of Y-142 and cetuximab were 4.1 nM and 38 nM, respectively.

sHB-EGF has been reported to be involved in multiple processes of angiogenesis (Abramovitch et al, 1998; Ushiro et al, 1996). I therefore studied the effect of Y-142 in the proliferation assay of a human umbilical vein endothelial cells (HUVEC). Y-142 neutralized sHB-EGF-induced HUVEC proliferation in a concentration dependent manner. Conversely, in the same assay, cetuximab and CRM197 showed no significant activity (Fig. 2-4B). To confirm this initial observation, I investigated the ability of Y-142, cetuximab, and CRM197 to block the angiogenic activities of sHB-EGF in a tube formation assay in which HUVEC and normal human dermal fibroblasts (NHDF) were co-cultured. Y-142 showed a complete inhibition of sHB-EGF-induced tube formation while cetuximab and CRM197 had no significant effect (Fig. 2-4C). To further evaluate the role of Y-142 in the angiogenic activity of sHB-EGF, I tested the neutralizing activity of Y-142 against sHB-EGF-induced VEGF production. I observed that Y-142 inhibited VEGF production induced by sHB-EGF while cetuximab and CRM197 showed no inhibitory effects (Fig. 2-4D). These results indicate that Y-142 could neutralize the angiogenic activities of sHB-EGF more effectively than cetuximab and CRM197.

I further compared the inhibitory activity of Y-142 against the sHB-EGF-induced tube formation with that of anti-VEGF antibody bevacizumab, which is used as a cancer therapeutic agent. As shown in Fig. 2-4E, bevacizumab only partially inhibited the sHB-EGF-induced tube formation, while Y-142 showed complete inhibition (Fig. 2-4C).

4.3.5. Conformational epitope recognition and epitope mapping of Y-142

These results show that Y-142 binds to HB-EGF and ARG and blocks the binding of HB-EGF to EGFR and ERBB4 as well as ARG to EGFR. These findings suggest Y-142 recognizes the EGF-like domain of HB-EGF because the EGF-like domain is required for the interaction of the EGF family of ligands and receptors. When probing HB-EGF by Western blot under reducing and non-reducing conditions, Y-142 only recognized sHB-EGF under non-reducing condition, suggesting it might recognize a conformational epitope (Fig. 2-5). To identify the Y-142 epitope, I tested its binding activity against a series of proHB-EGF mutants where an alanine point mutation was introduced in the EGF-like domain. Six cysteines in this domain were not replaced so as not to disrupt the disulfide bonds required for EGFR activation (Hoskins et al, 2008). Data demonstrated that the binding of Y-142 to G119A, G140A, and R142A mutants decreased by more than 70%, while binding to F115A, Y123A, and G137A mutants decreased by more than 50% (Fig. 2-6). These results indicate that Y-142 recognizes F115, G119, Y123, G137, G140, and R142 in the EGF-like domain of HB-EGF.

4.4. Discussion

In this study, I characterized an anti-HB-EGF mAb Y-142 and evaluated its therapeutic potential. The results show that Y-142 has unique properties with its potent neutralizing activity in multiple HB-EGF signaling.

My results clearly demonstrated that Y-142 inhibits sHB-EGF-induced cancer cell proliferation as well as sHB-EGF-induced angiogenic processes more effectively than cetuximab and CRM197, suggesting that Y-142 may have more promising therapeutic possibilities that cetuximab and CRM197. I hypothesized that the unique epitope of Y-142 and its high affinity to HB-EGF accounted for its superior activities in blocking cell proliferation and angiogenic activities of sHB-EGF. Previous studies have reported that the K_D value of sHB-EGF binding to EGFR is 3.8 nM (Jin

et al, 2009), the K_D of CRM197 binding to sHB-EGF is 27 nM (Brooke et al, 1998), and that the K_D of cetuximab binding to EGFR is 0.2 nM (Goldstein et al, 1995). Compared to these reported affinities, the K_D value of Y-142 measured in this study (1.5 pM) was several orders of magnitude lower (Fig. 2-2). More interestingly, the inhibitory activity of Y-142 seemed to be enhanced in the HUVEC proliferation and tube formation assays compared to that in the cancer cell proliferation assay (Figs. 2-4A, 2-4B and 2-4C). As shown in Fig. 2-4E, the sHB-EGF-induced tube formation was only partially blocked by bevacizumab, implying that sHB-EGF uses VEGF-independent and VEGF-dependent pathways. Therefore, I speculate that the complete inhibition of Y-142 against the function of sHB-EGF, which led to the subsequent inhibition of the VEGF function, resulted in the enhanced activity of Y-142.

I compared the neutralizing activity of Y-142 with that of KM3566, which is a parental antibody of KHK2866 (Miyamoto et al, 2011). KHK2866 is the humanized version of mouse anti-HB-EGF antibody KM3566. The IC_{50} value of KM3566 was estimated to be approximately 0.2 μg/mL (1.3 nM) in an MCAS cell growth assay using 3 ng/mL (0.32 nM) of sHB-EGF (Miyamoto et al, 2011). This estimated IC_{50} value was more than four-fold higher than the concentration of sHB-EGF used. In contrast, the IC_{50} value of Y-142 was 4.3 nM in an SK-OV-3 cell growth assay using 10 nM sHB-EGF (Fig. 2-4A). In the Chapter I, I identified the IC_{50} values of anti-HB-EGF monoclonal antibodies with a colony formation assay (Fig. 1-1B). In the assay, Y-142 showed an IC_{50} value of 0.02 nM against 0.11 nM sHB-EGF. Hence, each assay showed the IC_{50} values of Y-142 were less than half the concentrations of sHB-EGF used, indicating a superior neutralization activity of Y-142 compared to KM3566.

The study here also shed light on the functional epitope of Y-142. An alanine scanning approach to the whole EGF-like domain revealed six amino acids, F115, G119, Y123, G137, G140, and R142, as the Y-142 binding epitope (Fig. 2-6). This mapping result is consistent with the finding that Y-

142 did not recognize a linear conformational epitope (Fig. 2-5). Structural analyses by nuclear magnetic resonance and crystallography demonstrated that Y13 and R41 of EGF, corresponding to F115 and R142 of HB-EGF, were in close proximity to each other (Hommel et al, 1992; Ogiso et al, 2002). Mutational analyses of EGF identified Y13, I23, R41, and L47 of EGF as crucial amino acids in its binding to EGFR (Engler et al, 1992; Koide et al, 1992; Tadaki et al, 1993). R41 in EGF is an especially critical determinant for EGFR binding (Engler et al, 1992) because it forms a salt bridge with D355 in domain III of EGFR (Hommel et al, 1992). Y13 in EGF was reported to hydrophobically interact with the F357 side chain in domain III of EGFR (Ogiso et al, 2002). Consistent with the mutagenesis data of EGF, the neutralizing activity of Y-142 against sHB-EGF-induced EGFR was predicted to be attributed to the recognition of F115 and R142. In addition to the binding studies of EGF to EGFR, mutagenesis approaches with heregulinβ (HRGβ), a ligand for ERBB4, identified several residues critical for ERBB4 binding (Jones et al, 1998). Replacement of R44 in HRGβ with an alanine showed the greatest reduction of ERBB4 binding. Furthermore, the replacement of F13, G18, and G42 in HRGβ also resulted in an apparent reduction in ERBB4 binding. Similar to the binding between HRGβ and ERBB4, the binding activity of Y-142 to HB-EGF was reduced when R142, F115, G119, and G140 in HB-EGF were mutated. The HRGβ mutagenesis approach was consistent with the model that describes the neutralizing activity of Y-142 to ERBB4 as being attributed to the recognition of these amino acids on HB-EGF.

Species specificity and EGFR ligand specificity provided additional information of the epitope of Y-142. Of the six amino acids determined to be the Y-142 binding epitope (F115, G119, Y123, G137, G140, R142), all except for F115 were conserved between human, mouse, and rat HB-EGF (Fig. 2-1D), yet Y-142 binds to human HB-EGF specifically. This indicates that human HB-EGF specificity was determined by F115. Among the six amino acids which define the Y-142 epitope, F115 and Y123 are the only two which are shared between ARG and HB-EGF and not with other

EGF ligands (Fig. 2-1C). Therefore, I concluded that the cross-reactivity of Y-142 to ARG resulted from the recognition of the combination of F115 and Y123. Among EGF ligands, ARG and HB-EGF share common features. Both ARG and HB-EGF possess a heparin-binding domain (Inui et al, 1997) and bind to CD9, which potentiates their juxtacrine activities (Cook et al, 1991). In the Chapter II, however, Y-142 only partially neutralized ARG (Fig. 2-3F), whereas sHB-EGF-induced EGFR phosphorylation was completely neutralized by Y-142 (Fig. 2-3B). This finding may indicate that ARG uses amino acids not recognized by Y-142 when interacting with EGFR. Although the neutralizing activity of Y-142 was partial, interestingly, the co-expression of ARG with HB-EGF has been reported (Nakagawa et al, 2009), suggesting that Y-142 may be able to exert its synergistic anti-cancer activity by neutralizing sHB-EGF and ARG functionalities at the same time.

I have demonstrated the potent neutralizing activity of Y-142 against sHB-EGF and the superiority of Y-142 over cetuximab, CRM197, and bevacizumab in sHB-EGF neutralizing activities. My findings may expedite progress in the clinical research of HB-EGF.

4.5. Figures

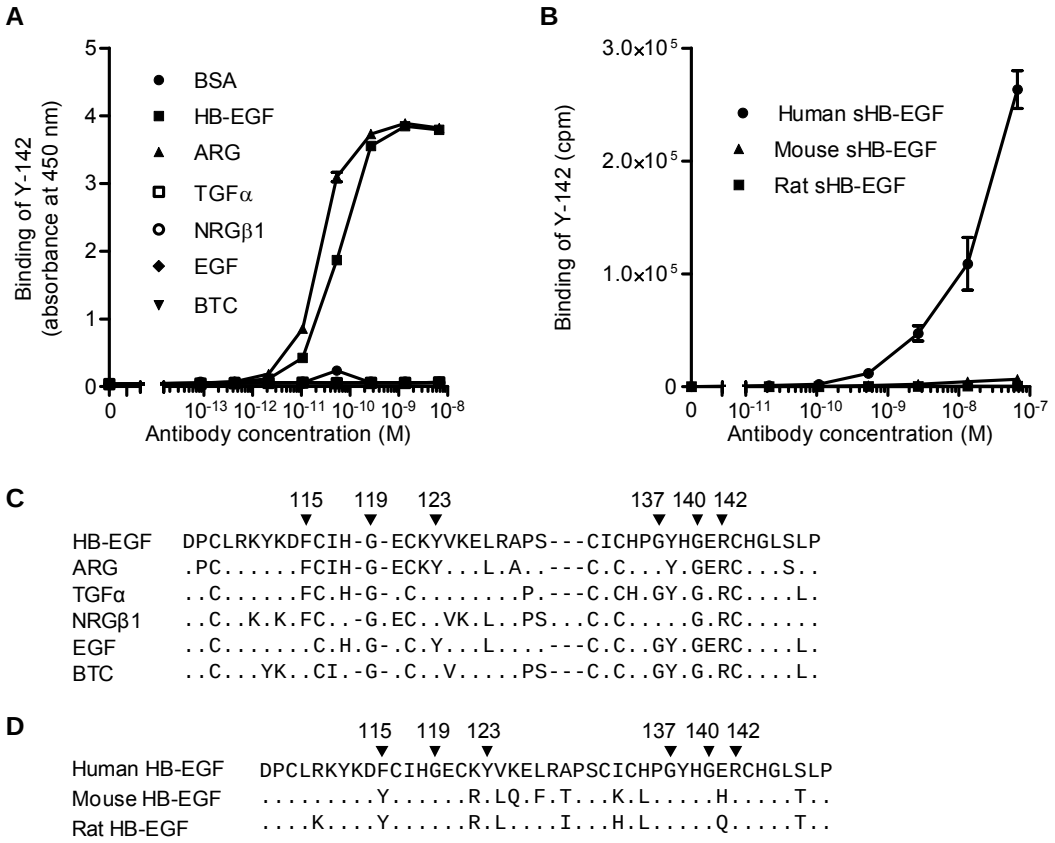

Fig. 2-1. Binding specificity of Y-142 to EGFR ligands and to different species of sHB-EGF

(A) The binding activity of Y-142 to EGFR ligands by ELISA. The various concentrations of Y-142 were incubated in an EGFR ligand-immobilized plate. The binding was then detected with HRP-labeled anti-mouse IgG antibody. Data points represent the mean ± standard deviation (SD) of values acquired in duplicate.

(B) The binding activity of Y-142 to human, mouse, and rat sHB-EGF by ELISA. The binding activity to different species sHB-EGF was measured by ELISA using an electroluminescence-based technology. The various concentrations of Y-142 were incubated in a sHB-EGF-immobilized plate. The binding was detected with sulfo-tagged anti-mouse IgG antibody. Data points represent the mean ± SD of values acquired in duplicate.

(C) Amino acid alignment of the EGF-like domain of EGFR ligands. A dot indicates an amino acid different than HB-EGF. A dash represents a gap. Arrowheads labeled with a number indicate the Y-142 binding epitopes identified in Fig. 2-6.

(D) Amino acid alignment of the EGF-like domain of human, mouse, and rat HB-EGF. A dot indicates an amino acid identical to human HB-EGF. Arrowheads labeled with a number indicate the Y-142 binding epitopes identified in Fig. 2-6.

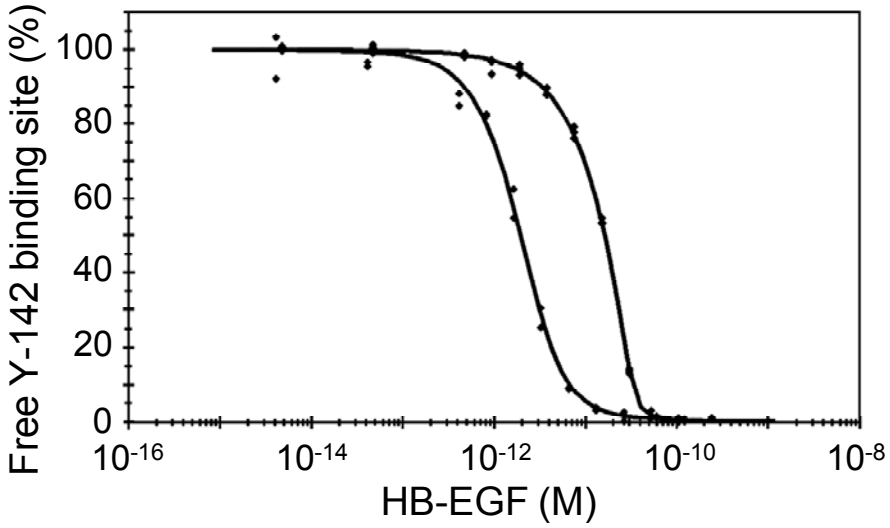

Fig. 2-2. Measuring the K_D of the Y-142/sHB-EGF complex

Dual-curve KinExA equilibrium titration of sHB-EGF binding to Y-142. K_D-controlled data (bottom fitted curve) were acquired by equilibrating sHB-EGF at a concentration range of 4.04 fM–207 pM with 1.03 pM Y-142 binding sites. Antibody-controlled data (top fitted curve) were acquired by equilibrating sHB-EGF at a concentration range of 4.67 fM–239 pM with 35.6 pM Y-142 binding sites. All data points were acquired in duplicate. Both curves were simultaneously fit to a standard positive cooperativity equilibrium model, yielding an effective K_D = 1.50 pM (0.31) where the number in parentheses is the 95% confidence interval of the fit, and a Hill coefficient n = 1.68.

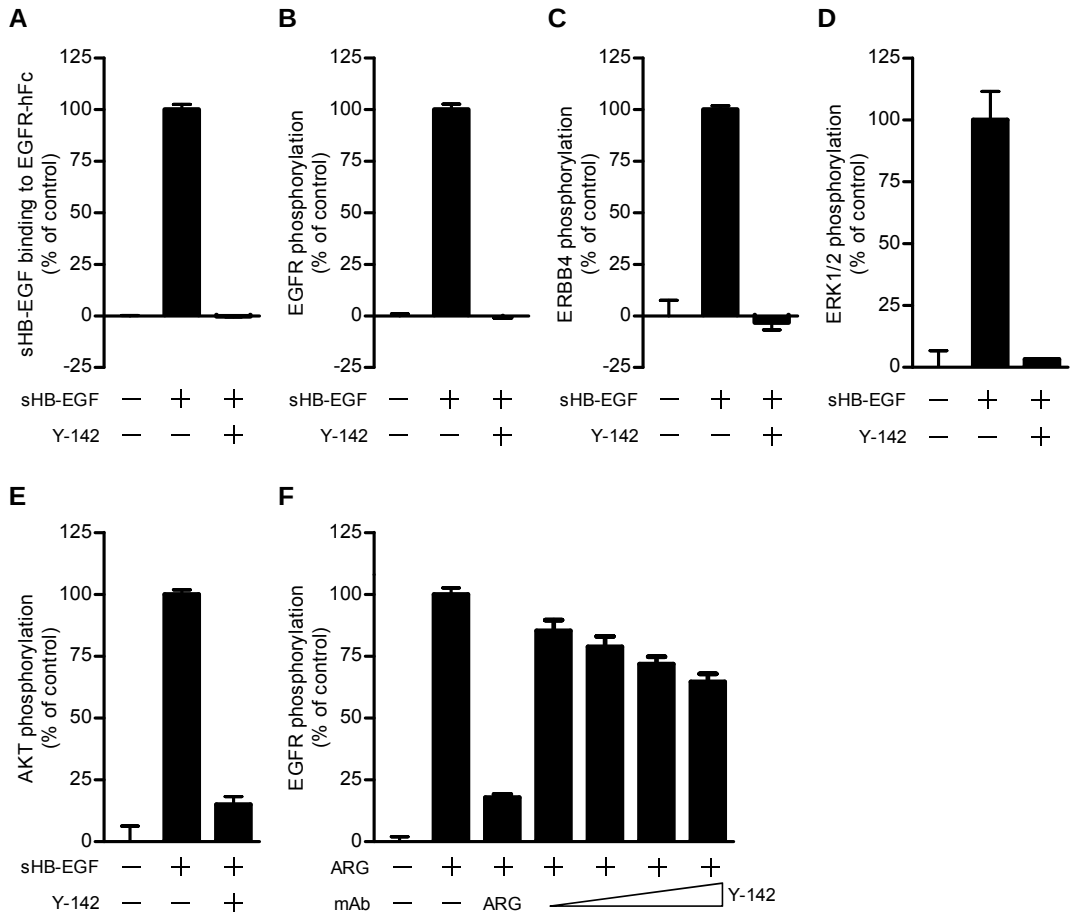

Fig. 2-3. Neutralizing activities of Y-142 against sHB-EGF and ARG signaling

(A) Inhibitory activity of Y-142 to sHB-EGF binding to EGFR. EGFR-hFc was incubated in an anti-human IgG Fc antibody-coated plate. Y-142 was then incubated at a concentration of 6.7 nM in the presence of 0.63 nM biotinylated sHB-EGF for 1 hour at 37°C. sHB-EGF bound to EGFR-hFc was detected by HRP-labeled streptavidin. sHB-EGF binding to EGFR-hFc in the presence of Y-142 was calculated as a percentage of the "control" sHB-EGF binding to EGFR which occurred without Y-142. Data points represent the mean + SD of values acquired in triplicate.

(B) Neutralizing activity of Y-142 against EGFR phosphorylation. SK-OV-3 cells were treated with 10 nM sHB-EGF and 67 nM Y-142. Cell lysates were incubated in an anti-EGFR antibody-coated plate, followed by an incubation with HRP-labeled anti-phosphorytosine antibody. EGFR phosphorylation in the presence of Y-142 was calculated as a percentage of the "control" EGFR phosphorylation which occurred without Y-142. Data points represent the mean + SD of values acquired in triplicate.

(C) Neutralizing activity of Y-142 against ERBB4 phosphorylation. Cell lysates of T47D cells as prepared in Fig. 2-3A were incubated on an anti-ERBB4 antibody-coated plate. The phosphorylation of ERBB4 was detected by a sulfo-tagged anti-phosphotyrosine antibody. ERBB4 phosphorylation in the presence of Y-142 was calculated as a percentage of the "control" ERBB4 phosphorylation which occurred without Y-142. Data points represent the mean + SD of values acquired in duplicate.

(D) and (E) Neutralizing activity of Y-142 against (D) ERK1/2 phosphorylation and (E) AKT phosphorylation. In (D) and (E) SK-OV-3 cells treated with 10 nM sHB-EGF and 200 nM Y-142 were stained with an anti-phosphorylated ERK1/2 antibody or an anti-phosphorylated AKT antibody, respectively, followed by an Alexa488-labeled anti-rabbit IgG antibody. Phosphorylated ERK1/2 and phosphorylated AKT were both detected with an ImageXpress Micro instrument and calculated as a percentage of the "control" phosphorylation levels which occurred without Y-142. Data points represent the mean + SD of values acquired in duplicate.

(F) Neutralizing activity of Y-142 to ARG. SK-OV-3 cells were treated with 10 nM ARG plus 67 nM anti-ARG antibody or various concentrations of Y-142 (2 nM, 6.7 nM, 20 nM, and 67 nM). Cell lysates were incubated in an anti-EGFR antibody-coated plate followed by an incubation with an HRP-labeled anti-phosphorytosine antibody. EGFR phosphorylation was calculated as a percentage of the "control" EGFR phosphorylation which occurred without Y-142. Data points represent the mean + SD of values acquired in triplicate.

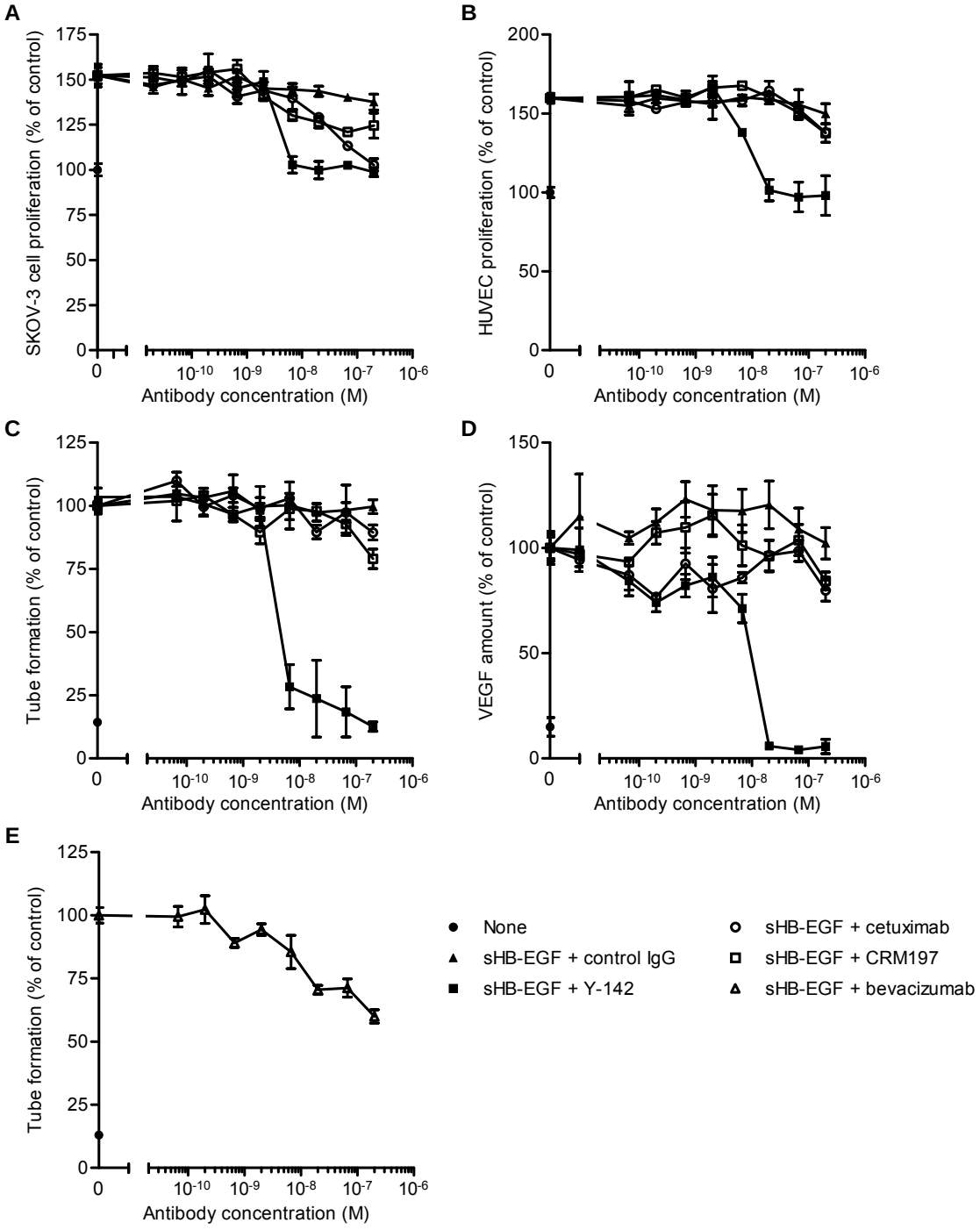
A
SKOV-3 cell proliferation (% of control)
175
150
125
100
75
50
25
0
0
10-10
10-9
10-8
10-7
10-6
Antibody concentration (M)
B
HUVEC proliferation (% of control)
200
150
100
50
0
0
10-10
10-9
10-8
10-7
10-6
Antibody concentration (M)
C
Tube formation (% of control)
125
100
75
50
25
0
0
10-10
10-9
10-8
10-7
10-6
Antibody concentration (M)
D
VEGF amount (% of control)
150
100
50
0
0
10-10
10-9
10-8
10-7
10-6
Antibody concentration (M)
E
Tube formation (% of control)
125
100
75
50
25
0
0
10-10
10-9
10-8
10-7
10-6
Antibody concentration (M)
None
sHB-EGF + control IgG
sHB-EGF + Y-142
sHB-EGF + cetuximab
sHB-EGF + CRM197
sHB-EGF + bevacizumab

Fig. 2-4. Inhibitory activity of Y-142 against sHB-EGF functions

(A) and (B) Neutralizing activities of Y-142 against (A) sHB-EGF-induced SK-OV-3 cell proliferation and (B) HUVEC proliferation. SK-OV-3 cells or HUVEC were cultured for 3 days in the presence of sHB-EGF and the indicated concentrations of Y-142, cetuximab, or CRM197. Cell proliferation was detected with a CellTiter-Glo instrument and calculated as a percentage of the "control" cell proliferation without sHB-EGF. Data points represent the mean ± SD of values acquired in triplicate.

(C) Inhibition of HUVEC tube formation by Y-142. HUVEC were cultured on a monolayer of NHDF in the presence of 50 nM sHB-EGF and the indicated concentrations of Y-142, cetuximab, or CRM197 for 4 days. HUVEC were then stained with FITC-labeled anti-CD31 antibody. Tube formation (CD31-positive area) was calculated as a percentage of the "control" amount of tube formation without the presence of sHB-EGF. Data points represent the mean ± SD of values acquired in triplicate.

(D) Inhibition of VEGF production by Y-142. HUVEC were prepared as in Figure 4C and treated with 50 nM sHB-EGF and the indicated concentrations of Y-142, cetuximab, or CRM197 for 4 days. VEGF concentration in the supernatant of co-culture was measured in an electrochemiluminescence-based method. VEGF production was calculated as a percentage of the "control" amount of VEGF produced without the presence of sHB-EGF. Data points represent the mean ± SD of values acquired in triplicate.

No sHB-EGF, closed circles; sHB-EGF plus control IgG, closed triangles; sHB-EGF plus Y-142, closed squares; sHB-EGF plus CRM197, open circles; sHB-EGF plus cetuximab, open squares.

(E) Inhibition of sHB-EGF-induced HUVEC tube formation by bevacizumab. HUVEC were prepared as in Figure 4C and treated with 50 nM sHB-EGF and the indicated concentrations of bevacizumab for 4 days. Tube formation was calculated as a percentage of the "control" amount of tube formation without the presence of sHB-EGF. Data represent mean ± SD of triplicate values.

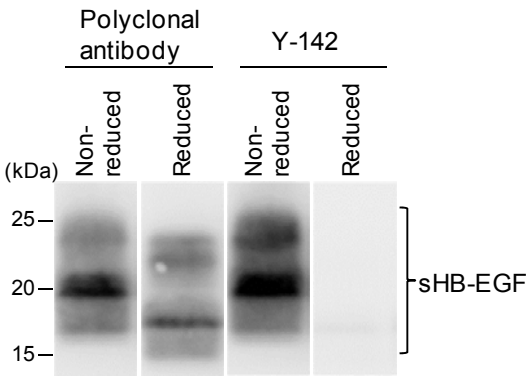

Fig. 2-5. Recognition of a conformational epitope by Y-142

The binding of Y-142 to a linear or conformational epitope was tested using Western blot. sHB-EGF was prepared in reducing or non-reducing conditions with or without dithiothreitol, respectively. The sHB-EGF was probed with an anti-HB-EGF polyclonal antibody and with Y-142.

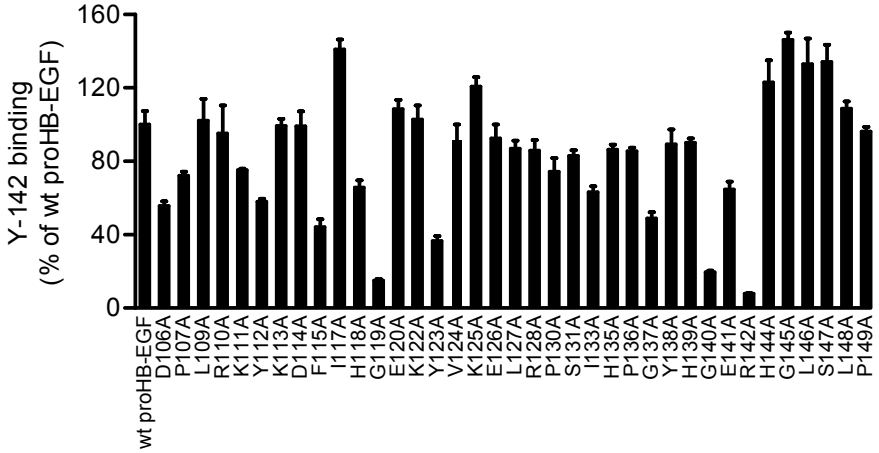

Fig. 2-6. Recognition of F115, G119, Y123, G137, G140, and R142 by Y-142

Epitope mapping of Y-142 was performed using alanine scanning. Each mutant proHB-EGF expression plasmid was transfected into SW480 cells. The binding activity of Y-142 to the cells was measured in a cell ELISA. The expression level of mutant proHB-EGF was normalized with the binding of anti-HB-EGF polyclonal antibody by each mutant. The binding of Y-142 to mutant proHB-EGF was calculated as a percentage of the "control" binding of Y-142 to wild-type proHB-EGF. Data points represent the mean + SD of values acquired in triplicate.

5. Chapter III: Identification of cancer cell proliferative and survival role of proHB-EGF using anti-HB-EGF antibody

5.1. Introduction

Other than as a precursor of sHB-EGF, membrane-bound form of HB-EGF, proHB-EGF has unique properties as a diphtheria toxin (DT) receptor (Naglich et al, 1992), a cell adhesion molecule (Raab et al, 1996), and a juxtacrine factor (Higashiyama et at, 1995). The functions of proHB-EGF in cell proliferation and survival have been evaluated by assessing its juxtacrine activity in a co-culture system, where proHB-EGF expressing cells were seeded on EGFR-over-expressing cells, or by analyzing the effects of proHB-EGF over-expression on autonomous cellular events (Higashiyama et al, 1995; Nakagawa et al, 1996; Takemura et al, 1997; Iwamoto et al, 1999; Miyoshi et al, 1997; Takemura et al, 1999). However, these studies have not reached to a definitive conclusion about if proHB-EGF promotes or inhibits cell proliferation and survival.

In this study, I report the functions of proHB-EGF in cancer cells by using 2 anti-HB-EGF mAbs that have different specificities toward proHB-EGF. These findings suggest that proHB-EGF plays roles in the cell proliferation and survival of cancer cells.

5.2. Materials and Methods

5.2.1. Materials

The anti-HB-EGF mAbs Y-073 and Y-142 were obtained through the KLH/BALB/c and KLH/cell/BALB/c immunizations, respectively, in the Chapter I. sHB-EGF was prepared in the Chapter I. I also used the following reagents: mouse control IgG and horseradish peroxidase-labeled (HRP-labeled) anti-mouse IgG antibody from Jackson ImmunoResearch Laboratories; Alexa488-labeled anti-mouse IgG antibody, HRP-labeled anti-goat IgG antibody, and HRP-labeled anti-rabbit

IgG antibody from Invitrogen; anti-amphiregulin (anti-ARG) mAb, anti-HB-EGF polyclonal antibody, anti-EGFR polyclonal antibody, and biotinylated anti-EGFR polyclonal antibody from R&D Systems; anti-β-actin antibody from Cell Signaling Technology; erlotinib from Selleck Chemicals; biotinylated anti-phosphotyrosine antibody from Millipore; sulfo-tagged streptavidin from Meso Scale Discovery; and phorbol 12-myristate 13-acetate (PMA) from Wako.

5.2.2. Cell culture

NUGC-3 gastric cancer cells (Japanese Collection of Research Bioresources), 5637 bladder cancer cells (American Type Culture Collection), and BxPC-3 pancreatic cancer cells (American Type Culture Collection) were maintained in RPMI1640 supplemented with 10% serum. EFO-27 ovarian cancer cells (DMSZ) were maintained in RPMI1640 with 20% serum. The cells were maintained in 2D cell culture plates, and 3D spheroid culture experiments, they were transferred to a Celltight Spheroid culture plate (Sumitomo Bakelite).

5.2.3. Flow cytometry

Cells were detached from a culture dish with cell dissociation buffer (Invitrogen) and incubated with anti-HB-EGF antibody, or anti-ARG antibody for 1 hour at 4°C. After washing with PBS containing 1% BSA, the cells were incubated with Alexa488-labeled secondary antibody for 1 hour at 4°C. Protein expression was measured using a FACS CantoII instrument (Becton Dickinson) and the data were then analyzed with the FlowJo software (Tree Star).

5.2.4. sHB-EGF binding assay

sHB-EGF or BSA was immobilized at 1 μg/mL on a 96-well plate overnight at 4°C. After non-specific binding was blocked with PBS containing 1% BSA, anti-HB-EGF mAb was incubated at

various concentrations in the plate. HRP-labeled anti-mouse IgG antibody was then reacted for 1 hour at room temperature. TMB Peroxidase EIA Substrate (Bio-rad) was then added into each well. Antibody binding to sHB-EGF was detected by measuring the absorbance at 450 nm by using a SPECTRA MAX plate reader (Molecular Devices).

5.2.5. EGFR phosphorylation assay

NUGC-3 cells were seeded at 1×10^4 cells/well in RPMI1640 with 1% serum. After a 1-day incubation period, the cells were treated with various concentrations of anti-HB-EGF antibody and 10 nM sHB-EGF for 15 minutes at 37°C. Cell lysates were prepared with cell lysis buffer (Cell Signaling Technology) containing protease inhibitor cocktail (Roche Applied Science) and phosphatase inhibitor cocktail (Sigma Aldrich), and were used for analysis with pEGFR detection ELISA kit (R&D Systems).

5.2.6. Cell proliferation and caspase assays

Cells were seeded at a concentration of 1×10^4 cells/well in RPMI1640 containing 1% serum into Celltight Spheroid culture plates. I measured caspase 3/7 activation after a 1-d incubation period by using Caspase-Glo 3/7 (Promega) and measured cell proliferation after a 3-d incubation period by using CellTiter-Glo (Promega). Measurements for both parameters were obtained using an Envision instrument (Perkin Elmer). Cell proliferation was calculated as the percentage of the proliferation level measured in the absence of antibody.

5.2.7. siRNA transfection

NUGC-3 cells were transfected with negative control siRNA or HB-EGF siRNA (Dharmacon) by using Lipofectamine2000 (Invitrogen) during 2D culture. After transfection, the cells were

transferred to a 3D spheroid culture. siRNA-transfected cells were then used in the cell proliferation assay. Reduction in HB-EGF protein expression was examined by Western blot. HB-EGF expression was detected by anti-HB-EGF polyclonal antibody and HRP-labeled anti-goat IgG antibody. β-actin, an internal loading control, was detected as an internal control with anti-β-actin antibody and HRP-labeled anti-rabbit IgG antibody.

5.2.8. Measurement of proHB-EGF juxtacrine activities

NUCG-3 cells were incubated with 200 nM Y-142 or Y-073 for the indicated times under the spheroid culture condition. Mouse control IgG (200 nM) and 1 nM erlotinib were also used in the assay as negative and positive controls, respectively. For the detection of EGFR phosphorylation, cell lysates prepared as described above were incubated in an MSD plate (Meso Scale Discovery) pre-coated with anti-EGFR polyclonal antibody. The plate was then incubated with biotinylated anti-phosphotyrosine antibody, followed by incubation with sulfo-tagged streptavidin. For the detection of total EGFR, the cell lysates were incubated in an MSD plate pre-coated with anti-EGFR polyclonal antibody. Biotinylated anti-EGFR polyclonal antibody was then incubated in the plate, followed by incubation with sulfo-tagged streptavidin. Read T buffer (Meso Scale Discovery) was then added and chemiluminescence was measured with a Sector Imager 6000 instrument (Meso Scale Discovery). The EGFR phosphorylation signal was normalized to the total EGFR signal, and then calculated as the percentage of the maximum EGFR phosphorylation that was measured in the absence of Y-142, Y-073, control IgG, and erlotinib.

For the detection of the phosphorylation of ERK1/2 and AKT, I used the phosphoERK1/2 and phosphoAKT kits (Meso Scale Discovery), respectively, according to the supplier's instructions. In brief, cell lysates prepared as described above were added to the plate with spots of anti-ERK1/2 and anti-phosphoERK1/2 antibodies, or with spots of anti-AKT and anti-phosphoAKT antibodies.

Then each plate was incubated with sulfo-tagged anti-ERK1/2 antibody or with sulfo-tagged anti-AKT antibody. Read T buffer with surfactant was then added and chemiluminescence was measured with a Sector Imager 6000 instrument. The ERK1/2 or AKT phosphorylation signal was normalized to the total ERK1/2 or AKT signal, respectively. ERK1/2 or AKT phosphorylation was then calculated as the percentage of the maximum ERK1/2 or AKT phosphorylation, respectively, which was measured in the absence of Y-142, Y-073, control IgG, and erlotinib.

5.2.9. Detection of CTF

NUGC-3 cells were treated with 200 nM Y-142 for 3 days or 50 nM PMA for 30 min as a control for ectodomain shedding induction and CTF production. Cell lysates prepared as described above were subjected to Western blot. The CTF fragment was detected using the anti-CTF polyclonal antibody and HRP-labeled anti-rabbit IgG antibody. Anti-CTF polyclonal antibody was generated by immunizing a rabbit with an antigen peptide corresponding to amino acids 185-208 of proHB-EGF, as described previously (Miyagawa et al, 1995).

5.3. Results

5.3.1. Characterization of Y-142 and Y-073

Anti-HB-EGF antibodies were generated using a hybridoma approach in the Chapter I. During the characterization of the antibodies, I found that Y-142 (epitope bin A1) and Y-073 (epitope bin C1) had a different binding profileto cancer cell lines endogenously expressing proHB-EGF. Y-142 bound to the tested cancer cell lines, whereas Y-073 showed no binding (Fig. 3-1A).

In the Chapter II, I showed that Y-142 recognizes another EGF ligand amphiregulin (ARG) in addition to HB-EGF. To confirm that the Y-142 binding to cells was attributable to its recognition of proHB-EGF, and not from ARG, ARG expression was examined by flow cytometry, and no

ARG expression was detected (Fig. 3-1B). To rule out the possibility that the anti-ARG antibody did not have binding activity for ARG, I used transfected ARG as a positive control. This result further confirmed that the binding of Y-142 to the tested cancer cell lines was attributable to its recognition of proHB-EGF.

To further examine the characteristics of the antibodies, I tested their binding activity to sHB-EGF by ELISA. Interestingly, Y-142 and Y-073 bound to sHB-EGF with comparable EC_{50} values of 56 pM and 110 pM, respectively, and neither of them bound to the negative control BSA (Fig. 3-2A). In addition, I tested their neutralizing activity on sHB-EGF-induced EGFR phosphorylation. The NUGC-3 gastric cancer cell line was used to detect EGFR phosphorylation because of the high EGFR expression. As shown in Fig. 3-2B, both the antibodies inhibited the phosphorylation of EGFR in a concentration-dependent manner with similar IC_{50} values (Y-142 = 3.8 nM; Y-073 = 4.1 nM). These findings indicated that only Y-142 had the ability to bind to proHB-EGF, although both Y-142 and Y-073 had similar binding and neutralizing activities toward sHB-EGF.

5.3.2. Cell proliferation and survival functions of proHB-EGF

A previous study has shown that proHB-EGF is involved in cell-cell contact (Raab et al, 1996). In a 3D spheroid culture, cancer cells undergo more extensive cell-cell contacts than in a 2D culture (Santini et al, 1999). I speculated that the cell-cell contact-mediated proHB-EGF effect might be more pronounced and easier to detect in the 3D spheroid culture. To this end, I established a 3D spheroid culture cell-based assay by using NUGC-3 cells. When NUGC-3 cells were seeded in a spheroid culture plate, they formed a spheroid with a small cell mass in the center core and loosely distributed cells surrounding the core (dark gray and light gray, respectively, in the PBS control in Fig. 3-3A). Interestingly, under the Y-142 treatment, the cells were more diffuse and had a smaller center core and a larger halo. The morphological change caused specifically by Y-142 suggested

that this change in spheroid morphology was attributable to the modulation of proHB-EGF functions. I further explored the proHB-EGF functions by using the 3D spheroid culture assay. In the cell proliferation assay, Y-142 significantly inhibited the proliferation of NUGC-3 in a concentration-dependent manner (Fig. 3-3B). The inhibition of cell proliferation reached 72% at the maximum antibody concentration. In contrast, Y-073 had no effect on proliferation. Similar results were obtained in the other cell lines tested, that is, 5637 and BxPC-3 (Fig. 3-3B). Since Y-073 inhibited the functions of sHB-EGF, and had no effect on any of the proHB-EGF cell lines in the spheroid culture, it was suggested that the function of endogenous proHB-EGF was dominant in the spheroid culture compared to the endogenous sHB-EGF function. These results indicated that proHB-EGF acted as an important cell proliferation factor in cancer cells.

To further confirm that the inhibition of cell proliferation was caused by the perturbation of proHB-EGF function, I evaluated the effect of HB-EGF siRNA on cell proliferation in the spheroid assay for NUGC-3 cells. Reduced expression of proHB-EGF due to HB-EGF siRNA was confirmed by Western blot (Fig. 3-3C). In accordance with the knockdown of proHB-EGF expression, HB-EGF siRNA caused reduced cell proliferation (Fig. 3-3D). I found that the extent of inhibition of cell proliferation by HB-EGF siRNA was similar that observed with Y-142. These results are consistent with the notion that Y-142 inhibits proHB-EGF function, which may lead to reduced cell proliferation.

To explore the molecular mechanism underlying the functions of proHB-EGF in cell survival, I measured caspase activation, a key event in apoptosis (Boatright et al, 2003), in NUGC-3 cells. As indicated in Fig. 3-4, Y-142 promoted the activation of caspase-3/7 (Fig. 3-4), while Y-073 had no effect. This result indicated that proHB-EGF has cell survival activity in cancer cells, and that inhibiting proHB-EGF triggers caspase-mediated apoptosis.

5.3.3. Inhibition of proHB-EGF juxtacrine activities by Y-142

Unlike sHB-EGF, which acts by autocrine and paracrine mechanisms, juxtacrine signaling is a mechanism unique to proHB-EGF (Higashiyama et al, 1995). I hypothesized that the effect of Y-142 may be mediated specifically through the inhibition of proHB-EGF juxtacrine signaling. Because the juxtacrine activity was reported to be EGFR-mediated (Higashiyama et al, 1995), I measured the phosphorylation of EGFR as well as of its downstream proteins ERK1/2 and AKT, which are involved in cell proliferation and caspase-mediated apoptosis, respectively, in NUGC-3 cells. The EGFR inhibitor erlotinib, used as a positive control, inhibited the phosphorylation of EGFR, ERK1/2, and AKT (Fig. 3-5). Similar to the effect of erlotinib, Y-142 decreased the phosphorylation of EGFR, ERK1/2, and AKT, whereas Y-073 as well as control IgG did not. The inhibition of their phosphorylation by Y-142 was significant at 15 minutes after the treatment and lasted for up to 3 days, suggesting that the juxtacrine signal was constitutively switched on in the spheroid. These data suggested that proHB-EGF juxtacrine activity leads to cell proliferation as well as cell survival activity.

5.3.4. No effect of Y-142 on CTF generation

CTF, which is produced along with sHB-EGF by ectodomain shedding, drives cell proliferation (Higashiyama et al, 2008). To evaluate the contribution of CTF in the inhibition of cell proliferation by Y-142, the CTF amount was examined in NUGC-3 cells. PMA (Hirata et al, 2001) was used as a control to stimulate the ectodomain shedding and CTF production. As shown in Fig. 3-6, the amount of CTF generated in the presence and absence of Y-142 was not substantially different, suggesting that Y-142 had no impact on the generation of CTF.

5.4. Discussion

HB-EGF consists of a membrane-bound form (proHB-EGF), a soluble form (sHB-EGF) and a C-terminal fragment (CTF), and each form has a unique biological activity. Among these 3 forms, the function of sHB-EGF has been widely evaluated using recombinant proteins. To date, the biological activity of proHB-EGF has been suggested on the basis of the effect of formalin-fixed proHB-EGF transfectants on the proliferation and survival of EGFR-expressing cells (Higashiyama et al, 1995; Nakagawa et al, 1996; Takemura, 1997) or the basis of the effect of proHB-EGF over-expression on autonomous cell proliferation (Miyoshi et al, 1997; Takemura et al, 1999). However, information on proHB-EGF function has been scanty and inconsistent possibly because of the lack of a method for specifically activating or inhibiting proHB-EGF. In some other studies, uncleavable mutant proHB-EGF (uc-proHB-EGF), which has 2 amino acid replacements (Leu148 and Pro149) in the cleavage site, was used to evaluate proHB-EGF function (Hirata et al, 2001). uc-proHB-EGF has been shown to possess juxtacrine activity in formalin-fixed EGFR-expressing cells (Yamazaki et al, 2003). If uc-proHB-EGF fully represents wild-type proHB-EGF functions even in live cells, this mutant might be useful in identifying proHB-EGF functions in spheroid culture. Recently, another version of uc-proHB-EGF, whose cleavage site was deleted, was used to study proHB-EGF functions. This uc-proHB-EGF prevented anoikis of Madin-Darby canine kidney cells (Singh et al, 2007). However, in comparison with these approaches used so far, there are some advantages in the approach here using a 3D spheroid culture and a functional anti-HB-EGF antibody: the functions of endogenously expressed proHB-EGF can be detected, and formalin fixation, which may cause artifacts, is not required because there is no endogenous sHB-EGF function.

The approach here will be useful for further identifying proHB-EGF functions. Accumulated reports showed that spheroid culture mimics the cancer environment better than a 2D culture in terms of cell-cell contacts, drug resistance, drug penetration, and nutrient efficiency (Santini et al, 1999; Friedrich et al, 2007); therefore, the functions of endogenously expressed proHB-EGF found

in the 3D spheroid suggest that proHB-EGF may play important roles in tumor progression. In this study, I used 3 cancer cell lines endogenously expressing proHB-EGF. Y-142 inhibited the proliferation of NUGC-3 cells by 72%, 5637 cells by 55%, and BxPC-3 cells by 24% at the maximum concentration (Fig. 3-3B). As shown in Fig. 3-1A, the 3 cell lines have different levels of proHB-EGF expression (NUGC-3 cells > 5637 cells > BxPC-3 cells), which may explain the relative effect of Y-142 on proliferation. The 3 cell lines are derived from gastric, bladder, and pancreatic cancer tissues, which are known to over-express HB-EGF (Naef et al, 1996; Thøgersen et al, 2001; Kobrin et al, 1994). HB-EGF has been reported to be up-regulated in other cancer types such as breast and ovarian cancers and glioblastoma (Suo et al, 2002; Miyamoto et al, 2004; Mishima et al, 1998); proHB-EGF may exert its functions in a broad range of cancer types.

In this study, to investigate proHB-EGF functions in cancer cells, I used 2 anti-HB-EGF antibodies Y-142 and Y-073, which had activities similar to those of sHB-EGF, but different specificities toward proHB-EGF (Figs. 3-1A and 3-2). The result in the Chapter II showed that the neutralizing activity of Y-142 is attributable to its recognition of amino acids in the EGF-like domain of HB-EGF. The EGF-like domain is required for the binding of HB-EGF to EGFR. I, therefore, presume that the epitope of neutralizing antibody Y-073 should also be located in the EGF-like domain. Y-073, however, did not bind to proHB-EGF. These findings allowed me to speculate that Y-073 may also recognize the newly exposed site in sHB-EGF after proHB-EGF ectodomain shedding. Consistent with my speculation, several antibodies to different molecules such as type II collagen, aggrecan, fibrin, and link protein have been reported to specifically recognize a newly exposed site resulting from a protein cleavage (Mort et al, 1999). Epitope mapping studies will provide detailed information about Y-073 functionality.

In the spheroid culture, the treatment with Y-142 increased the number of cells that diffused out of the spheroid core (Fig. 3-3A). The inhibition of proHB-EGF juxtacrine activity was detected

even 3 days after the Y-142 treatment (Fig. 3-5), when cell diffusion was seen. I speculate that the proHB-EGF-mediated cell-cell contact is directly associated with its proHB-EGF juxtacrine activity. The results of a previous study using uc-proHB-EGF supported this speculation in that the results indicated a cytoprotective role of proHB-EGF by enhancing EGFR-mediated cell-cell contact and showed that caspase activation was inhibited by the proHB-EGF-EGFR-AKT pathway (Singh et al, 2007). I also detected caspase activation and inhibited EGFR and AKT phosphorylation by Y-142 treatment in the spheroid culture (Figs. 3-4 and 3-5). These results may be derived from the blockage of the proHB-EGF cytoprotective role. While measuring the juxtacrine activity of proHB-EGF, I also noted the inhibition of ERK1/2 phosphorylation by Y-142, suggesting that the ERK1/2 pathway induced cell proliferation.

In summary, I have shown that the endogenously expressed proHB-EGF acts as a cell proliferation and cell survival factor in cancer cells and that it may play an important role in cell proliferation and survival in tumor tissues.

5.5. Figures

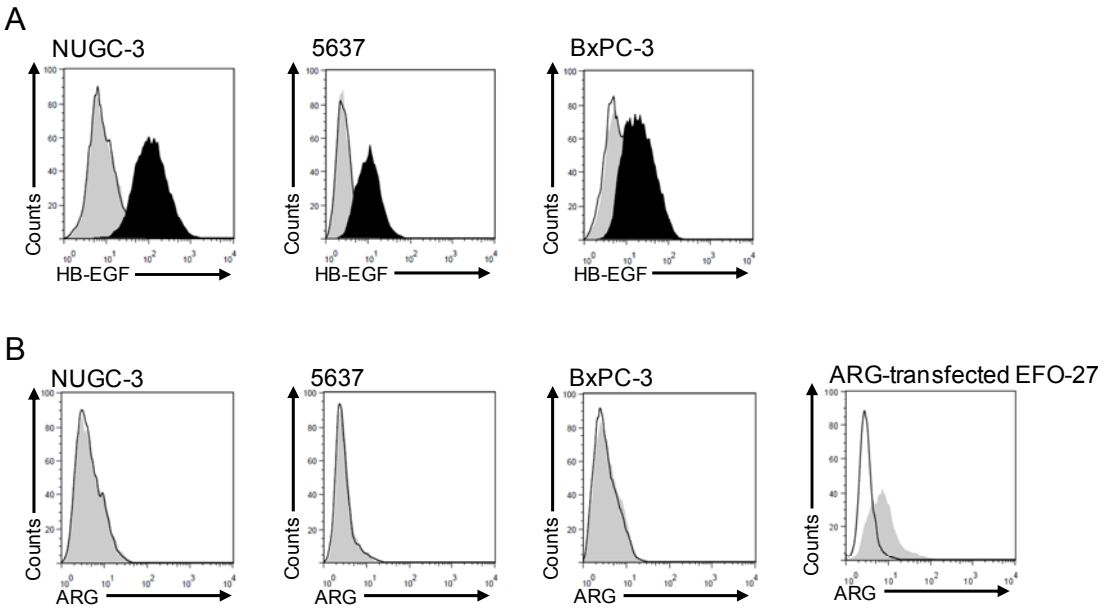

Fig. 3-1. Comparison of Y-142 and Y-073 binding activities toward proHB-EGF

A. Binding of anti-HB-EGF antibody to proHB-EGF. The cells were incubated with anti-HB-EGF antibody, followed by incubation with Alexa488-labeled anti-mouse IgG antibody. The binding was detected by flow cytometry. No IgG, black line; Y-142, black histogram; Y-073, gray histogram. B. Expression of amphiregulin (ARG) in the cancer cell lines. Cells were incubated with anti-ARG antibody, followed by incubation with Alexa488-labeled anti-mouse IgG antibody. The binding activity of anti-ARG antibody was confirmed using cells transfected with an ARG expression plasmid. No IgG, black line; anti-ARG antibody, gray histogram.

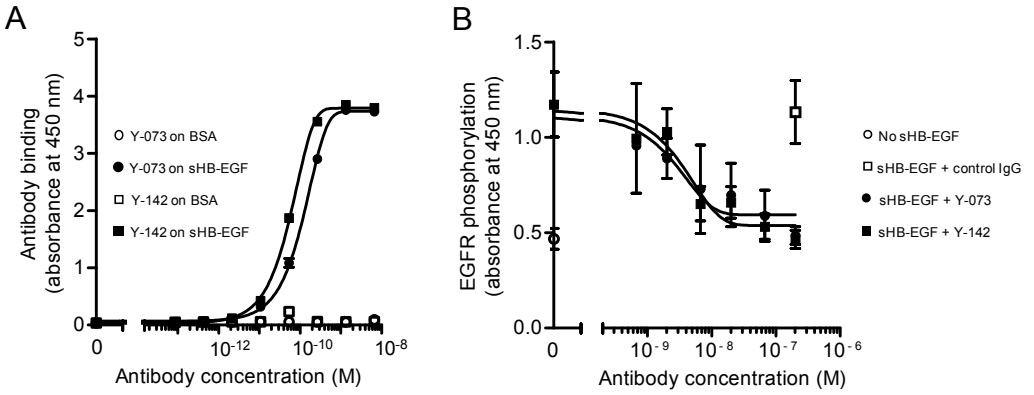

Fig. 3-2. Comparison of Y-142 and Y-073 biological activities toward sHB-EGF

A. Binding activity of Y-142 and Y-073 toward sHB-EGF. Anti-HB-EGF antibody was incubated at various concentrations in a sHB-EGF-coated or a BSA-coated plate. Antibody binding was detected with an HRP-labeled anti-mouse IgG antibody. The data points represent the mean ± standard deviation (SD) of values acquired in duplicate. B. Neutralizing activity of Y-142 and Y-073 against sHB-EGF-induced EGFR phosphorylation. Anti-HB-EGF antibody was incubated at the indicated concentrations in the presence of 10 nM sHB-EGF with NUGC-3 cells for 15 minutes at 37°C. Cell lysates were incubated on an anti-EGFR antibody-coated plate, followed by incubation with HRP-labeled anti-phosphotyrosine antibody. The data points represent the mean ± SD of values acquired in triplicate.

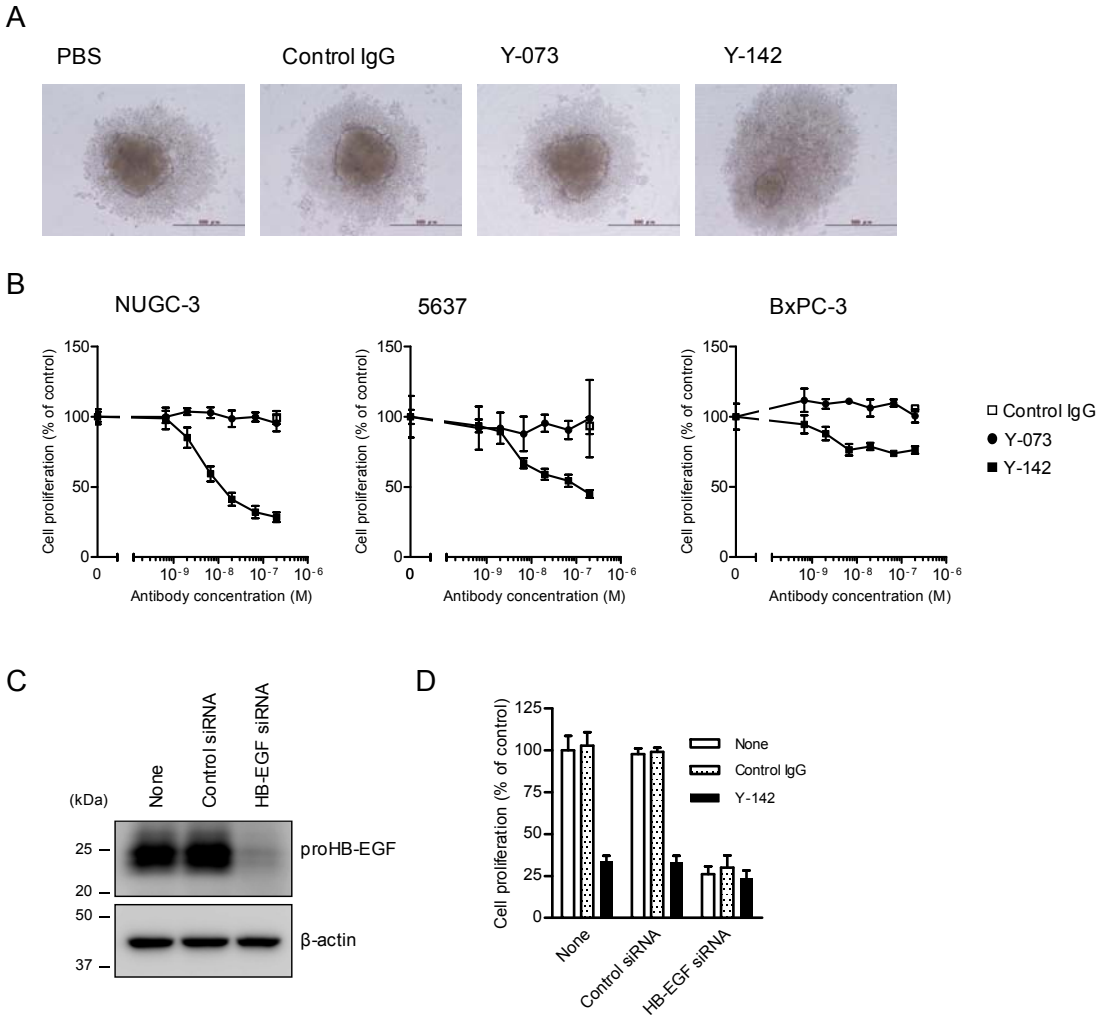

Fig. 3-3. Spheroid-forming and cell proliferation effects of proHB-EGF

Spheroid formation and cell proliferation by proHB-EGF function were assessed under Y-142 treatment. The cells were seeded into a spheroid culture plate in the presence of 1% serum. After a 1-day incubation period, the cells were treated with the indicated concentrations of anti-HB-EGF antibody and cultured for 3 days. A. Spheroid formation of NUGC-3 cells. The bar in each image indicates 500 μm. B. Inhibition of proHB-EGF-dependent cell proliferation by Y-142. Cell proliferation was measured by CellTiter-Glo and is shown as the percentage of the proliferation of PBS-treated cells. The data points represent the mean ± SD of values acquired in triplicate. C. Reduction in proHB-EGF protein expression by HB-EGF siRNA. Cell lysates of

siRNA-transfected NUGC-3 cells were subjected to SDS-PAGE. HB-EGF was detected by Western blot, with β-actin as the internal control. D. Confirmation of proHB-EGF-dependent cell proliferation by HB-EGF siRNA. NUGC-3 cells were transfected with HB-EGF siRNA prior to spheroid culture. One day after the siRNA transfection, the cells were seeded into a spheroid culture plate. Cell proliferation was measured by CellTiter-Glo and shown as a percentage of the cell proliferation of PBS-treated cells. The data points represent the mean + SD of values acquired in triplicate.

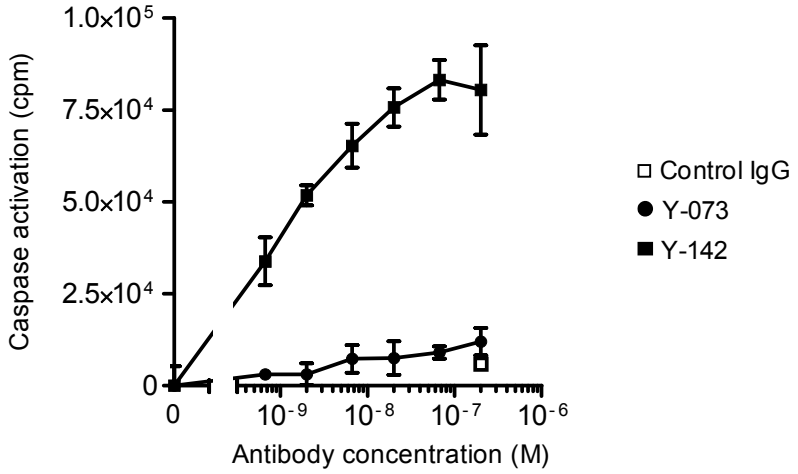

Fig. 3-4. Cell survival signaling through proHB-EGF

The cell survival activity of proHB-EGF was tested by measuring caspase activation. NUGC-3 cells were seeded into a spheroid culture plate in the presence of 1% serum. After a 1-day incubation period, the cells were treated with Y-142 and cultured for 1 day. Caspase activation was measured by Caspase-Glo 3/7.

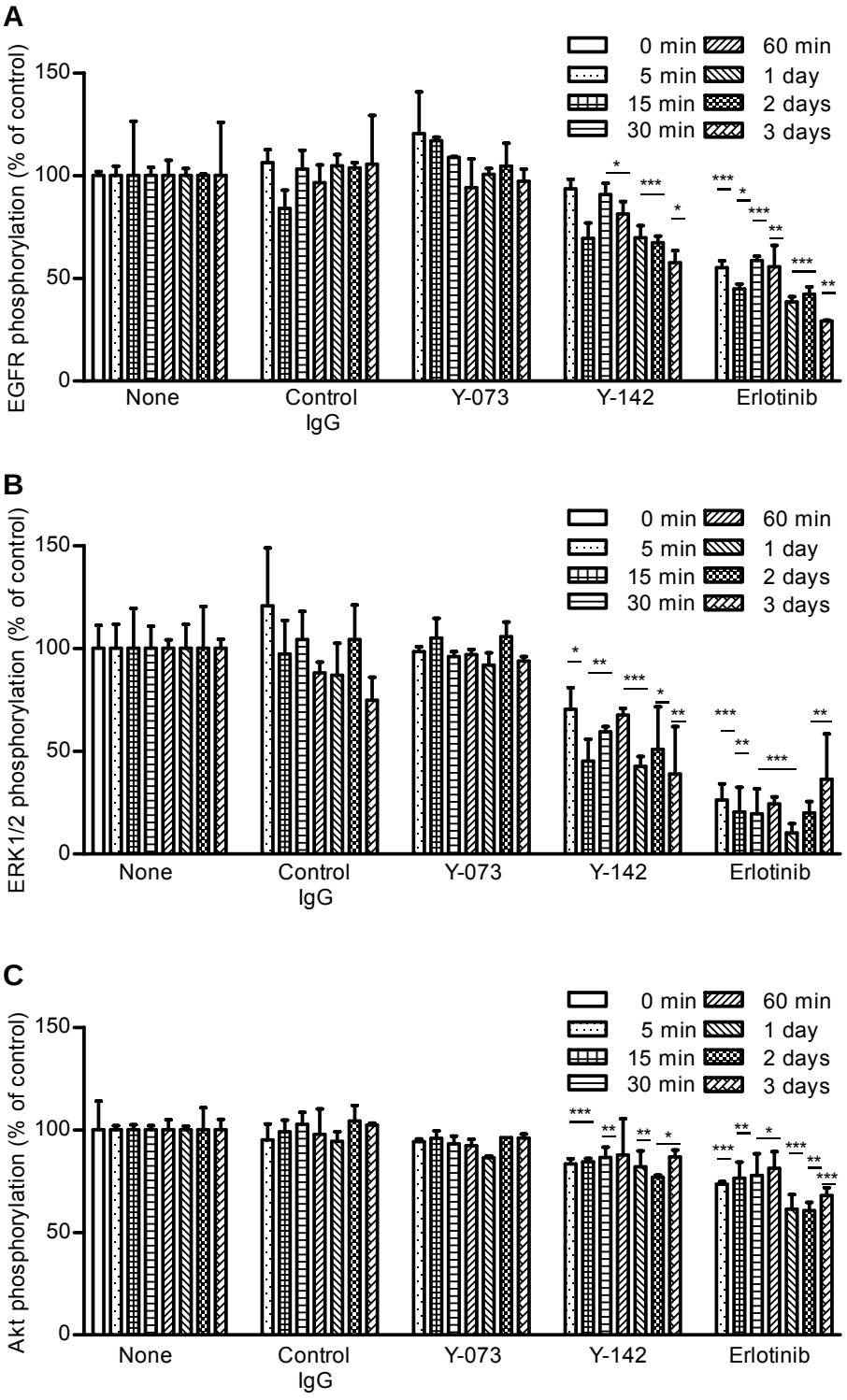
A
EGFR phosphorylation (% of control)
150
100
50
0
0 min
5 min
15 min
30 min
60 min
1 day
2 days
3 days
None
Control IgG
Y-073
Y-142
Erlotinib
B
ERK1/2 phosphorylation (% of control)
C
Akt phosphorylation (% of control)

Fig. 3-5. Inhibition of proHB-EGF juxtacrine activity by Y-142

proHB-EGF juxtacrine activity was measured using Y-142. NUGC-3 cells in a spheroid culture plate were treated with 200 nM control IgG, 200 nM Y-142, 200 nM Y-073, or 1 nM erlotinib for the indicated times. A. Phosphorylation of EGFR. B. Phosphorylation of ERK1/2. C. Phosphorylation of AKT. Phosphorylation was calculated as the percentage of the phosphorylation of PBS-treated cells. The data points represent the mean ± SD of values acquired in triplicate. Statistical analysis was performed using the unpaired t-test (one-tailed, vs PBS-treated sample at the corresponding time point). *, $p<0.05$; **, $p<0.005$; ***, $p<0.0005$.

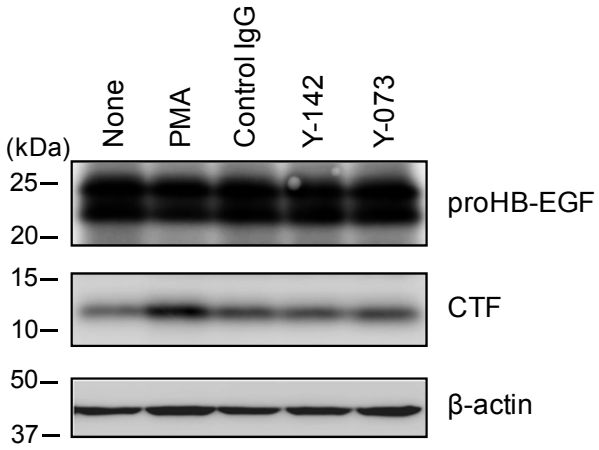

Fig. 3-6. Y-142 did not affect CTF production

The effect of CTF on the observed inhibition of cell proliferation (Fig. 3-3B) was examined by measuring the amount of CTF. Cell lysates of the PMA, control IgG, Y-142, or Y-073-treated NUGC-3 cells were subjected to SDS-PAGE. CTF was detected with anti-CTF polyclonal antibody in Western blot.

6. Conclusion

Cancer incidence has been increasing as the population ages. Patients with an unresectable cancer usually require anti-cancer drugs for treatment. However, cancer cells show heterogenous properties depending on tissue of origin as well as on microenvironment. Therefore, it is recommended to appropriately select anti-cancer drug that is efficacious to targeted cancer cells and less harmful to normal cells. The accumulated evidence on the tumor-progressing roles of HB-EGF has suggested that HB-EGF-targeted cancer therapy is expected to be promising. In the present research, with the aim of developing anti-cancer drug targeting HB-EGF, neutralizing anti-HB-EGF mAbs were generated, and the therapeutic possibility of Y-142 was evaluated. In addition, the functions of proHB-EGF in cancer cell were identified.

In the Chapter I, I challenged the generation of neutralizing anti-HB-EGF mAbs by a hybridoma approach using mice from different genetic backgrounds, as well as different types of HB-EGF immunogens. The populations of mAb bins and the production rates of the neutralizing mAbs were strikingly different by mouse strain and by immunogen type. The finding presented here is the first evidence of the effects of mouse strains and immunogen types on the characteristics of individual mAbs. This would provide important insight on the generation of functional antibodies against any target molecule.

In the Chapter II, the therapeutic possibility of Y-142 was explored by characterizing its biological activity. The antibody has a potent HB-EGF neutralizing activity that modulates multiple biological activities of HB-EGF including cancer cell proliferation and angiogenic activities. The results indicated that Y-142 may have a potential to be developed into a therapeutic agent for the treatment of HB-EGF-dependent cancers.

In the Chapter III, I utilized the anti-HB-EGF mAbs Y-142 and Y-073, which have differential specificities toward proHB-EGF, in order to elucidate proHB-EGF functions in cancer cells. The

use of 3D spheroid culture in combination with the monoclonal antibodies enabled to identify the cell proliferation and survival functions of proHB-EGF.

In the present research, the therapeutic possibilities of Y-142 against HB-EGF have been evaluated in terms of efficacy. Next challenge would be an assessment of adverse events of the HB-EGF-targeting therapy. As described in the General introduction section, EGFR inhibitors cause unnecessary adverse events possibly by excessively disturbing the activation of EGFR by multiple EGFR ligands. Previous reports evidenced that the expression of HB-EGF was significantly increased in ovarian cancer compared with that in normal ovaries, but those of other EGFR ligands were not (Miyamoto et al, 2004; Tanaka et al, 2005; Yagi et al, 2005). The differential expression of HB-EGF may lead to reduced adverse events in the HB-EGF-targeting therapy. To avoid immunogenicity against different species IgG, antibody drugs have to be human, humanized, or chimeric IgG. The antibodies obtained in this research are all mouse IgG; therefore, anti-HB-EGF antibodies here need to be engineered to humanized or chimerc IgG for the purpose of treatment. Fc region of IgG heavy chain binds to Fc receptor on NK cells, and the interaction leads to ADCC against target-expressing cells. Fc region is usually fucosylated at the position of N297. In contrast, IgG with the absence of fucose on N297 more strongly binds to Fc receptor and shows an enhanced ADCC. The non-fucosylated IgG can be produced by using fucosyltransferase-null cells. This finding is applied to mogamulizumab, which was approved for the treatment of T cell lymphoma in Japan. This approach may help to enhance the cytotoxicity of Y-142 against proHB-EGF-expressing cancer cells. I showed that Y-142 could simultaneously inhibit both proHB-EGF and sHB-EGF functions. In contrast, Y-073 was a sHB-EGF-specific neutralizer. Therefore, if Y-142 causes proHB-EGF-on-target adverse events, Y-073 can become an alternative antibody drug to inhibit only sHB-EGF pathways.

Multiple reports indicated the over-expression of HB-EGF in ovarian and gastric cancer tissues (Tanaka et al, 2005; Yagi et al, 2005; Miyamoto et al, 2004; Hirata et al, 2009; Yasumoto et al, 2001; Naef et al, 1996). Notably, in ovarian cancer, the over-expression of HB-EGF is not only associated with a poor prognosis of patients, but also noted in advanced cancer stage. More interestingly, the over-expression of HB-EGF is not exclusive to these cancer types. Glioblastoma, bladder, pancreas, and breast cancer tissues show the over-expression of HB-EGF (Mishima et al, 1998; Thøgersen et al, 2001; Kobrin et al, 1994; Suo et al, 2002). These facts enhance the value of development of Y-142 for the treatment of a broad range of cancer types.

The findings here would advance basic and clinical researches of HB-EGF, and furthermore, provide important insights into biological mechanisms of HB-EGF-dependent cancers. The concepts and approaches in the present research also would contribute to the development of an antibody drug field.

7. Acknowledgments

I would like to express deep thankfulness to Prof. Shiota K, Laboratory of Cellular Biochemistry, Animal Resource Sciences/Veterinary Medical Sciences, the University of Tokyo for helpful discussions. I am indebted to Dr. Drake AW and Mr. Oshima T at Takeda San Francisco, Inc., and Dr. Tsuji I, Messrs. Watanabe T, Otake K, and Kajiwara H at Takeda Pharmaceutical Company Limited for experimental collaboration, and to Drs. Masat L, and Landes G at Takeda San Francisco, Inc. and to Ms. Kamada H, Drs. Kurokawa T, Shintani Y, Kondo S, Kokubo T, Fujii R, and Takizawa M at Takeda Pharmaceutical Company Limited for insightful comments. My deepest appreciation goes to Dr. Fan J at Takeda San Francisco, Inc. for generous supports and discussions. I also would like to give thanks to Ms. Sato Y for continuous supports and encouragements.

8. References

Abramovitch R, Neeman M, Reich R, Stein I, Keshet E, Abraham J, Solomon A, Marikovsky M (1998) Intercellular communication between vascular smooth muscle and endothelial cells mediated by heparin-binding epidermal growth factor-like growth factor and vascular endothelial growth factor. FEBS Lett 425: 441–447.

Amagai M (2010) Autoimmune and infectious skin diseases that target desmogleins. Proc Jpn Acad, Ser B Phys Biol Sci 86: 524–537.

Asakura M, Kitakaze M, Takashima S, Liao Y, Ishikura F, Yoshinaka T, Ohmoto H, Node K, Yoshino K, Ishiguro H, Asanuma H, Sanada S, Matsumura Y, Takeda H, Beppu S, Tada M, Hori M, Higashiyama S (2002) Cardiac hypertrophy is inhibited by antagonism of ADAM12 processing of HB-EGF: metalloproteinase inhibitors as a new therapy. Nat Med 8: 35–40.

Aviezer D, Yayon A (1994) Heparin-dependent binding and autophosphorylation of epidermal growth factor (EGF) receptor by heparin-binding EGF-like growth factor but not by EGF. Proc Natl Acad Sci U S A 91: 12173–12177.

Baraldo K, Mori E, Bartoloni A, Petracca R, Giannozzi A, Norelli F, Rappuoli R, Grandi G, Del Giudice G (2004) N19 polyepitope as a carrier for enhanced immunogenicity and protective efficacy of meningococcal conjugate vaccines. Infect Immun 72: 4884–4887.

Beerli RR, Hynes NE (1996) Epidermal growth factor-related peptides activate distinct subsets of ErbB receptors and differ in their biological activities. J Biol Chem 271: 6071–6076.

Beguinot L, Lyall RM, Willingham MC, Pastan I (1984) Down-regulation of the epidermal growth factor receptor in KB cells is due to receptor internalization and subsequent degradation in lysosomes. Proc Natl Acad Sci U S A 81: 2384–2388.

Blake RCII, Delehanty JB, Khosraviani M, Yu H, Jones RM, Blake DA (2003) Allosteric binding properties of a monoclonal antibody and its Fab fragment. Biochemistry 42: 497–508.

Boatright KM, Salvesen GS (2003) Mechanisms of caspase activation. Curr Opin Cell Biol 15: 725-731.

Brooke JS, Cha JH, Eidels L (1998) Diphtheria toxin:receptor interaction: association, dissociation, and effect of pH. Biochem Biophys Res Commun 248: 297–302.

Buzzi S, Rubboli D, Buzzi G, Buzzi AM, Morisi C, Pironi F (2004) CRM197 (nontoxic diphtheria toxin): effects on advanced cancer patients. Cancer Immunol Immunother 53: 1041–1048.

Carpenter G, Wahl MI (1991) in: Sporn MB, Roberts AB (Eds) Peptide Growth Factors and Their Receptors, Vol. 1, Springer-Verlag, New York, 69–171.

Cegedim Strategic Data: http://www.utobrain.co.jp/news/20120730.shtml. Accessed on Aug 27th, 2012.

Chapman K, Pullen N, Graham M, Ragan I (2007) Preclinical safety testing of monoclonal antibodies: the significance of species relevance. Nat Rev Drug Discov 6: 120–126.

ClinicalTrials: http://clinicaltrials.gov/. Accessed on Aug 28th, 2012.

Cook PW, Mattox PA, Keeble WW, Pittelkow MR, Plowman GD, Shoyab M, Adelman JP, Shipley GD (1991) A heparin sulfate-regulated human keratinocyte autocrine factor is similar or identical to amphiregulin. Mol Cell Biol 11: 2547–2557.

Darling RJ, Brault PA (2004) Kinetic exclusion assay technology: characterization of molecular interactions. Assay Drug Dev Techn 2: 647–657.

Das SK, Wang XN, Paria BC, Damm D, Abraham JA, Klagsbrun M, Andrews GK, Dey SK (1994) Heparin-binding EGF-like growth factor gene is induced in the mouse uterus temporally by the blastocyst solely at the site of its apposition: a possible ligand for interaction with blastocyst EGF-receptor in implantation. Development 120: 1071–1083.

Defendini ML, Pierres M, Regnier-Vigouroux A, Rochat H, Granier C (1990) Epitope mapping of apamin by means of monoclonal antibodies raised against free or carrier-coupled peptide. Mol Immunol 27: 551–558.

Defize LH, Boonstra J, Meisenhelder J, Kruijer W, Tertoolen LG, Tilly BC, Hunter T, van Bergen en Henegouwen PM, Moolenaar WH, de Laat SW (1989) Signal transduction by epidermal growth factor occurs through the subclass of high affinity receptors. J Cell Biol 109: 2495–2507.

Elenius K, Paul S, Allison G, Sun J, Klagsbrun M (1997) Activation of HER4 by heparin-binding EGF-like growth factor stimulates chemotaxis but not proliferation. EMBO J 16: 1268–1278.

Engler DA, Campion SR, Hauser MR, Cook JS, Niyogi SK (1992) Critical functional requirement for the guanidinium group of the arginine 41 side chain of human epidermal growth factor as revealed by mutagenic inactivation and chemical reactivation. J Biol Chem 267: 2274–2281.

Engvall E, Perlmann P (1971) Enzyme-linked immunosorbent assay (ELISA). Quantitative assay of immunoglobulin G. Immunochemistry 8: 871–874.

EpiDatabase: http://kantarhealth.com. Accessed on Aug 27th, 2012.

Eslick GD (2006) Helicobacter pylori infection causes gastric cancer? A review of the epidemiological, meta-analytic, and experimental evidence. World J Gastroenterol 12: 2991–2999.

Friedrich J, Ebner R, Kunz-Schughart LA (2007) Experimental anti-tumor therapy in 3-D: spheroids-old hat or new challenge? Int J Radiat Biol 83: 849–871.

Fu S, Bottoli I, Goller M, Vogt PK (1999) Heparin-binding epidermal growth factor-like growth factor, a v-Jun target gene, induces oncogenic transformation. Proc Natl Acad Sci U S A 96: 5716–5721.

Giannini G, Rappuoli R, Ratti G (1984) The amino-acid sequence of two non-toxic mutants of diphtheria toxin:CRM45 and CRM197. Nucl Acids Res 12: 4063–4069.

Giorgio C, Hassan Mohamed I, Flammini L, Barocelli E, Incerti M, Lodola A, Tognolini M (2011) Lithocholic acid is an Eph-ephrin ligand interfering with Eph-kinase activation. PLoS One 2011; 6: e18128

Goldstein NI, Prewett M, Zuklys K, Rockwell P, Mendelsohn J (1995) Biological efficacy of a chimeric antibody to the epidermal growth factor receptor in a human tumor xenograft model. Clin Cancer Res 1: 1311–1318.

Hamaoka M, Chinen I, Murata T, Takashima S, Iwamoto R, Mekada E (2010) Anti-human HB-EGF monoclonal antibodies inhibiting ectodomain shedding of HB-EGF and diphtheria toxin binding. J Biochem 148: 55–69.

Higashiyama S, Abraham JA, Miller J, Fiddes JC, Klagsbrun M (1991) A heparin-binding growth factor secreted by macrophage-like cells that is related to EGF. Science 251: 936–939.

Higashiyama S, Lau K, Besner GE, Abraham JA, Klagsbrun M (1992) Structure of heparin-binding EGF-like growth factor. Multiple forms, primary structure, and glycosylation of the mature protein. J Biol Chem 267: 6205–6212.

Higashiyama S, Abraha, JA, Klagsbrun M (1993) Heparin-binding EGF-like growth factor stimulation of smooth muscle cell migration: dependence on interactions with cell surface heparin sulfate. J Cell Biol 122: 933–940.

Higashiyama S, Iwamoto R, Goishi K, Raab G, Taniguchi N, Klagsbrun M, Mekada E (1995) The membrane protein CD9/DRAP 27 potentiates the juxtacrine growth factor activity of the membrane-anchored heparin-binding EGF-like growth factor. J Cell Biol 128: 929–938.

Higashiyama S, Iwabuki H, Morimoto C, Hieda M, Inoue H, Matsushita N (2008) Membrane-anchored growth factors, the epidermal growth factor family: beyond receptor ligands. Cancer Sci 99: 214–220.

Hirata M, Umata T, Takahashi T, Ohnuma M, Miura Y, Iwamoto R, Mekada E (2001) Identification of serum factor inducing ectodomain shedding of proHB-EGF and studies of noncleavable mutants of proHB-EGF. Biochem Biophys Res Commun 283: 915–922.

Hirata Y, Ogasawara N, Sasaki M, Mizushima T, Shimura T, Mizoshita T, Mori Y, Kubota E, Wada T, Tanida S, Kataoka H, Kamiya T, Higashiyama S, Joh T (2009) BCL6 degradation caused by the interaction with the C-terminus of pro-HB-EGF induces CCND2 expression in gastric cancers. Br J Cancer 100: 1320–1329.

Hoffenbach A, Lagrange PH, Bach MA (1985) Strain variation of lymphokine production and specific antibody secretion in mice infected with Mycobacterium lepraemurium. Cell Immunol 91: 1–11.

Hoffmann AC, Danenberg KD, Taubert H, Danenberg PV, Wuerl P (2009) A three-gene signature for outcome in soft tissue sarcoma. Clin Cancer Res 15: 5191–5198.

Hommel U, Harvey TS, Driscoll PC, Campbell ID (1992) Human epidermal growth factor. High resolution solution structure and comparison with human transforming growth factor alpha. J Mol Biol 227: 271–282.

Hoskins JT, Zhou Z, Harding PA (2008) The significance of disulfide bonding in biological activity of HB-EGF, a mutagenesis approach. Biochem Biophys Res Commun 375: 506–511.

Inui S, Higashiyama S, Hashimoto K, Higashiyama M, Yoshikawa K, Taniguchi N (1997) Possible role of coexpression of CD9 with membrane-anchored heparin-binding EGF-like growth factor and amphiregulin in cultured human keratinocyte growth. J Cell Physiol 171: 291–298.

Iwamoto R, Handa K, Mekada E (1999) Contact-dependent growth inhibition and apoptosis of epidermal growth factor (EGF) receptor-expressing cells by the membrane-anchored form of heparin-binding EGF-like growth factor. J Biol Chem 274: 25906–25912.

Iwamoto R, Mekada E (2000) Heparin-binding EGF-like growth factor: a juxtacrine growth factor. Cytokine Growth Factor Rev 11: 335–344.

Iwamoto R, Yamazaki S, Asakura M, Takashima S, Hasuwa H, Miyado K, Adachi S, Kitakaze M, Hashimoto K, Raab G, Nanba D, Higashiyama S, Hori M, Klagsbrun M, Mekada E (2003) Heparin-binding EGF-like growth factor and ErbB signaling is essential for heart function. Proc Natl Acad Sci U S A 100: 3221–3226.

Izumi Y, Hirata M, Hasuwa H, Iwamoto R, Umata T, Miyado K, Tamai Y, Kurisaki T, Sehara-Fujisawa A, Ohno S, Mekada E (1998) A metalloprotease-disintegrin, MDC9/meltrin-γ/ADAM9 and PKCδ are involved in TPA-induced ectodomain shedding of membrane-anchored heparin-binding EGF-like growth factor. EMBO J 17: 7260–7272.

Jackson LF, Qiu TH, Sunnarborg SW, Chang A, Zhang C, Patterson C, Lee DC (2003) Defective valvulogenesis in HB-EGF and TACE-null mice is associated with aberrant BMP signaling. EMBO J 22: 2704–2716.

Jin P, Zhang J, Beryt M, Turin L, Brdlik C, Feng Y, Bai X, Liu J, Jorgensen B, Shepard HM (2009) Rational optimization of a bispecific ligand trap targeting EGF receptor family ligands. Mol Med 15: 11–20.

Jones JT, Ballinger MD, Pisacane PI, Lofgren JA, Fitzpatrick VD, Fairbrother WJ, Wells JA, Sliwkowski MX (1998) Binding interaction of the heregulinbeta egf domain with ErbB3 and ERBB4 receptors assessed by alanine scanning mutagenesis. J Biol Chem 273: 11667–11674.

Jung KW, Park S, Kong HJ, Won YJ, Lee JY, Park EC, Lee JS (2011) Cancer statistics in Korea: incidence, mortality, survival, and prevalence in 2008. Cancer Res Treat 43: 1–11.

Kageyama T, Ohishi M, Miyamoto S, Mizushima H, Iwamoto R, Mekada E (2007) Diphtheria toxin mutant CRM197 possesses weak EF2-ADP-ribosyl activity that potentiates its anti-tumorigenic activity. J Biochem 142: 95–104.

Karle S, Nishiyama Y, Taguchi H, Zhou YX, Luo J, Planque S, Hanson C, Paul S (2003) Carrier-dependent specificity of antibodies to a conserved peptide determinant of gp120. Vaccine 21: 1213–1218.

Kasai K, Teuscher C, Smith S, Matzner P, Tung KS (1987) Strain variations in anti-sperm antibody responses and anti-fertility effects in inbred mice. Biol Reprod 36: 1085–1094.

Keizer RJ, Huitema AD, Schellens JH, Beijnen JH (2010) Clinical pharmacokinetics of therapeutic monoclonal antibodies. Clin Pharmacokinet 49: 493–507.

Khong TF, Fraser S, Katerelos M, Paizis K, Hill PA, Power DA (2000) Inhibition of heparin-binding epidermal growth factor-like growth factor increases albuminuria in puromycin aminonucleoside nephrosis. Kidney Int 58: 1098–1107.

Kinugasa Y, Hieda M, Hori M, Higashiyama S (2007) The carboxyl-terminal fragment of pro-HB-EGF reverses Bcl6-mediated gene repression. J Biol Chem 282: 14797–14806.

Knudson AG (2001) Two genetic hits (more or less) to cancer. Nat Rev Cancer 1: 157–162.

Kobrin MS, Funatomi H, Friess H, Buchler MW, Stathis P, Korc M (1994) Induction and expression of heparin-binding EGF-like growth factor in human pancreatic cancer. Biochem Biophys Res Commun 202: 1705–1709.

Koide H, Muto Y, Kasai H, Kohri K, Hoshi K, Takahashi S, Tsukumo K, Sasaki T, Oka T, Miyake T, Fuwa T, Kohda D, Inagaki F, Miyazawa T, Yokoyama S (1992) A site-directed mutagenesis study on the role of isoleucine-23 of human epidermal growth factor in the receptor binding. Biochim Biophys Acta 1120: 257–261.

Ladner RC (2007) Mapping the epitopes of antibodies. Biotechnol Genet Eng Rev 24: 1–30.

Lax I, Bellot F, Howk R, Ullrich A, Givol D, Schlessinger J (1989) Functional analysis of the ligand binding site of EGF-receptor utilizing chimeric chicken/human receptor molecules. EMBO J 8: 421–427.

Lax I, Fischer R, Ng C, Segre J, Ullrich A, Givol D, Schlessinger J (1991) Noncontiguous regions in the extracellular domain of EGF receptor define ligand-binding specificity. Cell Regul 2: 337–345.

Lemjabbar H, Basbaum C (2002) Platelet-activating factor receptor and ADAM10 mediate responses to Staphylococcus aureus in epithelial cells. Nat Med 8: 41–46.

Li JY, English MA, Ball HJ, Yeyati PL, Waxman S, Licht JD (1997) Sequence-specific DNA binding and transcriptional regulation by the promyelocytic leukemia zinc finger protein. J Biol Chem 272: 22447–22455.

Lin J, Hutchinson L, Gaston SM, Raab G, Freeman MR (2001) BAG-1 is a novel cytoplasmic binding partner of the membrane form of heparin-binding EGF-like growth factor: a unique role for proHB-EGF in cell survival regulation. J Biol Chem 276: 30127-30132.

Livneh E, Prywes R, Kashles O, Reiss N, Sasson I, Mory Y, Ullrich A, Schlessinger J (1986) Reconstitution of human epidermal growth factor receptors and its deletion mutants in cultured hamster cells. J Biol Chem 261: 12490-12497.

Lunet N, Lacerda-Vieira A, Barros H (2005) Fruit and vegetables consumption and gastric cancer: a systematic review and meta-analysis of cohort studies. Nutr Cancer 53: 1–10.

Matsuda T, Marugame T, Kamo KI, Katanoda K, Ajiki W, Sobue T and The Japan Cancer Surveillance Research Group (2012) Cancer Incidence and Incidence Rates in Japan in 2006: Based on Data from 15 Population-based Cancer Registries in the Monitoring of Cancer Incidence in Japan (MCIJ) Project. Jpn J Clin Oncol, 42: 139-147.

Mekada E, Okada Y, Uchida T (1988) Identification of diphtheria toxin receptor and a nonproteinous diphtheria toxin-binding molecule in Vero cell membrane. J Cell Biol 107: 511–519.

Mine N, Iwamoto R, Mekada E (2005) HB-EGF promotes epithelial cell migration in eyelid development. Development 132: 4317–4326.

Mishima K, Higashiyama S, Asai A, Yamaoka K, Nagashima Y, Taniguchi N, Kitanaka C, Kirino T, Kuchino Y (1998) Heparin-binding epidermal growth factor-like growth factor stimulates mitogenic signaling and is highly expressed in human malignant gliomas. Acta Neuropathol 96: 322–328.

Mitamura T, Iwamoto R, Umata T, Yomo T, Urabe I, Tsuneoka M, Mekada E (1992) The 27-kD diphtheria toxin receptor-associated protein (DRAP27) from vero cells is the monkey homologue of human CD9 antigen: expression of DRAP27 elevates the number of diphtheria toxin receptors on toxin-sensitive cells. J Cell Biol 118: 1389–1399.

Mitamura T, Higashiyama S, Taniguchi N, Klagsbrun M, Mekada E (1995) Diphtheria toxin binds to the epidermal growth factor (EGF)-like domain of human heparin-binding EGF-like growth factor/diphtheria toxin receptor and inhibits specifically its mitogenic activity. J Biol Chem 270: 1015–1019.

Miyagawa J, Higashiyama S, Kawata S, Inui Y, Tamura S, Yamamoto K, Nishida M, Nakamura T, Yamashita S, Matsuzawa Y, Taniguchi N (1995) Localization of heparin-binding EGF-like

growth factor in the smooth muscle cells and macrophages of human atherosclerotic plaques. J Clin Invest 95: 404–411.

Miyamoto S, Hirata M, Yamazaki A, Kageyama T, Hasuwa H, Mizushima H, Tanaka Y, Yagi H, Sonoda K, Kai M, Kanoh H, Nakano H, Mekada E (2004) Heparin-binding EGF-like growth factor is a promising target for ovarian cancer therapy. Cancer Res 64: 5720–5727.

Miyamoto S, Yagi H, Yotsumoto F, Horiuchi S, Yoshizato T, Kawarabayashi T, Kuroki M, Mekada E. (2007) New approach to cancer therapy: heparin binding-epidermal growth factor-like growth factor as a novel targeting molecule. Anticancer Res 27: 3713–3721.

Miyamoto S, Iwamoto R, Furuya A, Takahashi K, Sasaki Y, Ando H, Yotsumoto F, Yoneda T, Hamaoka M, Yagi H, Murakami T, Hori S, Shitara K, Mekada E (2011) A novel anti-human HB-EGF monoclonal antibody with multiple antitumor mechanisms against ovarian cancer cells. Clin Cancer Res 17: 6733–6741.

Miyoshi E, Higashiyama S, Nakagawa T, Hayashi N, Taniguchi N (1997) Membrane-anchored heparin-binding epidermal growth factor-like growth factor acts as a tumor survival factor in a hepatoma cell line. J Biol Chem 272: 14349–14355.

Mort JS Buttle DJ (1999) The use of cleavage site specific antibodies to delineate protein processing and breakdown pathways. Mol Pathol 52: 11-18.

Naef M, Yokoyama M, Friess H, Büchler MW, Korc M (1996) Co-expression of heparin-binding EGF-like growth factor and related peptides in human gastric carcinoma. Int J Cancer 66: 315–321.

Naglich JG, Metherall JE, Russell DW, Eidels L (1992) Expression cloning of a diphtheria toxin receptor: identity with a heparin-binding EGF-like growth factor precursor. Cell 69: 1051–1061.

Nakagawa M, Nabeshima K, Asano S, Hamasaki M, Uesugi N, Tani H, Yamashita Y, Iwasaki H (2009) Up-regulated expression of ADAM17 in gastrointestinal stromal tumors: coexpression with EGFR and EGFR ligands. Cancer Sci 100: 654–662.

Nakagawa T, Higashiyama S, Mitamura T, Mekada E, Taniguchi N (1996) Amino-terminal processing of cell surface heparin-binding epidermal growth factor-like growth factor up-regulates its juxtacrine but not its paracrine growth factor activity. J Biol Chem 271: 30858–30863.

Nakamura K, Iwamoto R, Mekada E (1995) Membrane-anchored heparin-binding EGF-like growth factor (HB-EGF) and diphtheria toxin receptor-associated protein (DRAP27)/CD9 form a complex with integrin alpha 3 beta 1 at cell-cell contact sites. J Cell Biol 129: 1691–1705.

Nanba D, Mammoto A, Hashimoto K, Higashiyama S (2003) Proteolytic release of the carboxy-terminal fragment of proHB-EGF causes nuclear export of PLZF. J Cell Biol 163: 489–502.

Ogiso H, Ishitani R, Nureki O, Fukai S, Yamanaka M, Kim JH, Saito K, Sakamoto A, Inoue M, Shirouzu M, Yokoyama S (2002) Crystal structure of the complex of human epidermal growth factor and receptor extracellular domains. Cell 110: 775–787.

Ono M, Raab G, Lau K, Abraham JA, Klagsbrun M (1994) Purification and characterization of transmembrane forms of heparin-binding EGF-like growth factor. J Biol Chem 269: 31315–31321.

Peoples GE, Blotnick S, Takahashi K, Freeman MR, Klagsbrun M, Eberlein TJ (1995) T lymphocytes that infiltrate tumors and atherosclerotic plaques produce heparin-binding epidermal growth factor-like growth factor and basic fibroblast growth factor: a potential pathologic role. Proc Natl Acad Sci U S A 92: 6547–6551.

Plummer M, Franceschi S, Muñoz N (2004) Epidemiology of gastric cancer. IARC Sci Publ: 311–326.

Powell PP, Klagsbrun M, Abraham JA, Jones RC (1993) Eosinophils expressing heparin-binding EGF-like growth factor mRNA localize around lung microvessels in pulmonary hypertension. Am J Pathol 143: 784–793.

Prat J, Ribé A, Gallardo A (2005) Hereditary ovarian cancer. Hum Pathol 36: 861–870.

Prenzel N, Zwick E, Daub H, Leserer M, Abraham R, Wallasch C, Ullrich, A (1999) EGF receptor transactivation by G-protein-coupled receptors requires metalloproteinase cleavage of proHB-EGF. Nature 402: 884–888.

Raab G, Kover K, Paria BC, Dey SK, Ezzell RM, Klagsbrun M (1996) Mouse preimplantation blastocysts adhere to cells expressing the transmembrane form of heparin-binding EGF-like growth factor. Development 122: 637–645.

Riese DJ, Kim ED, Elenius K, Buckley S, Klagsbrun M, Plowman GD, Stern DF (1996) The epidermal growth factor receptor couples transforming growth factor-alpha, heparin-binding epidermal growth factor-like factor, and amphiregulin to Neu, ErbB-3, and ErbB-4. J Biol Chem 271: 20047–20052.

Salomon DS, Brandt R, Ciardiello F, Normanno N (1995) Epidermal growth factor-related peptides and their receptors in human malignancies. Crit Rev Oncol Hematol 19: 183–232.

Santini MT, Rainaldi G (1999) Three-dimensional spheroid model in tumor biology. Pathobiology 67: 148–157.

SEER: http://seer.cancer.gov/. Accessed on Aug 28th, 2012.

Singh AB, Sugimoto K, Harris RC (2007) Juxtacrine activation of epidermal growth factor (EGF) receptor by membrane-anchored heparin-binding EGF-like growth factor protects epithelial cells from anoikis while maintaining an epithelial phenotype. J Biol Chem 282: 32890–32901.

Shin SY, Takenouchi T, Yokoyama T, Ohtaki T, Munekata E (1994) Chemical synthesis and biological activity of the EGF-like domain of heparin-binding epidermal growth factor-like growth factor (HB-EGF). Int J Pept Protein Res 44: 485–490.

Shirakata Y, Kimura R, Nanba D, Iwamoto R, Tokumaru S, Morimoto C, Yokota K, Nakamura M, Sayama K, Mekada E, Higashiyama S, Hashimoto K (2005) Heparin-binding EGF-like growth factor accelerates keratinocyte migration and skin wound healing. J Cell Sci 118: 2363–2370.

Shishido Y, Sharma KD, Higashiyama S, Klagsbrun M, Mekada E (1995) Heparin-like molecules on the cell surface potentiate binding of diphtheria toxin to the diphtheria toxin receptor/membrane-anchored heparin-binding epidermal growth factor-like growth factor. J Biol Chem 270: 29578–29585.

Stollar BD, Fuchs S, Mozes E (1973) Immune response of mice to nucleic acids: strain-dependent differences in magnitude and class of antibody production. J Immunol 111: 121–129.

Sueblinvong T, Carner ME (2010) Current understanding of risk factors for ovarian cancer. Current Treatment Options in Oncology 10: 67-81.

Sunnarborg SW, Hinkle CL, Stevenson M, Russell WE, Raska CS, Peschon JJ, Castner BJ, Gerhart MJ, Paxton RJ, Black RA, Lee DC (2002) Tumor necrosis factor-alpha converting enzyme (TACE) regulates epidermal growth factor receptor ligand availability. J Biol Chem 277: 12838–12845.

Suo Z, Risberg B, Karlsson MG, Villman K, Skovlund E, Nesland JM (2002) The expression of EGFR family ligands in breast carcinomas. Int J Surg Pathol 10: 91–99.

Suzuki M, Raab G, Moses MA, Fernandez CA, Klagsbrun M (1997) Matrix metalloproteinase-3 releases active heparin-binding EGF-like growth factor by cleavage at a specific juxtamembrane site. J Biol Chem 272: 31730–31737.

Swartzman EE, Miraglia SJ, Mellentin-Michelotti J, Evangelista L, Yuan PM (1999) A homogeneous and multiplexed immunoassay for high throughput screening using fluorometric microvolume assay technology. Anal Biochem 271: 143–151.

Tadaki DK, Niyogi SK (1993) The functional importance of hydrophobicity of the tyrosine at position 13 of human epidermal growth factor in receptor binding. J Biol Chem 268: 10114–10119.

Takemura T, Kondo S, Homma T, Sakai M, Harris RC (1997) The membrane-bound form of heparin-binding epidermal growth factor-like growth factor promotes survival of cultured renal epithelial cells. J Biol Chem 272: 31036–31042.

Takemura T, Hino S, Murata Y, Yanagida H, Okada M, Yoshioka K, Harris RC (1999) Coexpression of CD9 augments the ability of membrane-bound heparin-binding epidermal growth factor-like growth factor (proHB-EGF) to preserve renal epithelial cell viability. Kidney Int 55: 71–81.

Takenobu H, Yamazaki A, Hirata M, Umata T, Mekada E (2003) The stress- and inflammatory cytokine-induced ectodomain shedding of heparin-binding epidermal growth factor-like growth

factor is mediated by p38 MAPK, distinct from the 12-O-tetradecanoylphorbol-13-acetate- and lysophosphatidic acid-induced signaling cascades. J Biol Chem 278: 17255–17262.

Tanaka Y, Miyamoto S, Suzuki SO, Oki E, Yagi H, Sonoda K, Yamazaki A, Mizushima H, Maehara Y, Mekada E, Nakano H (2005) Clinical significance of heparin-binding epidermal growth factor-like growth factor and a disintegrin and metalloprotease 17 expression in human ovarian cancer. Clin Cancer Res 11: 4783–4792.

Thøgersen VB, Sørensen BS, Poulsen SS, Orntoft TF, Wolf H, Nexo E (2001) A subclass of HER1 ligands are prognostic markers for survival in bladder cancer patients. Cancer Res 61: 6227–6233.

Tramacere I, Negri E, Pelucchi C, Bagnardi V, Rota M, Scotti L, Islami F, Corrao G, La Vecchia C, Boffetta P (2012) A meta-analysis on alcohol drinking and gastric cancer risk. Ann Oncol 23: 28–36.

Thompson SA, Higashiyama S, Wood K, Pollitt NS, Damm D, McEnroe G, Garrick B, Ashton N, Lau K, Hancock N, Klagsbrun M, Abraham JA (1994) Characterization of sequences within heparin-binding EGF-like growth factor that mediate interaction with heparin. J Biol Chem 269: 2541–2549.

The United Nations, World Population Prospects: The 2010 Revision.

Tsujioka H, Fukami T, Yotsumoto F, Ueda T, Hikita S, Takahashi Y, Kondo H, Kuroki M, Miyamoto S (2011) A possible clinical adaptation of CRM197 in combination with conventional chemotherapeutic agents for ovarian cancer. Anticancer Res 31: 2461–2465.

Uchida T, Gill DM, Pappenheimer AM Jr (1971) Mutation in the structural gene for diphtheria toxin carried by temperate phage b. Nature New Biol 233: 8–11.

Ushiro S, Ono M, Izumi H, Kohno K, Taniguchi N, Higashiyama S, Kuwano M (1996) Heparin-binding epidermal growth factor-like growth factor: p91 activation induction of plasminogen activator/inhibitor, and tubular morphogenesis in human microvascular endothelial cells. Jpn J Cancer Res 87: 68–77.

Wang F, Liu R, Lee SW, Sloss CM, Couget J, Cusack JC (2007) Heparin-binding EGF-like growth factor is an early response gene to chemotherapy and contributes to chemotherapy resistance. Oncogene 26: 2006–2016.

Yagi H, Miyamoto S, Tanaka Y, Sonoda K, Kobayashi H, Kishikawa T, Iwamoto R, Mekada E, Nakano H (2005) Clinical significance of heparin-binding epidermal growth factor-like growth factor in peritoneal fluid of ovarian cancer. Br J Cancer 92: 1737–1745.

Yamazaki S, Iwamoto R, Saeki K, Asakura M, Takashima S, Yamazaki A, Kimura R, Mizushima H, Moribe H, Higashiyama S, Endoh M, Kaneda Y, Takagi S, Itami S, Takeda N, Yamada G, Mekada E (2003) Mice with defects in HB-EGF ectodomain shedding show severe developmental abnormalities. J Cell Biol 163: 469–475.

Yan Y, Shirakabe K, Werb Z (2002) The metalloprotease Kuzbanian (ADAM10) mediates the transactivation of EGF receptor by G protein-coupled receptors. J Cell Biol 158: 221–226.

Yang P, Zhou Y, Chen B, Wan HW, Jia GQ, Bai HL, Wu XT (2009) Overweight, obesity and gastric cancer risk: results from a meta-analysis of cohort studies. Eur J Cancer 45: 2867–2873.

Yasumoto K, Yamada T, Kawashima A, Wang W, Li Q, Donev IS, Tacheuchi S, Mouri H, Yamashita K, Ohtsubo K, Yano S (2011) The EGFR ligands amphiregulin and heparin-binding egf-like growth factor promote peritoneal carcinomatosis in CXCR4-expressing gastric cancer. Clin Cancer Res 17: 3619–3630.

Yeyati PL, Shaknovich R, Boterashvili S, Li J, Ball HJ, Waxman S, Nason-Burchenal K, Dmitrovsky E, Zelent A, Licht JD (1999) Leukemia translocation protein PLZF inhibits cell growth and expression of cyclin A. Oncogene 18: 925–934.

Yu WH, Woessner Jr JF, McNeish JD, Stamenkovic I (2002) CD44 anchors the assembly of matrilysin/MMP-7 with heparin-binding epidermal growth factor precursor and ErbB4 and regulates female reproductive organ remodeling. Genes Dev 16: 307–323.

9. Abstract in Japanese

高齢化や生活習慣の変化に伴い癌の発生率は上昇しており、新たな治療法の開発が望まれている。進行性、転移性癌においては抗癌剤が広く用いられてきたが、癌細胞は画一的な細胞集団ではなく、発生組織だけではなく癌細胞を取り巻く微小環境によって異なる性質を獲得するため、従来の化学療法を主体とした治療法では効果が不十分で副作用も無視できないという問題があった。標的とする癌細胞の特定と分子標的を基礎にした抗癌剤として、近年、抗体医薬が注目されている。本研究では、ヘパリン結合性上皮成長因子（HB-EGF）を標的とした抗癌剤の開発を目的とし、HB-EGF の機能に対する活性を測定することで抗 HB-EGF 抗体の医薬品としての可能性を検証すると同時に、これまで不明瞭であった細胞膜結合型 proHB-EGF の癌細胞における機能を見出した。HB-EGF は上皮成長因子受容体である EGFR のリガンドとして機能し、細胞の増殖・生存を誘導する分子である。HB-EGF は、卵巣癌、胃癌、膀胱癌、膵臓癌、乳癌、肺癌、神経芽腫を含む多種の癌組織において発現亢進していることが報告され、癌組織における発現と癌患者の予後不良に相関が見られることが知られている。

本論文は三章より構成され、第一章では HB-EGF に対する中和抗体の作出と、それらの性状解析、第二章では上市された医薬品と比較することにより抗 HB-EGF 中和抗体 Y-142 の癌治療への可能性検証、第三章では作出した抗体を用いた proHB-EGF の癌細胞における機能解析を行なった。

第一章： Characterization of a variety of neutralizing anti-HB-EGF monoclonal antibodies by different immunization methods

（複数の免疫法を用いて取得した多様性を有した抗 HB-EGF 中和抗体の性状解析）

HB-EGF は細胞増殖活性を有し、特定の癌細胞において発現の亢進が見られることから、抗癌剤の標的分子としての可能性が示唆されてきた。しかし、これまで HB-EGF 中和抗体作製の成功例は少なく、成功したとする報告例においても十分な癌細胞増殖を抑制する活性を有しているとは言い難い。

本章では、中和活性を有する抗 HB-EGF 抗体の作出を目的とした。抗体作製の困難さを考慮し、異なる遺伝的背景を有するマウスと、複数の免疫原を用い、ハイブリドーマ法

による抗体の作製に挑戦した。ハイブリドーマの産生には電気融合法を用いた。抗体産生ハイブリドーマの選択には fluorometric microvolume assay technology を用いた。

用いたマウス種のうち、主に BALB/c、CD1 マウスより抗 HB-EGF 中和抗体が得られ、合計 146 種の中和抗体を機能評価に用いた。これらの抗体は可溶性 HB-EGF（sHB-EGF）に対する競合的結合性により 7 種のエピトープビンに分類された。得られた中和抗体は、sHB-EGF に対する中和活性、ヒト sHB-EGF に対する結合性、マウス/ラット sHB-EGF に対する交差結合性、及び細胞膜結合型 HB-EGF（proHB-EGF）に対する結合活性のいずれにおいても、エピトープビン毎に特徴的な活性を示していた。中和抗体の産生効率、及びエピトープビンの割合はマウス種、免疫原種によって著しく異なることも示された。

本章において多様性を有した抗 HB-EGF 抗体が作製され、マウス種、免疫原種の違いが、個々の抗体の活性に強く影響することが示された。本知見は HB-EGF のみならず他の標的分子に対する機能性抗体の取得時にも有用な情報となり得る。また、取得した抗体の中には強い中和活性を有する抗体も含まれていた。

第二章： An anti-HB-EGF monoclonal antibody inhibits cancer cell proliferation and multiple angiogenic activities of HB-EGF: a potential anti-cancer therapeutic agent

（抗 HB-EGF モノクローナル抗体よる HB-EGF 誘導性癌細胞増殖・血管誘導の阻害）

本章では、第一章において作製した抗 HB-EGF 中和抗体のうち、HB-EGF に対して強い中和活性を示した Y-142 の癌細胞の増殖および血管新生に対する中和活性を測定し、抗癌抗体としての可能性を検証した。

Y-142 の EGFR リガンドに対する結合、および種特異性結合は ELISA 法により決定し、sHB-EGF に対する中和活性の評価は、受容体である EGFR および ERBB4 の細胞内シグナルの活性化を測定することにより行った。Y-142 の生物活性は、ジフテリアトキシン変異体 HB-EGF 機能阻害タンパク質 CRM197、抗 EGFR 抗体 cetuximab、抗 VEGF 抗体 bevacizumab と比較し、Y-142 のエピトープ同定にはアラニンスキャニング法を用いた。

Y-142 は EGFR リガンドである HB-EGF、及び amphiregulin（ARG）に対して結合性を示した。また、Y-142 はマウス、ラット HB-EGF へは結合せず、ヒト HB-EGF に対する種特異的結合性を示した。Y-142 は sHB-EGF によって誘導された EGFR、ERBB4 のリン酸

化、細胞内シグナルの下流に位置する ERK1/2、および AKT のリン酸化を阻害した。さらに、Y-142 は CRM197、および cetuximab に比べ、低濃度において HB-EGF 誘導性の癌細胞の増殖、血管内皮細胞 HUVEC の増殖、管腔形成、VEGF の産生を抑制した。また、sHB-EGF 誘導性の HUVEC の管腔形成に対する Y-142 の阻害活性は、bevacizumab と比較して強いものであった。Y-142 のエピトープとして EGF 様ドメインに存在する 6 アミノ酸が同定され、このうち F115、および Y123 によって ARG に対する交差結合性、F115 によって Y-142 の種交差性が決定されていることが示唆された。Y-142 の強力な中和活性は、Y-142 が EGFR への結合に重要な HB-EGF の R142、Y123 を認識すること、および高親和性に由来していると推察された。

本章において、Y-142 の HB-EGF への結合様式を明らかにし、Y-142 が sHB-EGF の活性を強力に抑制することで、癌細胞の増殖、および複数の血管新生プロセスを抑制することを見出した。Y-142 は本章で用いた卵巣癌細胞を含め、HB-EGF シグナルに依存した癌の治療薬としての可能性が期待された。

第三章：Identification of cancer cell proliferative and survival role of proHB-EGF using anti-HB-EGF antibody

（抗 HB-EGF 抗体を用いた proHB-EGF の癌細胞増殖・生存促進機能の同定）

細胞膜結合型 proHB-EGF は sHB-EGF の前駆体として存在する。これまで sHB-EGF の機能は幅広く検証され、細胞の増殖・生存を促進することが知られている。ところが、proHB-EGF についての研究は少なく、機能解明は進んでいない。第一章で作製した 2 種の抗体（Y-142、Y-073）は proHB-EGF に対して異なる結合性を示す。そこで本章では Y-142 と Y-073 を利用し proHB-EGF の機能解析を試みた。

その結果、Y-142、及び Y-073 は sHB-EGF に対し同程度の結合活性、中和活性を有するものの、Y-142 のみが proHB-EGF に対する結合活性を有していることが判明した。Y-142 を用いて proHB-EGF の機能を抑制したところ、胃癌細胞 NUGC-3 のスフェロイド形成抑制と、細胞増殖抑制が見られ、カスパーゼ活性化も誘導されることが明らかとなった。

これらの結果から、proHB-EGF が癌細胞の増殖・生存を促進する機能を有することが示され、proHB-EGF が癌の進行に重要な役割を担っていることが示唆された。

本研究では、取得した抗 HB-EGF 抗体、特に Y-142 の評価を行い、上市されている抗 EGFR 抗体や他の HB-EGF 阻害剤に比べ HB-EGF に対する中和活性が強いことを見出した。HB-EGF を標的とした Y-142 による癌治療が副作用の面からも優れていることが示されれば、Y-142 の開発価値はさらに高まると考えられる。抗 EGFR 抗体を含めた EGFR 阻害剤は重度の発疹が副作用として出現する。この副作用は EGFR 阻害剤に共通して出現するため、EGFR シグナル遮断によるものと考えられる。EGFR 阻害剤は、複数の EGFR リガンドの機能を阻害するが、例えば、卵巣癌組織において HB-EGF の発現亢進が報告されているが、他の EGFR リガンドの発現亢進は見られていない。抗 HB-EGF 抗体は、癌組織で発現亢進を示す HB-EGF シグナルを特異的に阻害するため、EGFR 阻害剤に比較し副作用の面で優れている可能性が考えられる。Y-142 は sHB-EGF 及び proHB-EGF の機能を阻害する。一方、Y-073 は sHB-EGF の機能のみを阻害する。そのため、proHB-EGF の機能を阻害することで副作用が出現する場合には、Y-073 を用い sHB-EGF シグナルのみを阻害するという選択も可能である。また、本研究においては、卵巣癌、胃癌細胞株を主に用いて検討を実施したが、神経芽腫、膀胱癌、膵臓癌、乳癌組織においても HB-EGF の発現亢進は報告されているため、Y-142 は幅広い癌種に対して有効であると期待される。

本研究において、筆者は抗 HB-EGF 抗体の医薬品としての価値を見出すだけではなく、proHB-EGF の癌細胞における機能の重要性を見出した。これらの知見は、HB-EGF を標的とした抗体医薬の開発、並びに癌の増殖メカニズムの解明に重要な知見となった。